OCS Study
BOEM 2022-006

Coastal Marine Institute

An Assessment of Mud-Capped Dredge Pit Evolution on the Outer Continental Shelf in the Northern Gulf of Mexico

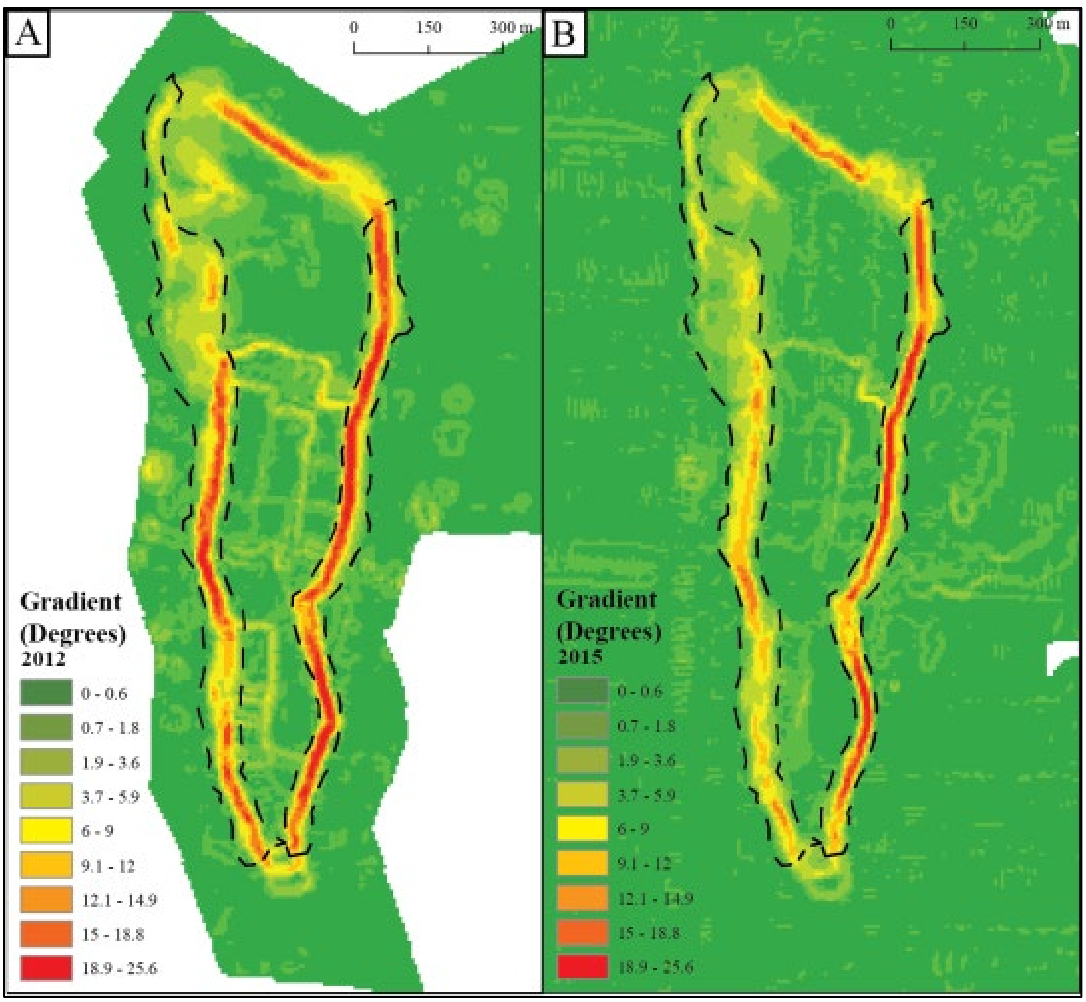

BOEM
Bureau of Ocean Energy Management

U.S. Department of the Interior
Bureau of Ocean Energy Management
Gulf of Mexico Regional Office

LSU

Cooperative Agreement
Coastal Marine Institute
Louisiana State University

OCS Study
BOEM 2022-006

Coastal Marine Institute

An Assessment of Mud-Capped Dredge Pit Evolution on the Outer Continental Shelf in the Northern Gulf of Mexico

Authors

KH Xu
SJ Bentley
C Li
N Chaichitehrani
J Obelcz
M O'Connor
P Robichaux
J Wang

January 2022

Prepared under BOEM Cooperative Agreement
M14AC00023
by
Louisiana State University
Coastal Marine Institute
Baton Rouge, Louisiana 70803

Published by

U.S. Department of the Interior
Bureau of Ocean Energy Management
Gulf of Mexico Regional Office

Cooperative Agreement
Coastal Marine Institute
Louisiana State University

DISCLAIMER

Study collaboration and funding were provided by the US Department of the Interior, Bureau of Ocean Energy Management (BOEM), Environmental Studies Program, Washington, DC, under Agreement Number M14AC00023. This report has been technically reviewed by BOEM, and it has been approved for publication. The views and conclusions contained in this document are those of the authors and should not be interpreted as representing the opinions or policies of the US Government, nor does mention of trade names or commercial products constitute endorsement or recommendation for use.

REPORT AVAILABILITY

To download a PDF file of this report, go to the US Department of the Interior, Bureau of Ocean Energy Management Data and Information Systems webpage (http://www.boem.gov/Environmental-Studies-EnvData/), click on the link for the Environmental Studies Program Information System (ESPIS), and search on 2022-006. The report is also available at the National Technical Reports Library at https://ntrl.ntis.gov/NTRL/.

CITATION

Xu KH, Bentley SJ, Li C, Chaichitehrani N, Obelcz J, O'Connor M, et al. 2019. An assessment of mud-capped dredge pit evolution on the outer continental shelf of the Gulf of Mexico. 89 p. New Orleans (LA): US Dept. of the Interior, Bureau of Ocean Energy Management. Contract No.: GM-14-03-05. Report No.: BOEM 2022-006.

ABOUT THE COVER

Slopes (gradient) of Sandy Point Dredge Pit walls in 2012 and 2015 derived from bathymetric data collected during this study.

CONTENTS

List of Figures

List of Tables

Abbreviations and Acronyms

Short Form	Long Form
ABS	acoustic backscatter sensor
ADCP	acoustic Doppler current profiler
ADV	acoustic Doppler velocimeter
BBL	bottom boundary layer
BOEM	Bureau of Ocean Energy Management
LSU	Louisiana State University
MCDP	mud-capped dredge pit
OBS	optical backscatter sensor
OCS	Outer Continental Shelf
WAVCIS	Wave-Current-Surge Information System

1. Introduction

Barrier islands are sandy sedimentary environments separated from the mainland by estuary or lagoon environments. They protect the mainland coast and interior wetlands from meteorological and marine forcings and help to regulate estuarine conditions. A major component of the State of Louisiana's effort to manage coastal land loss is to restore degraded barrier shorelines by dredging sand resources from offshore borrow sites and delivering those resources to the barrier systems to supplement a deficit in the coastal sand budget. However, dredging offshore alters seafloor topography; this has the potential to affect oil and gas infrastructure or other resources of concern located proximal to dredge pits. Direct impacts from dredging are well understood and mitigated for BOEM's environmental review and coordination throughout the sand leasing process. However, knowledge of long term changes in borrow pit geometry is poor; this is particularly true for some recent cases in the Gulf of Mexico where targeted sand resource deposits underlie muddy overburden, resulting in relatively deep pits with a "muddy cap" (pit walls are characterized by cohesive muds overlying unconsolidated sands). Though dredge pit evolution is expected (e.g., expansion of pit beyond extent of dredging activity) and mitigations are applied to protect adjacent areas, the effectiveness of mitigations has not been evaluated. This study provides empirical data to quantify mud-capped dredge pit evolution, building on earlier investments by BOEM to predict pit evolution based on numerical model simulations (Narin et al. 2005; 2007). The results are also applied to evaluate the effectiveness of existing mitigations (e.g., setback distances from pipelines) to determine if cultural resources and infrastructure are being protected.

1.1 Background

Approximately 90% of the Mississippi-Atchafalaya River system sediment load is suspended mud, defined as sediment finer than 63 µm in diameter, and only about 10% is sand (Nittrouer et al. 2008). Understanding the spatial and temporal variations of the formation of limited sand resources along the Mississippi Delta Plain is critical to the projects that require high-quality sand resources. Penland et al. (1989) proposed a conceptual model of inner shelf shoal evolution offshore the Mississippi Delta Plain. After river abandonment of a delta lobe, an abandoned deltaic headland is reworked by marine processes to form transgressive barrier islands and, ultimately, an inner shelf shoal that continues to be reworked by marine processes.

There are several prominent sandy shoals in Louisiana coasts, such as Trinity Shoal, Ship Shoal and Tiger Shoal. Much of northern Gulf of Mexico, however, is characterized by a dominantly muddy seafloor with a paucity of restoration-quality sand within several kilometers (km) to the shorelines. The sandy shoals are a considerable distance from most barrier shorelines that are in need of sand and have been cost-prohibitive as an option for many restoration projects. However, discrete sand deposits associated with ancient river channels that flowed across the shelf during the earlier stages of shelf and delta evolution do occur close to shore on the Outer Continental Shelf (OCS) (Figure 1). These channels were filled with sandy sediments as sea-levels rose, and ultimately were buried by recent mud deposition associated primarily with the modern rivers (Figure 1). During the past several decades, there have been extensive geophysical studies of incised fluvial systems along the northern Gulf of Mexico. Suter et al. (1987), for instance, identified many incised fluvial systems offshore of the western Louisiana Chenier Plain (Figure 2). These river channels were widely distributed along the 800-km long Louisiana coast and were formed in the geological past when the sea levels rose and fell and the rivers switched lobes. These shelf channel-filling sands have been targeted for coastal restoration projects, resulting in significant cost savings over using more distal deposits. These savings benefit the project's effectiveness and sustainability since greater quantities of sand can be placed for lower cost. However, identifying the location of these former, and now buried, channel sands can be challenging.

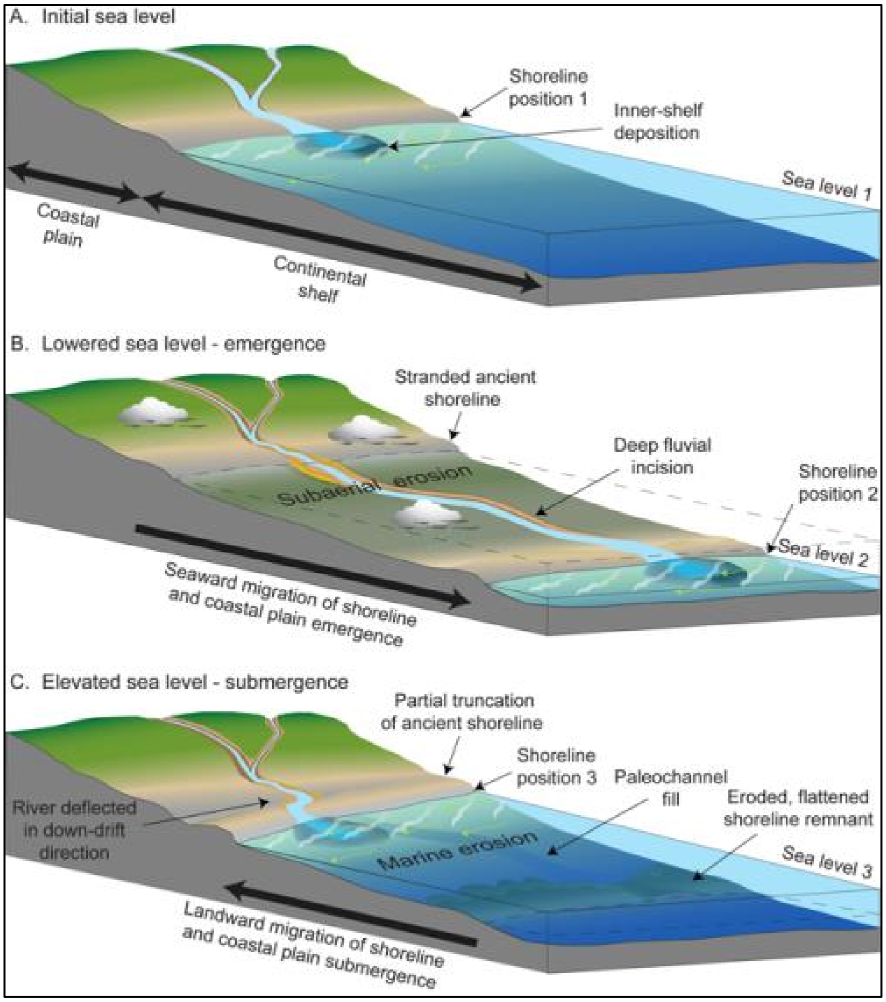

Figure 1. Changes in river sediment deposits and shorelines under the influence of sea level fluctuations.

Based on (Barnhardt et al. 2009). River paleochannel fills can be used as potential sand resources.

Because most of these sandy river paleochannels are now covered by muddy overburden associated with more recent shelf mud deposition, Nairn et al. (2005) defined this kind of sediment deposit as "mud-capped". These sandy river paleochannels are usually narrow and deep (e.g., ~10m below seafloor). After mud-capped sandy resources have been dredged, a deep pit is produced that has walls composed of muds overlying sands. Because of contrasting characteristics of two types of sediments (mud and sand), the long-term evolution of these pits is not well understood in relation to their more common sand-only counterparts. There is an urgent need to understand the sediment dynamics and the related hydrodynamics in "mixed" sediment environments.

Figure 2. Map showing the distribution of incised fluvial systems offshore of the western Louisiana Chenier Plain.

From Suter et al. 1987.

The study areas of this project include three mud-capped dredge pits: Sandy Point southeast in the eastern, Raccoon Island in the central, and Peveto Channel in the western Louisiana shelf (Figure 3).

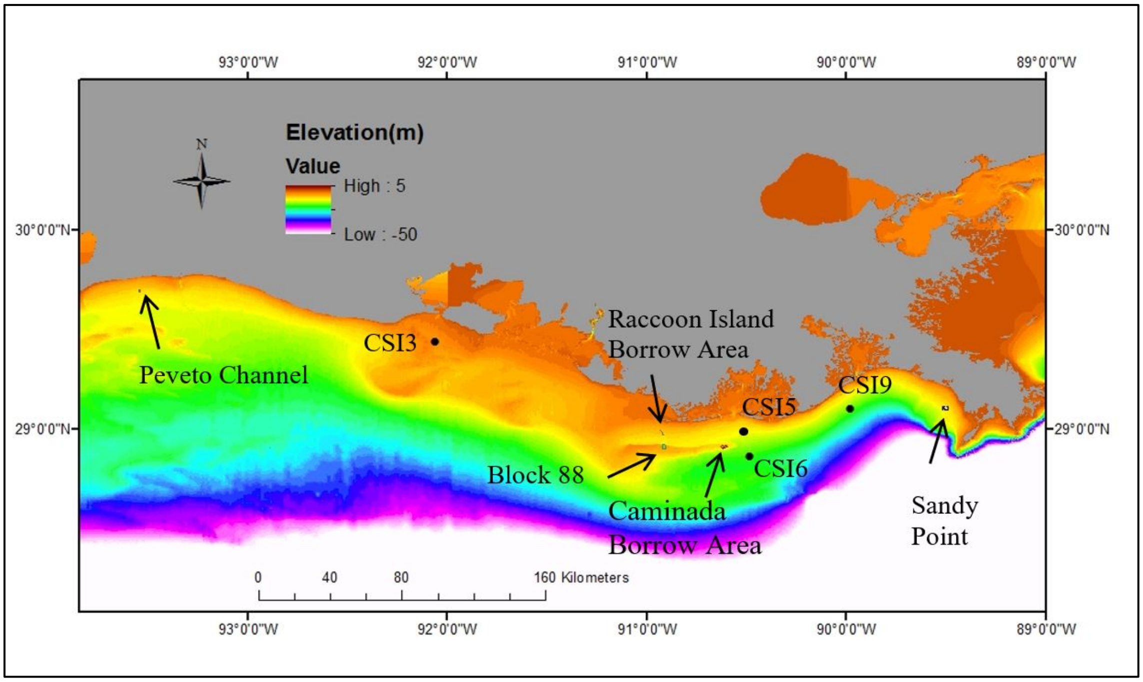

Figure 3. The map of locations of three mud-capped dredge pits: Peveto Channel, Raccoon Island, Sandy Point.

In blue: Peveto Channel, Raccoon Island, and Sandy Point, and two sandy dredge pits. In bold black: Caminada and Block 88 in Ship Shoal area. Black dots are active LSU WAVCIS (wave-current information system) stations, including CSI3, CSI5, CSI6, and CSI9.

Sandy Point southeast borrow area is about 13 km south of Sandy Point, Louisiana and is located to the west of the modern bird-foot Mississippi Delta (Figure 4). Water depths in this area range from 9.9 to 10.8 m. Sandy Point southeast was formed as relict channel fill sands with extensive muddy overburden. The borrow area contained about 3.9 million m^3 of sandy sediment and the average mean grain size of sand deposits is 0.12 mm (Tetra Tech 2004; Coastal Planning and Engineering, Inc. 2013). In November 2012, the dredging of this borrow site was completed for construction of the Pelican Island restoration project (Figure 4).

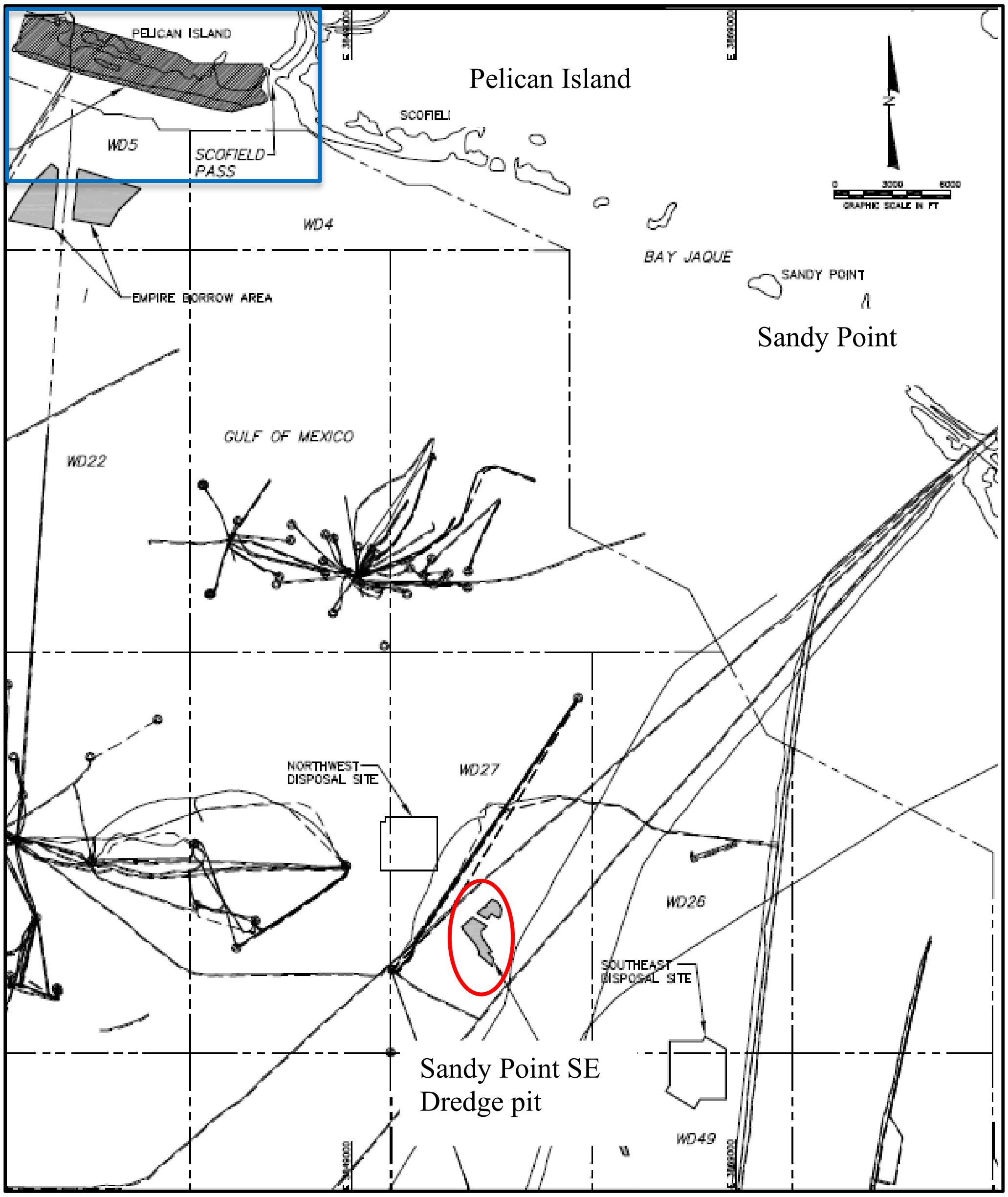

Figure 4. Sandy Point southeast dredge pit, Pelican Island, and Sandy Point of Louisiana.

Red oval: Sandy Point southeast dredge pit. Blue box: Pelican Island and Sandy Point of Louisiana. From Coastal Planning and Engineering 2013.

Before this study, limited site-specific empirical data were available as inputs for Sandy Point southeast borrow area model predictions. This dredge pit is located near the Barataria Bight, where the modern Mississippi Delta results in complex wave climate and current circulation patterns; the proximity to the river provides increased muddy sediment supply and helps the development of a clockwise gyre west of the Mississippi Delta; this gyre was also confirmed in a ROMS sediment transport modeling work by Xu et al. (2011).

In 2013, another dredge pit was excavated offshore Raccoon Island for the Raccoon Island Back-barrier Marsh Restoration Project. This pit is located south of Isles Dernieres and is between Raccoon Island and Ship Shoal (Figs. 3 and 5). The Isles Dernieres barrier island chain in central coastal Louisiana experienced some of the highest rates of erosion in the world from the 1890s to 1988. The rapid degradation of these islands has reduced the ability of the island chain to protect adjacent landward coastal marshes and swamps from the effects of storm surge, saltwater intrusion, an increased tidal prism, and frequent storm waves. Raccoon Island is the western-most island in the Isles Dernieres chain (Broussard and Boustany, 2005; Figure 5). The Raccoon Island project targeted paleo-channel muddy sands with no overburden, but produced a deep dredge pit.

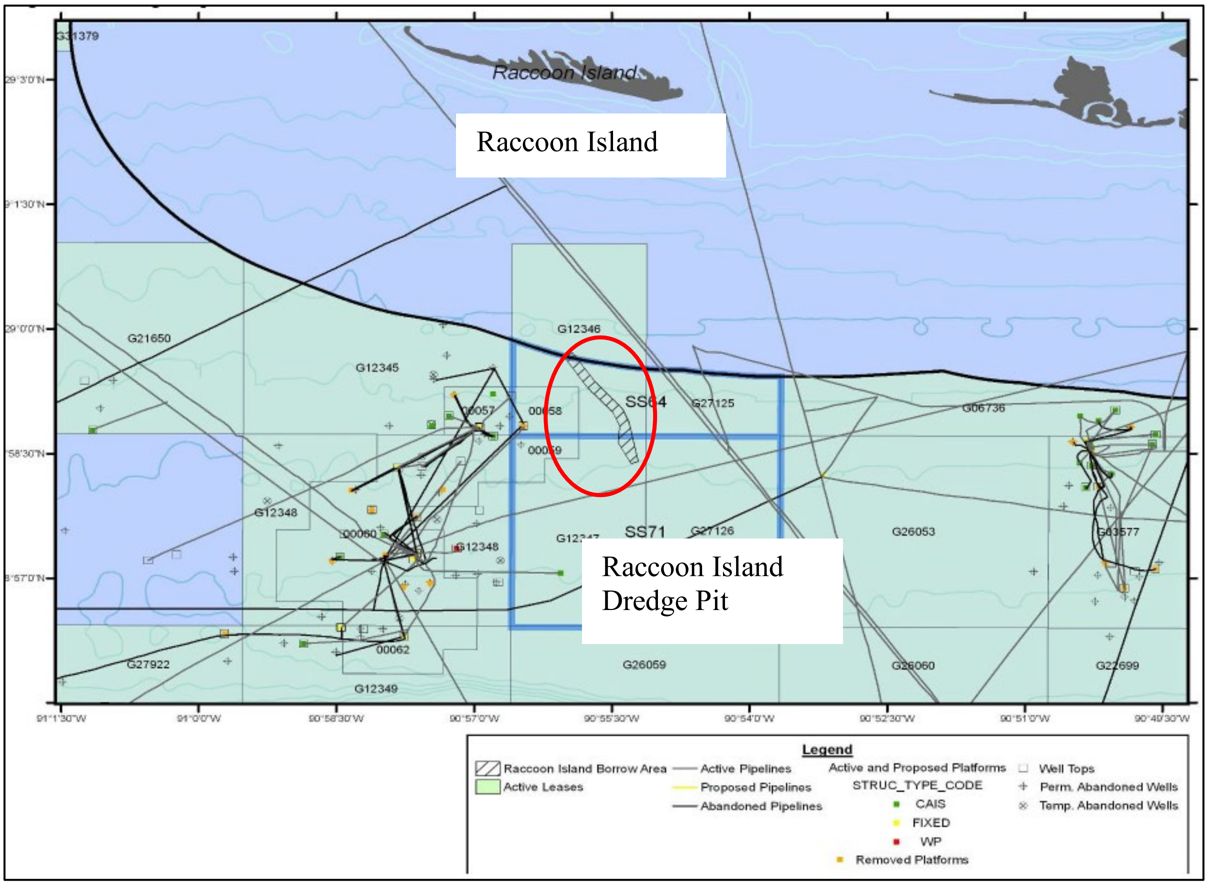

Figure 5. Raccoon Island Shore Protection-Marsh Creation Project.

Note that the dredge pit (red oval) is located on an identified paleo river channel (hatched elongated polygon) and is surrounded by many pipelines and oil platforms. From Broussard and Boustany (2005).

Previous studies of Stone et al. (1996, 2000, and 2009) and Kobashi (2009) showed that sediment transport processes on Ship Shoal include contrasting non-cohesive sand and cohesive mud transport. Muds from the Atchafalaya Bay sometimes are delivered to the Ship Shoal area, and then resuspended and transported to elsewhere; these “transient muds” may greatly impact the Raccoon Island dredge pit. Hydrodynamics and sediment dynamics in Raccoon Island dredge pit are probably steered in part by the boundaries of the mainland-island chain in the north and Ship Shoal in the south. This dredging pit is also surrounded by many pipelines and oil platforms, as illustrated in Figure 5.

The Peveto Channel dredge pit offshore Holly Beach of western Louisiana was excavated in 2003. It is located in federal waters offshore western Louisiana between Calcasieu Ship Channel and Sabine Pass, and approximately 7 km offshore in 8 m of water (Figure 6). The pit has dimensions of 400 m (shore-parallel) by 600 m (shore-normal) and was about 8 m deep immediately after dredging (Nairn et al.; 2004, and 2005; Figure 6). Site-specific data were collected to study the evolution of this pit over a period of two years following excavation. Predictive numerical models have been developed specifically for this mud-capped dredge pit in response to physical forcings including hydrodynamics, sediment dynamics, and local pit wall-seafloor stability (Nairn et al.; 2004, 2005, and 2007).

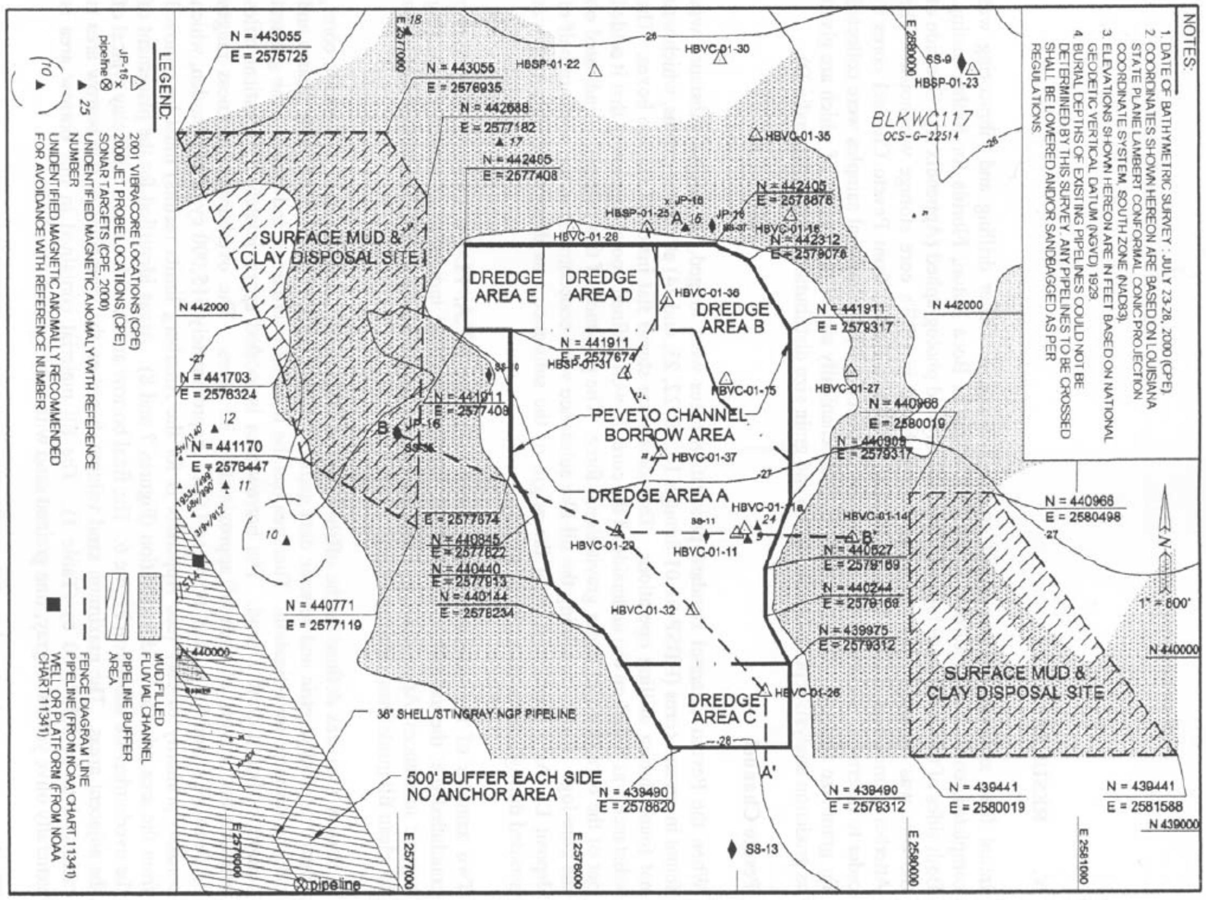

Figure 6. Peveto Channel dredge pit, disposal sites, and its surrounding pipelines.

From Coastal Planning & Engineering 2002.

Below are the major findings of the Peveto Channel dredge pit from Nairn et al. (2007):

a. Infilling of the pit to a near horizontal surface;
b. Slope flattening in areas where the pit edges were sandy;
c. The observation of little or no slope adjustment from the immediate post-dredge slopes for areas where the pit slope (or at least the upper part) consisted of clay or silt;
d. Pit margin erosion generally around the outer edge of the pit over a distance of at least 500 to 650 ft (150 to 200 m); and
e. Minor erosion and perhaps some migration towards the northwest of the dredge disposal mound (for stripped sediment) was evident.

Besides bathymetric surveys, Nairn et al. (2007) also did hydrodynamic work and found that tidal currents are in the range of +/- 1 ft/s (30 cm/s) driven by the dominant diurnal tides of the Gulf of Mexico (i.e., K1 and O1 constituents). The dominant S to SE winds drive residual westerly directed currents throughout much of the year which is equally important or at times greater than the tide-driven component (Cochrane and Kelly 1986; Nowlin et al. 1998a and 1998b). During the survey in March 5, 2007, Nairn et al. (2007) found that acoustic Doppler current profiler (ADCP) current velocity reversed at a depth of approximately 16.4 ft (5 m) below the water surface (Figure 7). Near-surface velocities over the pit and outside the pit ranged between 0.5 to 1.0 ft/s (0.15 and 0.30 m/s). They also found that the measured velocity profiles were mainly driven by winds and flow speed was reduced in the pit bottom.

Based on their comprehensive studies, Nairn et al. (2005) proposed a conceptual diagram of pit infilling and pit margin erosion processes (Figure 7). At the Peveto Channel dredge pit, erosion was observed in the pit margin area. As flow leaves the pit and water depth is reduced, flow becomes more confined, increasing velocity increases to match the ambient flow velocity in the absence of the pit. The sediment load capacity of the flow at the outgoing edge is similar to the load capacity at the incoming edge based on the conservation of water mass. However, the suspended sediment concentration at the outgoing edge is less than capacity once the flow accelerates to ambient flow speed due to deposition in the pit (Figure 7). Based on this assumed scenario, Nairn et al. (2005) predict bed erosion beyond the outgoing edge. Finally, Nairn et al. (2005) recommended some buffer distances for dredge pits in a muddy setting.

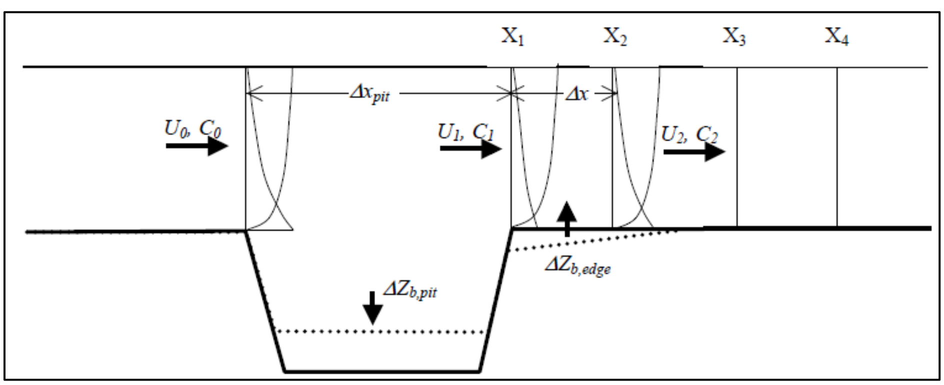

Figure 7. Pit infilling and pit margin erosion processes conceptual diagram.

From Nairn et al., 2005. U is velocity, C is sediment concentration, x is horizontal distance and z is sediment erosion or deposition.

1.2 Project Goals

In this project, new physical oceanographic, geological, and geophysical studies were conducted in Sandy Point southeast, and the Peveto Channel and Raccoon Island dredge pits to quantify and improve our understanding of mud-capped dredge pit evolution in the northern Gulf of Mexico. Alterations to seafloor topography from dredging OCS sediment resources have the potential to affect oil and gas infrastructure or other resources of concern that are located proximal to dredge pits. Direct impacts from dredging of sandy shoals are relatively well understood, but our understanding of long-term changes in mud-capped dredge pits is poor.

BOEM has devoted funding toward better understanding how dredge pits evolve and the potential impacts to infrastructure and/or resources of concern located adjacent to the pits (e.g., Stone et al., 1996, 2000, and 2009; Nairn et al. 2004, 2005, and 2007). Though dredge pit evolution is expected and mitigations are applied to protect adjacent areas, the effectiveness of mitigations has not been evaluated. Site-specific data required to make accurate predictions and empirical measurements to test and validate predictive models were only available for Peveto Channel (dredged in 2003) offshore of Holly Beach, Louisiana. Our study builds on BOEM's investment toward better understanding this problem by filling data gaps and validating predictive models developed during previous studies. We also evaluate the effectiveness of mitigations applied to existing dredge pits (e.g., setback distances from pipelines) to determine if resources and infrastructure are being protected. Our results can increase BOEM's decision-making ability regarding safety and protecting environmental and cultural resources, and better management of valuable OCS sand resources.

The main goals of this study are to:

1) Collect new hydrographic, geological, and geophysical data in three dredging pits: Sandy Point, Raccoon Island and Peveto Channel, respectively.
2) Validate and/or refine existing Nairn et al. predictive numerical model for dredge pit evolution using newly collected data from three dredge pits.
3) Develop a slope-failure model, a 1-D bottom boundary layer (BBL) sediment-transport model, and a 3-D hydrodynamics and sediment transport model, and apply them in the dredging pits.
4) Provide recommendations for future research and pit monitoring protocols (e.g., assigned setback buffer zone), and suggest mitigations based on empirical measurements.

1.3 Study Approach

The research was conducted by an interdisciplinary team of two geological oceanographers (Kehui Xu and Samuel Bentley, with expertise in sediment dynamics of dredging pits, seabed coring, geophysical methods, radionuclides) and a physical oceanographer (Chunyan Li, director of WAVCIS, with expertise in coastal dynamical processes influenced by tides, weather, river, and bathymetry), supervising multiple graduate and undergraduate students. New geological and physical data were collected mainly at Raccoon Island (dredged in 2013), Sandy Point southeast (dredged in 2012), and the Peveto Channel (dredged in 2003) pits. These field data collections are designed to capture the rapid changes at Raccoon Island and Sandy Point southeast before too much time has elapsed after excavations.

Our detailed field methods include mainly vessel-based hydrodynamics study to capture spatial variation of velocity profiles, tripod observation to study BBL hydrodynamics and sediment dynamics, a suite of geophysical surveys (bathymetry, sidescan, subbottom and magnetometer), and sediment corings using a multicorer and a submersible vibracorer. Lab approaches include mainly laser grain size analysis, loss-on-ignition, core logging, and radionuclide analysis. Modeling approaches include a slope-failure Henkel (1970) model to investigate slope stability, a 1-D bottom boundary layer sediment-transport model, and a 3-D hydrodynamics and sediment transport DELFT-3D model (Deltares 2014).

1.4 Team Organization

Our team from Louisiana State University consisted of the following key personnel fulfilling the listed roles:

Kehui Xu, Ph.D., Associate Professor, Department of Oceanography and Coastal Sciences
Principal Investigator and primary author of the final report

Samuel J. Bentley, Sr., Ph.D., Professor, Department of Geology and Geophysics
Co-Principal Investigator, coring, radionuclide, grain size and core logging

Chunyan Li, Ph.D., Professor, Department of Oceanography and Coastal Sciences
Co-Principal Investigator, hydrodynamics, 3-D modeling

Nazanin Chaichitehrani, Ph.D. student, Department of Oceanography and Coastal Sciences
3-D modeling study, advised by Li;

Jeffrey Obelcz, Ph.D. student, Department of Oceanography and Coastal Sciences,
Geophysical study, advised by Xu;

Meg O'Connor, M.S. student, LSU Department of Geology and Geophysics
Coring and radiochemistry study, advised by Bentley;

Patrick Robichaux, M.S. student, Department of Oceanography and Coastal Sciences
Geophysical study, advised by Xu;

Jiaze Wang, Ph.D. student, Department of Oceanography and Coastal Sciences,
Tripod BBL study, advised by Xu.

Based on our group effort, there are six published peer-review papers: Wang et al. (2018), Obelcz et al. (2018), Chaichitehrani et al. (2019), Robichaux et al. (2020), Liu et al. (2020) and Xu et al. (2021).

2. Field and Lab Methods and Results

2.1 Methods

All ADCP and geophysical (bathymetry, sidescan ,and subbottom) data acquisitions were performed at the same time aboard the LSU Coastal Studies Institute R/V *Coastal Profiler*, a 41 ft Lafitte skiff designed for conducting geophysical surveys and geologic sampling in Louisiana's estuaries and on the shallow coastal shelf. About three to four times of water depth (~10 m) were used as the survey line spacings which are about 30–40 m in three dredge pits.

2.1.1 Vessel-based Hydrodynamic Survey

The purpose of the ADCP study is to capture ***spatial*** variation of 3-D flow surrounding the pits. ADCP survey at Sandy Point was done using an ADCP on May 20, 2015 from 10:26 to 20:34, covering the dredged pit with repeated transects in the west-east and north-south directions. There were a total of 23 east-west transects, and the length of these lines are about ~ 1,746 m. There were a total of 15 north-south transects, and the length of these lines are about ~ 3,210 m.

The vessel-based survey at the Raccoon Island dredge pit was done on June 1, 2015 from 09:24 to 14:58, covering the pit with repeated transects. There were a total of 25 east-east transects, and the length of these transect lines are about ~ 1,457 m. There were a total of 5 north-south transects, and the length of these transects are about ~ 2,775 m.

The vessel survey at the Peveto Channel dredge pit was done on June 6, 2016 from 10:19 to 18:57 and on June 8, 2016 from 8:25 to 16:32. For the June 6 survey, there were a total of 31 east-west transects. For the June 8 survey, there were a total of 11 west-east transects with a total length of ~ 2,218 m. There were a total of 5 north-south transects totaling ~ 2,440 m.

2.1.2 Tripod Study

The above vessel-based surveys provide great spatial coverage but only last for 10s hours in fair weather conditions. They are short in time and do not provide a continuous time series of the variations. In order to get continuous data, bottom tripod-mounted sensors were deployed to collect hourly data for the study of *temporal* variations. Multiple acoustic and optical instruments are used in this study, including an optical backscatter sensor (OBS), an acoustic backscatter sensor (ABS), an acoustic Doppler velocimeter (ADV), an acoustic Doppler current profiler (ADCP), and a pulse-coherent acoustic Doppler profiler (PC-ADP). Two tripods, made by the Field Support Group of Coastal Studies Institute of LSU, were used for the mounting of acoustic and optical sensors.

In summer 2015, two tripods were deployed outside (station T1) and inside (station T2) of the Sandy Point dredge pit to study the hydrodynamics and sediment dynamics on the seabed around the pit. Station T1 has a water depth of 9.4 m; T2 is located at a 20 m water depth inside the pit. Three sensors, including OBS 3A, ADV Ocean, and one wave gauge, were deployed at station T1. However, due to a battery problem, the OBS3A did not work during the observation period. Inside the pit at station T2, the OBS 5+, wave gauge, and ADCP were mounted on the tripod. Table 1 shows all of the sensors and sample parameters for the deployments at stations T1 and T2.

Figure 8. Pictures of a tripod deployed at station T2 in Sandy Point dredge pit.

Left is before deployment and right is after retrieval.

Table 1. Sampling parameters of tripods near Sandy Point dredge pit

cmab is centimeter above bed

Station	Sensor	Sample Rate (burst interval/duration)	Sensor Height above bed (cmab)	Observation period
T1 (Out pit)	Wave Gauge	10 Hz (1200s/60min)	69 cmab	7/15/2015–8/21/2015
	ADV Ocean	1 Hz (1024s/60min)	48 cmab	
T2 (In pit)	OBS 5+	1 Hz (60s/60min)	97 cmab	
	Wave Gauge	10 Hz (1200s/60min)	90 cmab	
	ADCP	60min /0.5 m bin size	120 cmab	

In summer 2016, one tripod was deployed outside the Raccoon Island dredge pit at station R1 in a water depth of about 8.5 m. Multiple sensors were deployed: Table 2 lists sensors and their parameters.

The following paragraphs describe the methods used in ADV and ADCP data processing. The ADV current data were de-spiked before analyzing the currents (Goring and Nikora 2002; Wahl 2002). The toolbox developed by Karimpour (2015) was used to process the pressure data for waves, with correction of water depth effect. Wave-current combined shear stress near the bottom was calculated by the turbulent kinetic energy (TKE) method (Kim et al. 2002; Soulsby and Dyer 1981). Turbidity was calculated in a mixing chamber in a lab at LSU using "local" sediment collected next to the tripods to get the suspended sediment concentration.

ADCP data collected at station T2 inside the Sandy Point pit provide information for a harmonic and spectrum analysis to determine different flow constituents in the summer time in this area within the dredged pit. Our methods of analysis include: 1) visualization of the horizontal velocity measured by ADCP on the research vessel at various levels below the surface; 2) harmonic analysis of the tidal water level variations and tidal currents; 3) spectrum analysis of the tides and tidal velocity components; 4) low pass filtering of the time series data; and 5) coherence analysis of the low pass filtered flow velocity vectors.

Table 2. Settings and parameters of optical and acoustic sensors used near Raccoon Island dredge pit

T is temperature, S is salinity, Vel is velocity, and P is pressure. mab is meter above bed. From Xu et al. 2021.

Sensor	Provider	Orientation	Measuring Parameters (partial list)	Measuring Elevations (mab)	Sampling Interval (min)	Sampling Duration (min)
OBS3A	Campbell Scientific, USA	side looking	T, S, P and Turbidity	0.67	15	1
OBS5	Campbell Scientific, USA	side looking	Turbidity	0.35	15	1
ADV Ocean 5MHz	Sontek, xylem	downward looking	T, Vel and P	0.77	60	20
Wave Gauge OSSI-010-003C, 10Hz	Ocean Sensor Systems, USA	downward looking	T and P	0.50	60	20
ABS AQUAscat 1000R	Aquatec, UK	downward looking	Turbidity	0 - 1.08, with 0.01 m bin size	60	20
Up ADCP, Sentinel 1200 kHz	Teledyne RD Instruments	upward looking	T, Vel and Wave	1.33 - sea surface, with 0.5 m bin size	60	20
Down ADCP, Sentinel 1200 kHz	Teledyne RD Instruments	downward looking	T and Vel	0.53, with 0.5 m bin size	60	20
CSI06 ADCP, Sentinel 600 kHz	Teledyne RD Instruments	upward looking	T, Vel and Wave	5.13 - sea surface, with 1 m bin size	60	20

For the harmonic analysis, it is aimed at the tidal components mainly focused on the eight tidal constituents, i.e. the M2, S2, N2, K1, O1, S1, M1, and P1 tides. The harmonic analysis for the time series is expressed as (Li et al. 2000; Li 2002):

$$v_r = v_0 + \sum_{i=1}^{M} A_i \cos(\omega_i t - \varphi_i) = v_0 + \sum_{i=1}^{M} [a_i \cos(\omega_i t) + b_i \sin(\omega_i t)] \quad (1)$$

in which M is the total number of tidal constituents selected (in our case M=8); ω_i the i'th frequency among eight selected, (a_i, b_i) the cosine and sine coefficients; i an integer between 1 and M; A_i, φ_i are the amplitudes and phase of the i'th tidal constituents; and t is time. For each scalar (either the water level or any component of a velocity vector), the time series forms a column vector V of length N (total number of observations) and Eq. (1) can be expressed in a matrix form

$$V = Ax \quad (2)$$

in which x is the vector of the coefficients of Eq. (1):

$$x = (v_0, x_1, x_2, x_3, \dots, , x_{2M})^T \quad (3)$$

where $x_{2k-1} = a_k$, $x_{2k} = b_k, k = 1,2, \dots, M$, and T in Eq. (3) is a transpose of the row vector to a column vector. A in Eq. (2) is a matrix of the sine and cosine base functions dependent on the selected tidal constituents:

$$A = \begin{bmatrix} 1 & a_{1,1} & a_{1,2} & \cdots & a_{1,2M} \\ 1 & a_{2,1} & a_{2,2} & \cdots & a_{2,2M} \\ \vdots & \vdots & \vdots & \vdots & \vdots \\ 1 & a_{N,1} & a_{N,2} & \cdots & a_{N,2M} \end{bmatrix} \qquad (4)$$

In the above matrix, the elements are all the sine and cosine base functions defined by

$$a_{i,2k-1} = \cos(\omega_k t_i)\,, a_{i,2k} = \sin(\omega_k t_i) \qquad (5)$$

(i indicates the i'th observation, $k = 1,2,\ldots,M;\ i = 1,2,\ldots,N$)
The observed water level or velocity time series vector is simply

$$V = (v_1, v_2, \ldots, v_N)^T \qquad (6)$$

In matrix format, the harmonic coefficients can be shown to have the following format as the statistical solution:

$$\hat{x} = (A^T A)^{-1} A^T V \qquad (7)$$

We used this method to obtain the statistical estimate of the tidal amplitudes and phase for the eight selected diurnal and semi-diurnal tidal constituents.

The low pass filtering was done using an infinite impulse response (IIR) filter with a cut off frequency of 0.6 cycle per day which is equivalent to a 40-hour filter. The filter is implemented with a convolution in time domain which was applied twice (forward and backward) so that the phase shift is eliminated. This is applied to all the data.

The spectrum analysis and coherence analysis were based on commonly accepted theories (e.g., Bendat and Piersol, 2000). The coherence as a function of frequency *f*, ranging between 0 and 1, defined by

$$\gamma_{xy}^2(f) = \frac{\left|S_{xy}(f)\right|^2}{S_{xx}(f)S_{yy}(f)} \qquad (8)$$

in which *x* and *y* represent two sets of time series, respectively; $S_{xx}(f)$, $S_{yy}(f)$, and $S_{xy}(f)$, are the spectra of x and y, and cross spectrum of x and y, respectively. Here the coherence $\gamma_{xy}^2(f)$ is calculated based on Welch's averaged periodogram method (Bendat and Piersol, 2000).

2.1.3 Geophysical Survey and Data Processing

An Edgetech 4600 interferometric swath bathymetry and sidescan sonar system (Figure 9) was used to collect data with a swath width about three–five times of water depth. This 4600 system produces real-time high-resolution three-dimensional maps of the seafloor while providing co-registered simultaneous sidescan and bathymetric data. Seafloor features, such as pit edges, failure scarps, and bedforms as small as 10–20 cm can be imaged. This Edgetech 4600 was used to collect bathymetry and sidescan data simultaneously using a frequency at 540 kHz. A ship motion control inertial measurement unit (IMU) was used to collect pitch, roll, and yaw data. A Hemisphere™ Vector™ VS330 differential GPS unit was used for geopositioning, and its horizontal and vertical accuracies are 0.3 m and 0.6 m, respectively.

Edgetech 0512i and Edgetech 2000 (Figure 9) DSS systems were used simultaneously for collection of subbottom profiles. The Edgetech 0512i was run at a lower frequency (0.5-4.5 kHz) and produced images with a deep penetration depth of 50 m, while the Edgetech 2000 used a higher frequency (2-15 kHz), producing higher resolution with a shallow penetration depth of ~15m. This also minimized the “cross-talk” of two chirp systems. Edgetech 0512i, 4600, and 2000 systems were used in all three study sites:

Sandy Point, Raccoon Island, and Peveto Channel. In addition, a magnetometer survey was done only in the Peveto Channel dredge pit using a Geometrics G-882 Magnetometer. The primary purpose of including this magnetometer was pipeline detection, as a pipeline had been constructed in the middle of the Peveto Channel pit since a previous survey in 2007.

All geophysical data acquisition was performed aboard the R/V *Coastal Profiler*. The bathymetry and sidescan acquisition device (Edgetech 4600) were pole-mounted and fixed from a bowsprit ahead of the vessel (Figure 9) to mitigate vessel related noise. Sub-bottom profilers were towed off of the port (Edgetech 0512i) and starboard (Edgetech 2000) sides of the vessel about 0.5 m below the water surface around mid-vessel to minimize variations in pitch and roll (Freeman, 2010). The magnetometer was moored to the stern of the vessel and towed ~22.5 m behind the vessel to minimize interference from any metallic objects onboard.

Figure 9a. The bow-mounted Edgetech 4600 swath system on the R/V *Coastal Profiler*

Figure 9b. The Edgetech DSS 2000 system: combined sidescan sonar and sub-bottom profiler

Bathymetric data from all the surveys were processed using Caris HIPS and SIPS. Processing began with automatic filtering (including swath width and depth filters) to remove the majority of noise data. Manual cleaning was then used to further remove spurious data. These datasets were corrected for sound velocity artifacts (using the closest sound velocity profiler casts in time and space), and tidal corrections and vertical referencing were derived from mean sea level of the NOAA tidal stations. Hourly water level data of Southwest Pass, Grand Isle, and Calcasieu Pass were used for the Sandy Point, Raccoon Island, and Peveto Channel dredge pits, respectively. Digital elevation models (DEMs) were then constructed from point clouds using the CUBE (combined uncertainty and bathymetry estimator) algorithm. The DEMs were referenced to mean water level of the NAVD88 vertical datum. DEMs were exported from Caris and imported at 1 m^2 resolution into Esri ArcGIS™ for further analysis and interpretation. All morphometric analyses (cut and fill, cross sections, measurements, surface differencing) were done in ArcGIS™. Multiple maps were regirded using Kriging interpolation method using Golden Software® Surfer®.

To acquire an estimate of uncertainty for the difference of depths (DoDs), the “fixed reference uncertainty” was calculated, following the methods detailed in Schimel et al. (2015). The general premise behind this method is to use a “reference area” that is assumed to be relatively stable between two surveys to acquire a statistical estimate of the DEMs’ vertical uncertainty. For this study, the seafloor >100 m away from the dredge pits was used as a reference area. Values were extracted from the reference area, and statistical parameters were calculated. A 2σ (95% confidence interval for normally distributed data) value was used as the uncertainty range (e.g., 0.2 m for the Sandy Point pit); i.e., values within two standard deviations of 0 m were considered within the range of uncertainty and therefore not interpreted as actual change.

To spatially quantify slope change, the sharpest gradient breaks between the ambient seafloor and the pit floor at pit walls were studied. Uncertainty of slope derived from a DEM is largely a function of terrain complexity and DEM resolution. An empirically derived formula from Tang et al. (2003) was used to quantify the slope uncertainty of each DEM.

Sidescan mosaics for Peveto Channel were constructed in Caris HIPS and SIPS. SonarWiz was used for the sidescan processing for Sandy Point and Raccoon Island dredge pits. During the mosaic generation in SonarWiz, the “cover up” method was used to lay the user-selected high quality layers on tops of the others whereas the “shine-through” method was used to merge multiple layers.

Chirp subbottom profiles were processed using the SioSeis software package. Original JSF formatted files were converted to full-waveform SEG-Y files, which were then swell filtered, trace mixed, and deconvolved. These files were then loaded into a Kingdom Suite, a seismic and geological interpretation software (IHS 2016). Thicknesses of layer of interest (e.g., high turbidity layer in the Sand Point dredge pit) were extracted from the subbottom profiles and the isopach of the layer was generated using Kriging interpolation method in Golden Surfer. The magnetometer data collected in Peveto Channel were cleaned, processed, and interpolated using Magpick software provided by Geometrics.

2.1.4 Sediment Core Sampling

Multicores and vibracores were collected during two separate 2015 cruises on the R/V *Coastal Profiler*, one to Sandy Point (SP, July 14–15, 2015) and one to Raccoon Island (RI, July 21–22, 2015). Cores were collected from 4 sites within the SP pit (SP1, SP2, SP3, and SP5) and four sites within the RI pit (RI1, RI2, RI3, RI4). Two cores (one outside each pit) were also collected from outside the pits on adjacent seafloor (SP4 and RI5).

A submersible vibracorer with electric motor was used to collect cores up to about 5 m long (Figure 10). The 5 m long vibracore aluminum barrel had a 7.5 cm internal diameter. The aluminum core was attached to the electric vibrating head, allowing the vibracore to liquefy sediment and penetrate more deeply. Although compaction can occur in vibracores, stratigraphy remains intact and vibracores are complemented the relatively undisturbed, but shorter, multicores. After collection, the vibracores were cut into 1.5 m sections on deck to facilitate both transport and analysis.

An Ocean Instruments MC-400 multicorer (Figure 10) was used to collect four cores of up to 50 cm depth and 10 cm diameter per site. One of these cores was extruded into 2 cm sections on deck for radiochemical and grain size analyses. A lateral slice was removed from the second replicate core to transfer on deck into a 2 cm thick translucent plastic tray with a sliding lid for future x-radiography of undisturbed sedimentary structures. The remaining samples were archived in plastic tubes for future study. After being transported to a lab at LSU, all multicore samples and subsamples were refrigerated in a 4˚ C cold room.

Samples for grain-size analysis were dispersed in 0.05% sodium phosphate solution, then agitated with an ultrasonic probe, and pre-sieved at 850 um to remove large particles that might interfere with the instrument. The pretreated samples were analyzed on LS 13 320 Beckman-Coulter Laser Diffraction Particle Size Analyzer (0.04–2000 um). The loss-on-ignition (LOI) analysis was done in the muffle furnace. Samples were dried at 60^0C to a constant weight, and then grounded to powder. About 1.00 g sample was weighed in crucible and heated for two hours at 550 ^{0}C. Multiple sea surface water samples were filtered with the 0.7 um fabric filters to get the total suspended solids (TSS).

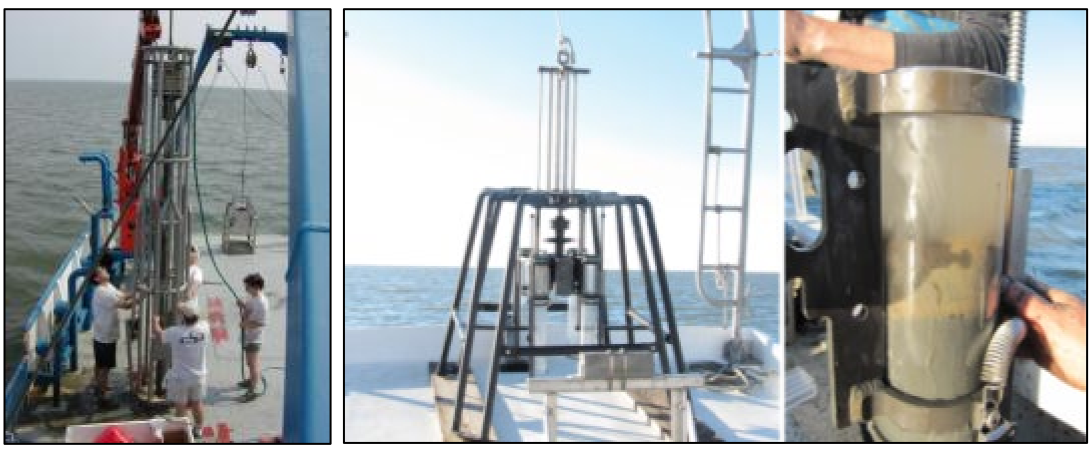

Figure 10. The submersible vibracorer (left), multicorer (middle), and an example of a multicore (right)

2.1.5 Lab Methods and Data Analyses

With aluminum core liners still intact, whole-core gamma ray density and p-wave velocity in each vibracore at 1 cm intervals were analyzed using a Geotek MSCL-S multi-sensor core logger. Data were used to produce sediment density and porosity profiles. Each vibracore was split lengthwise with a circular saw to produce two halves exhibiting clear stratigraphy. A Geotek Geoscan core logger was used to capture high-resolution imagery of one half of the split vibracore, which was used to produce lithologic logs for up to 5 m of core.

The multicore samples from SP and RI were dehydrated overnight at 100^0C to determine water content from gravimetric analysis. The dried samples were ground into a fine powder with a mortar and a pestle, then packed and sealed into petri dishes. The petri dishes of dried sediment were analyzed for 12–24 hours each on Canberra BEGe, LEGe, and REGe low-background planar gamma detectors to look for the penetration depth of ^{7}Be. ^{7}Be activity can be recognized by its signature of a 477 keV spectral line. The half-life $T_{1/2}$ of ^{7}Be is ~53 days and the detectors can identify about 1–3 half-lives of ^{7}Be, leading to time constraints that necessitated prioritizing identification of each multicore's ^{7}Be penetration depth rather than full profile collection. The unit used for radionuclide activity is a decay-per-minute-per-gram of dry sediment, or dpm/g.

Using the software SigmaPlot, depth profiles were generated to show ^{7}Be activity plotted against depth for each core with a regression analysis to calculate the sediment accumulation rate using the following equation for a one-dimensional steady state model from Muhammad et al. (2008):

$$A_z=A_0\, e^{(-\lambda/S)}$$

In this equation, A_z is the activity at depth z, A_0 is the activity at surface (depth 0), λ is the decay constant, or ($\ln(2)/T_{1/2}$), and $T_{1/2}$ is half-life. The equation is solved for S, or the sedimentation rate in the unit of cm/day (Muhammad et al. 2008).

X-radiographs of the multicore replicates were captured using a Thales Flashscan 35 digital x-ray detector, illuminated by a Medison Acoma portable x-ray unit operating at 60 keV and between 3.7 and 5.4 mA. These images were equalized and adjusted to an appropriate level of brightness and contrast using the software ImageJ, and Adobe® Photoshop® was used for subsequent editing.

2.2 Results

2.2.1 Vessel-based Hydrodynamics Study

The vessel-based ADCP measurements were done continuously as the vessel moved along a predefined route, consisting lines in the east-west and north-south directions. This type of survey was performed at the Sandy Point, Raccoon Island, and Peveto Channel dredge pits.

The flow velocity at the Sandy Point dredge pit shows a strong southeastward and southward flow field on the surface. The bottom flow was weak. Figures 11–13 show the composite horizontal flow velocity at 2, 6, and 11 m below the sea surface, respectively. It is apparent that the flow at 2 m below surface was the strongest; the flow at 6 m below the surface was weaker but essentially having the same overall characteristics; while the flow at 11 m below the surface is dramatically different: it was much weaker. The top layer of the flow is above the pit and that should have a thickness of ~ 10 m. Below this layer, the water inside the pit was sluggish and therefore had much reduced flow and less defined direction of the flow. It would not have similarity with the surface layer flows.

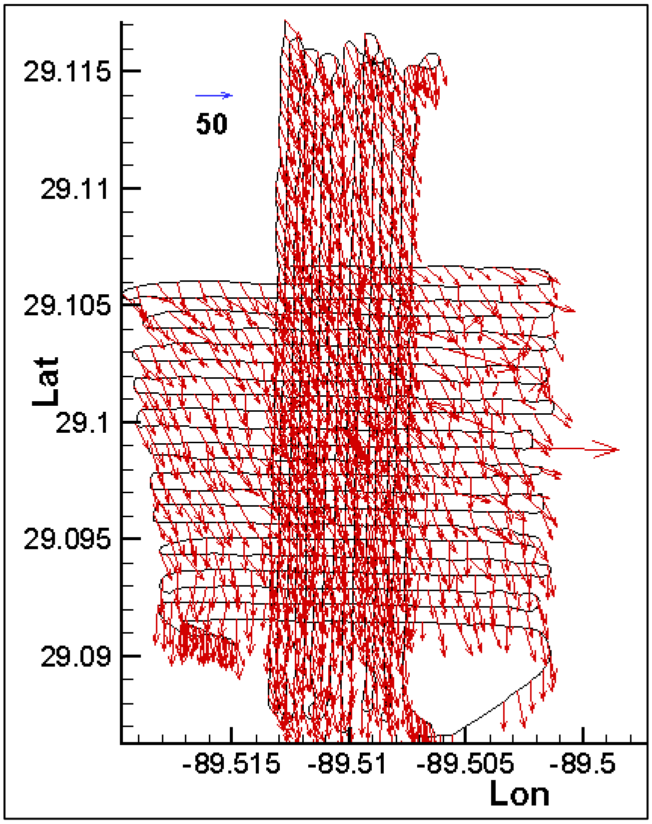

Figure 11. Subsurface flow velocity at about 2 m below the sea surface at the Sandy Point dredge pit on May 20, 2015

The scale of 50 cm/s is shown at the upper left. The black lines are the ship track. The coordinates use latitude and longitude in degrees.

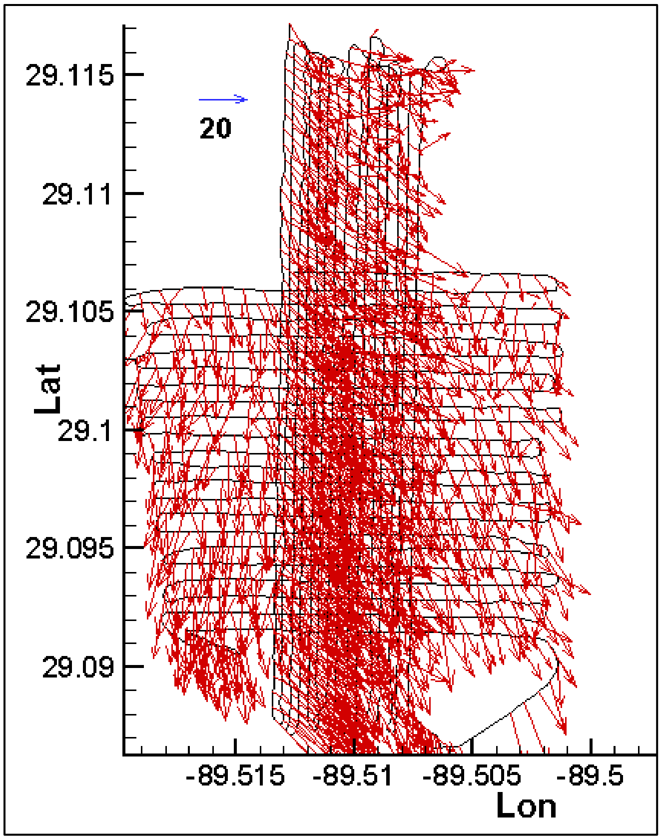

Figure 12. Subsurface flow velocity at about 6 m below the sea surface at the Sandy Point dredge pit on May 20, 2015

The scale of 20 cm/s is shown at the upper left. The black lines are the ship track. The coordinates use latitude and longitude in degrees.

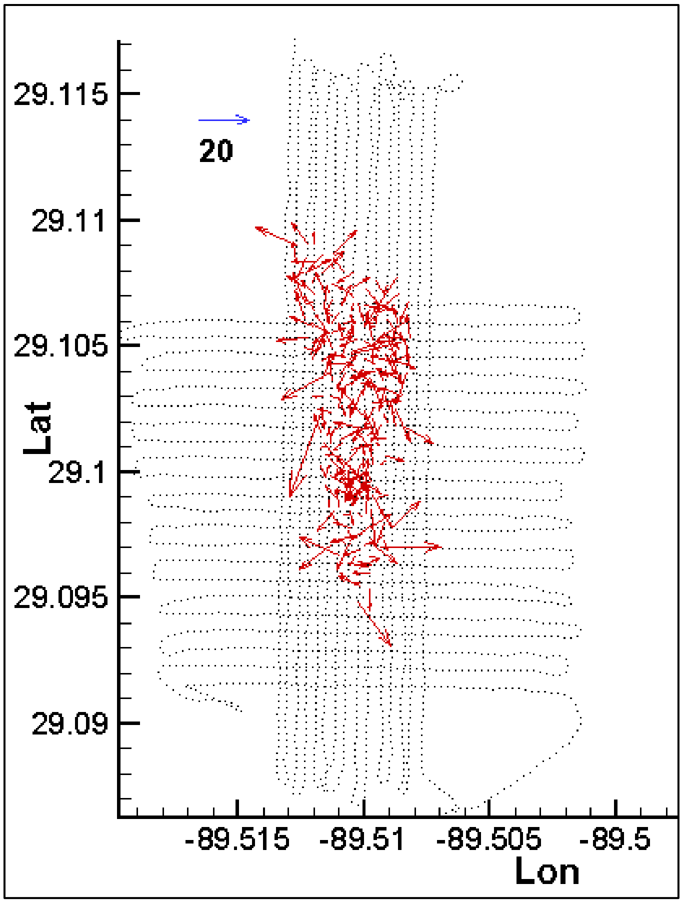

Figure 13. Subsurface flow velocity at about 11 m below the sea surface at the Sandy Point dredge pit on May 20, 2015

The scale of 20 cm/s is shown at the upper left. The black dotted lines are the ship track. The coordinates use latitude and longitude in degrees.

The ADCP flow field over the Raccoon Island site was similar to that of Sandy Point except that the surface layer had a westward flow. The velocity magnitude was also smaller. Figures 14 and 15 show the flow field at the Raccoon Island site 1 m and 7 m below the sea surface, respectively. The surface flow is westward-northwestward, with a magnitude less than that observed at Sandy Point. The lower-level flow field showed less directionality and some increased randomness of the data.

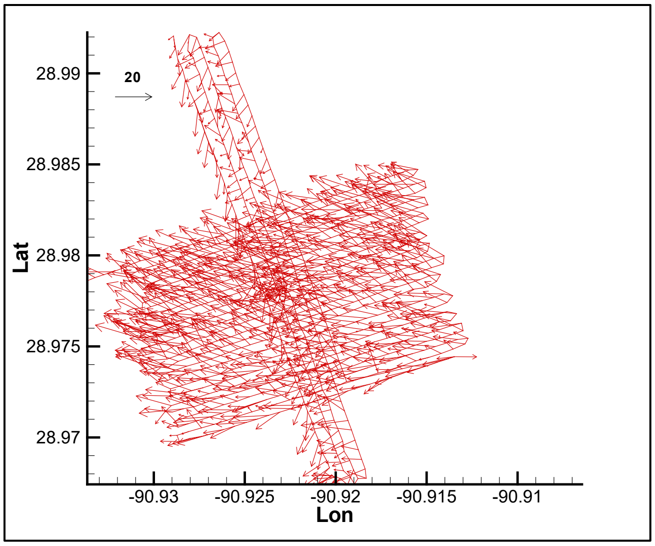

Figure 14. Subsurface flow velocity at about 1 m below the sea surface at the Raccoon Island dredge pit on June 1, 2015

The scale of 20 cm/s is shown at the upper left. The red lines are the ship track. The coordinates use latitude and longitude in degrees.

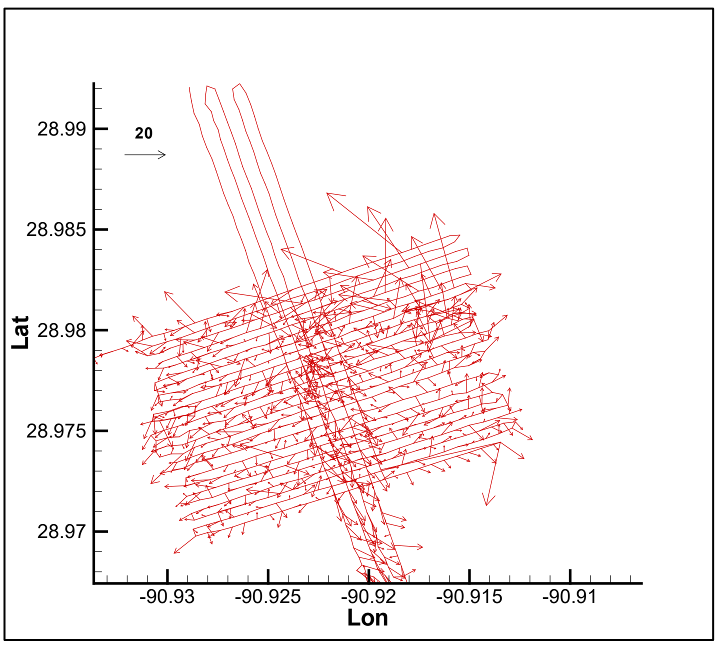

Figure 15. Subsurface flow velocity at about 7 m below the sea surface at the Raccoon Island dredge pit on June 1, 2015

The scale of 20 cm/s is shown at the upper left. The red lines are the ship track. The coordinates use latitude and longitude in degrees.

The flow field at the Peveto Channel dredge pit also showed similar characteristics. The survey over here was done on June 6 and 8, 2016. Figures 16 and 18 are the surface flows (1 m below surface) that had predominantly westward-northwestward flows; Figure 17 shows the flow at ~ 6 m below the surface, with mostly southward flows.

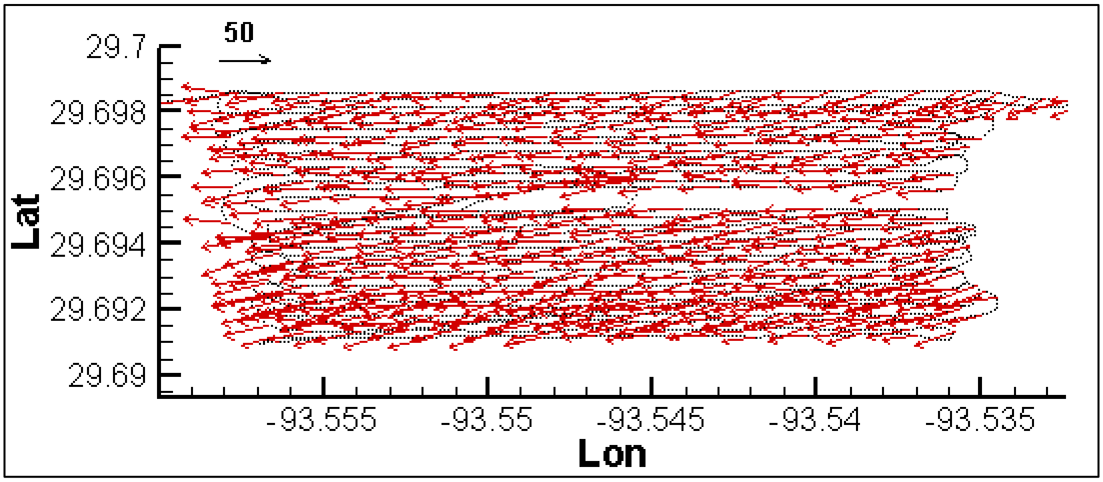

Figure 16. Subsurface flow velocity at about 1 m below the surface at the Peveto Channel dredge pit on June 6, 2016

The scale of 50 cm/s is shown at the upper left. The dotted black lines are the ship track. The coordinates use latitude and longitude in degrees.

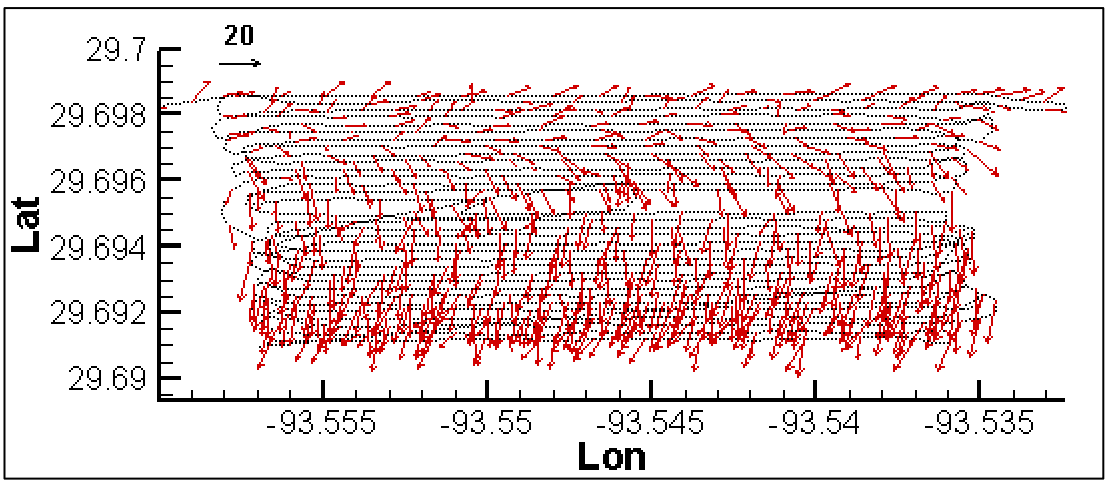

Figure 17. Subsurface flow velocity at about 6 m below the surface at the Peveto Channel dredge pit on June 6, 2016

The scale of 20 cm/s is shown at the upper left. The dotted black lines are the ship track. The coordinates use latitude and longitude in degrees.

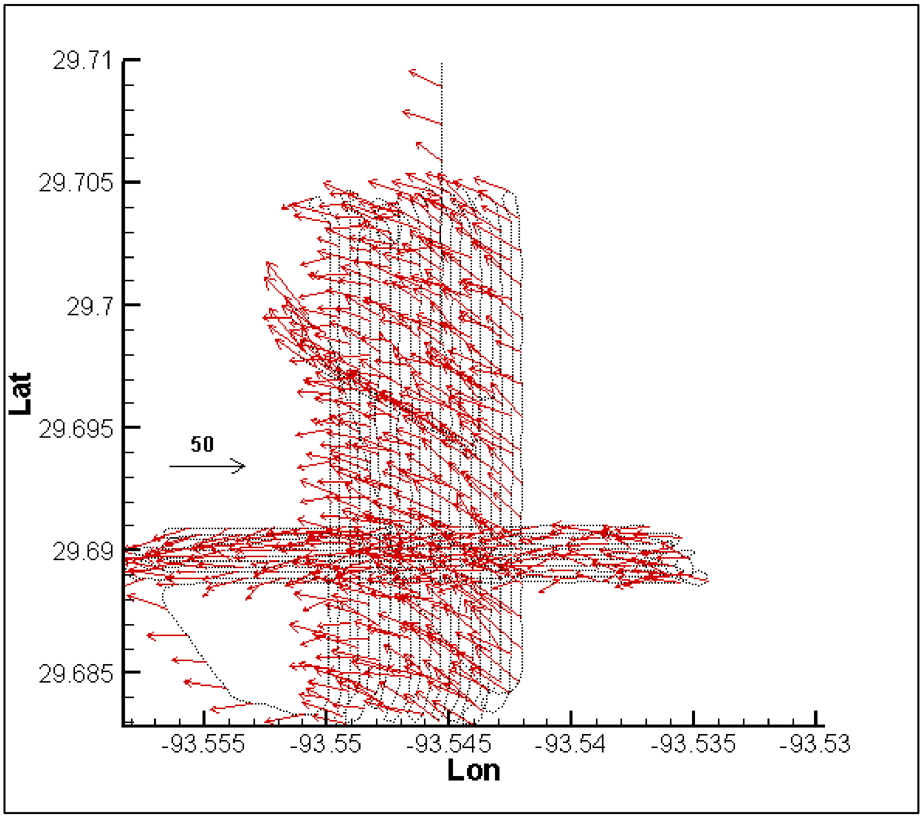

Figure 18. Subsurface flow velocity at about 1 m below the surface at the Peveto Channel dredge pit on June 8, 2016

The scale of 50 cm/s is shown at the upper left. The dotted black lines are the ship track. The coordinates use latitude and longitude in degrees.

2.2.2 Tripod

A. The Sandy Point Dredge Pit

Figure 19 shows the locations of two tripod stations deployed outside (T1) and inside (T2) the Sandy Point southeast dredge pit. Multiple analyses were performed on the data collected using the tripod-mounted ADCP in station T2, including harmonic, spectrum, low-pass filtering, and coherent analyses.

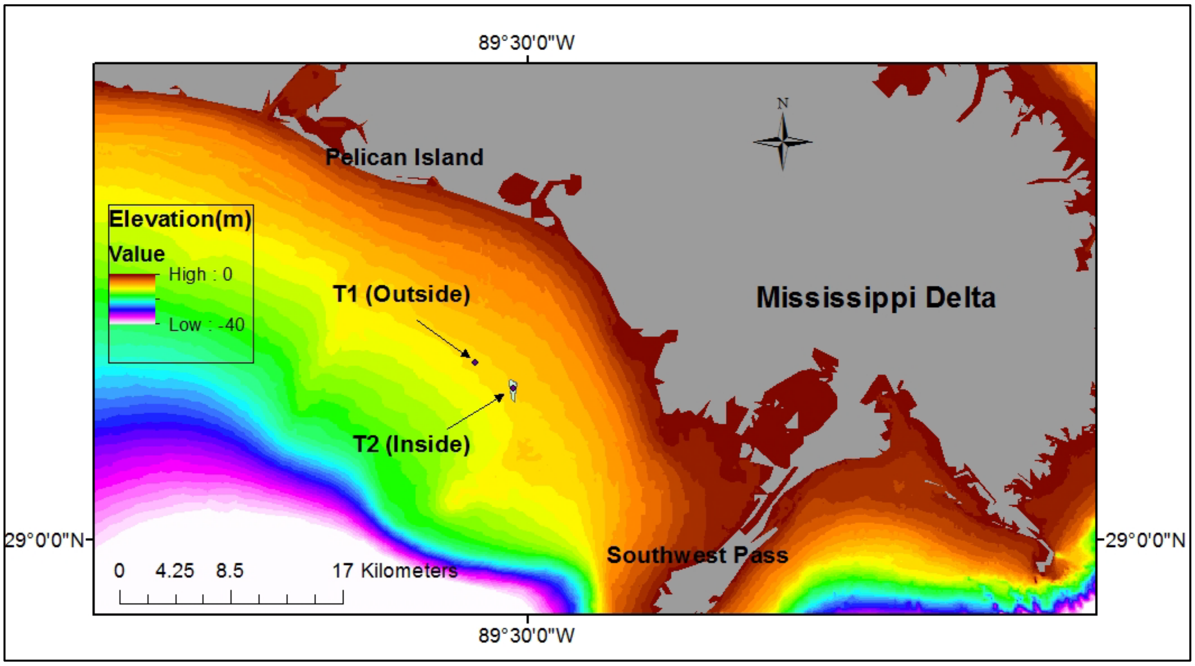

Figure 19. Location of the Sandy Point dredge pit, two deployments sites

T1(outside) and T2(inside), and restoration site at Pelican Island.

Harmonic Analysis

The harmonic analysis for the pressure or water level (Figures 20 and 21) using the eight tidal constituents showed a quite reliable fit between the reconstructed water level signal and the observed data. The harmonic constants thus confirmed that the dominant tidal constituents are diurnal and the semi-diurnal constituents are much smaller in magnitude (Figure 21). Among the diurnal tidal components, three of them (K1, S1, P1) are significant, but the other two (O1, M1) are almost negligible.

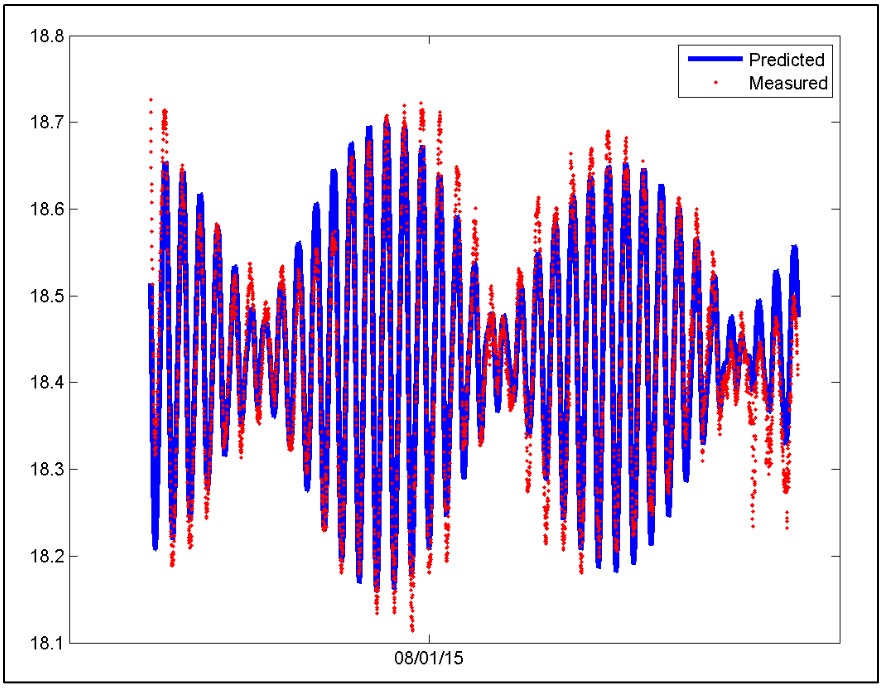

Figure 20. Bottom mounted ADCP water level time series data (red dots) and harmonic analysis regression (blue line) at station T2 inside the Sandy Point dredge pit in summer 2015

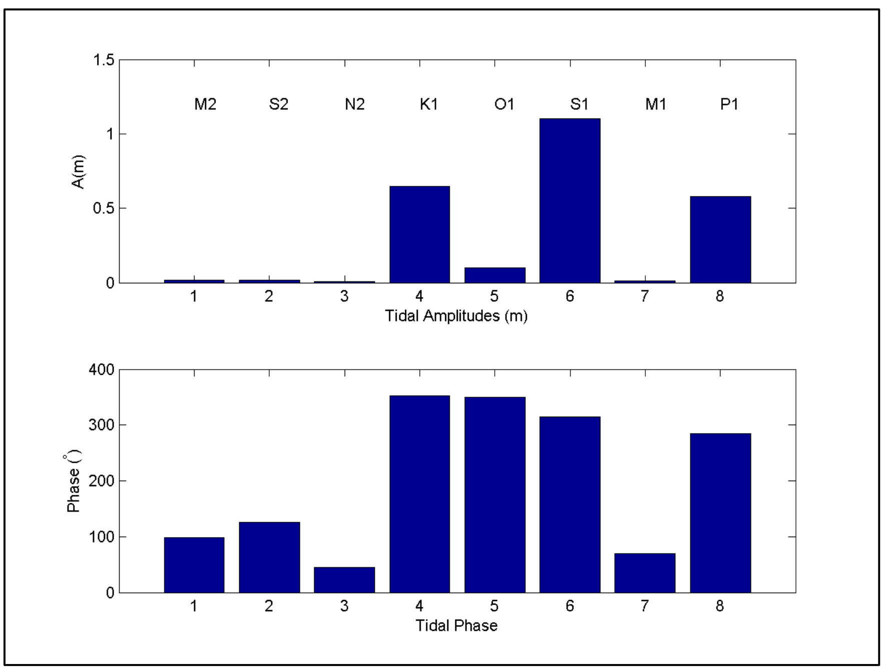

Figure 21. Harmonic coefficients for the M2, S2, N2, K1, O1, S1, M1, and P1 tides at station T2 inside the Sandy Point dredge pit in summer 2015

Upper panel: amplitude in meters; lower panel: phase in degrees.

Spectrum (Fourier Transform)

The water level spectrum shows clearly tidal constituents at diurnal and semi-diurnal bands (Figure 22). It is obvious that the semi-diurnal tidal constituents are much smaller than the diurnal constituents. The spectra velocity components (Figure 23) also show the tidal constituents but are obscured by significant noise in the data, partly because of the nonlinear nature of the hydrodynamics in this environment. There are additional over-tides and near-tide frequencies from the dynamical processes. These frequencies, with a unit of cycle per day (CPD), are listed in the following two matrices.

$$f_{m,n}^{(1)} = \begin{bmatrix} 3.8645 & 3.9323 & 3.8283 & 2.9350 & 2.8618 & 2.9323 & 2.8987 & \mathbf{2.9295} \\ - & 4.0000 & 3.8960 & 3.0027 & \mathbf{2.9295} & 3.0000 & 2.9664 & 2.9973 \\ - & - & 3.7920 & 2.8987 & 2.8255 & 2.8960 & 2.8624 & 2.8932 \\ - & - & - & 2.0055 & 1.9323 & 2.0027 & 1.9692 & \mathbf{2.0000} \\ - & - & - & - & 1.8591 & 1.9295 & 1.8960 & 1.9268 \\ - & - & - & - & - & \mathbf{2.0000} & 1.9664 & 1.9973 \\ - & - & - & - & - & - & 1.9329 & 1.9637 \\ - & - & - & - & - & - & - & 1.9945 \end{bmatrix} \quad (9)$$

Here there are two pairs of duplicate frequencies ($f_{2,5}^{(1)}$ and $f_{1,8}^{(1)}$) and ($f_{6,6}^{(1)}$ and $f_{4,8}^{(1)}$) as highlighted with bold.

$$f_{m,n}^{(2)} = \begin{bmatrix} - & \mathbf{0.0677} & \mathbf{0.0363} & \mathbf{0.9295} & \mathbf{1.0027} & 0.9323 & 0.9658 & 0.9350 \\ - & - & 0.1040 & 0.9973 & 1.0705 & 1.0000 & 1.0336 & \mathbf{1.0027} \\ - & - & - & 0.8932 & 0.9664 & 0.8960 & \mathbf{0.9295} & 0.8987 \\ - & - & - & - & 0.0732 & \mathbf{0.0027} & \mathbf{0.0363} & 0.0055 \\ - & - & - & - & - & 0.0705 & 0.0369 & \mathbf{0.0677} \\ - & - & - & - & - & - & 0.0336 & \mathbf{0.0027} \\ - & - & - & - & - & - & - & 0.0308 \\ - & - & - & - & - & - & - & - \end{bmatrix} \quad (10)$$

Here there are five pairs of duplicate frequencies ($f_{1,5}^{(2)}$ and $f_{2,8}^{(2)}$, $f_{1,4}^{(2)}$ and $f_{3,7}^{(2)}$,$f_{1,3}^{(2)}$ and $f_{4,7}^{(2)}$, $f_{1,2}^{(2)}$ and $f_{5,8}^{(2)}$, $f_{4,6}^{(2)}$ and $f_{6,8}^{(2)}$) as highlighted with bold fonts. With eight major tidal frequencies, without considering the effect of the nonlinear bottom friction effect, the nonlinearity from the advective acceleration, and that from the continuity would introduce 57 new frequencies (Eqn. 9 and 10). Most of these are concentrated around diurnal, semidiurnal and over tidal bands. The process in the Sandy Point pit is complicated and many more frequencies are added, especially for the flow field.

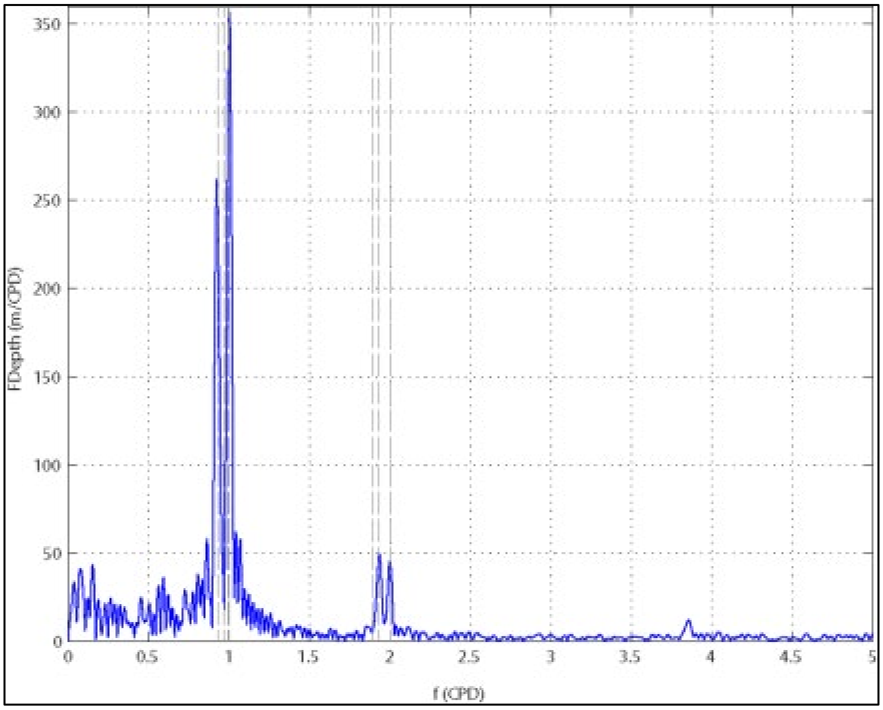

Figure 22. Fast Fourier Transform result showing the spectrum of water level at station T2 inside the Sandy Point dredge pit in summer 2015

The vertical dashed lines indicate the frequency of the eight tidal constituents (the M2, S2, N2, K1, O1, S1, M1, and P1 tides). CPD, cycles per day.

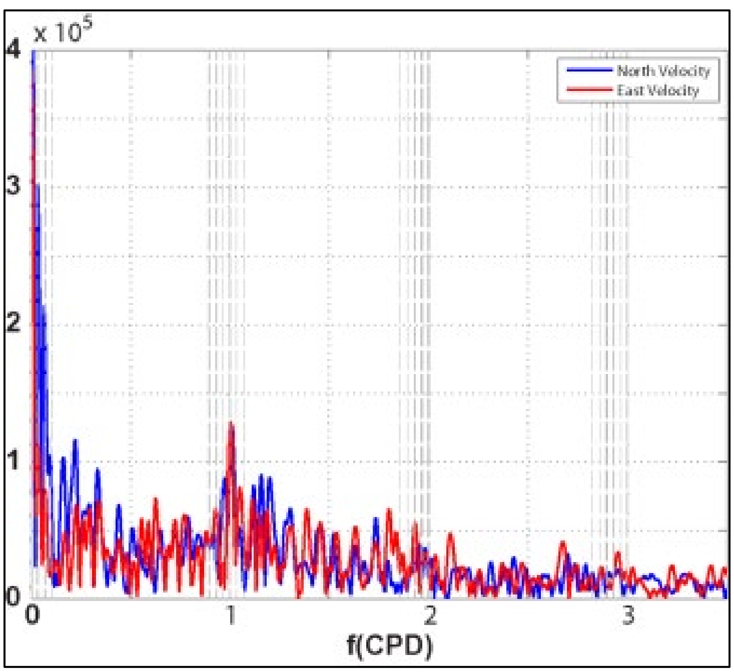

Figure 23. Fast Fourier Transform result showing the spectrum of the north and east velocity components at station T2 inside the Sandy Point dredge pit in summer 2015

The vertical dashed lines indicate eight tidal constituents (the M2, S2, N2, K1, O1, S1, M1, and P1 tides) plus added frequencies due to nonlinearity and low frequency tides. CPD, cycles per day.

Low-pass filtered flows

With the double filtering using an infinite impulse response filter with a cut-off frequency of 40 hours, the low-pass filtered flow components for both shore-parallel and shore-normal velocity components are demonstrated to have mostly positive shore-parallel flows (Figure 24). Here shore-parallel is defined as the southeast orientation along the western Mississippi Delta shoreline nearest to station T2 (Figure 19). The vertical structure shows a clear two-layered character with an upper layer of stronger flow regime and a bottom stagnant layer (Figs 25 and 26). The thickness of the top layer is obviously less than 10 m. This is consistent with the vessel-based measurements but with a much-detailed time series over a month.

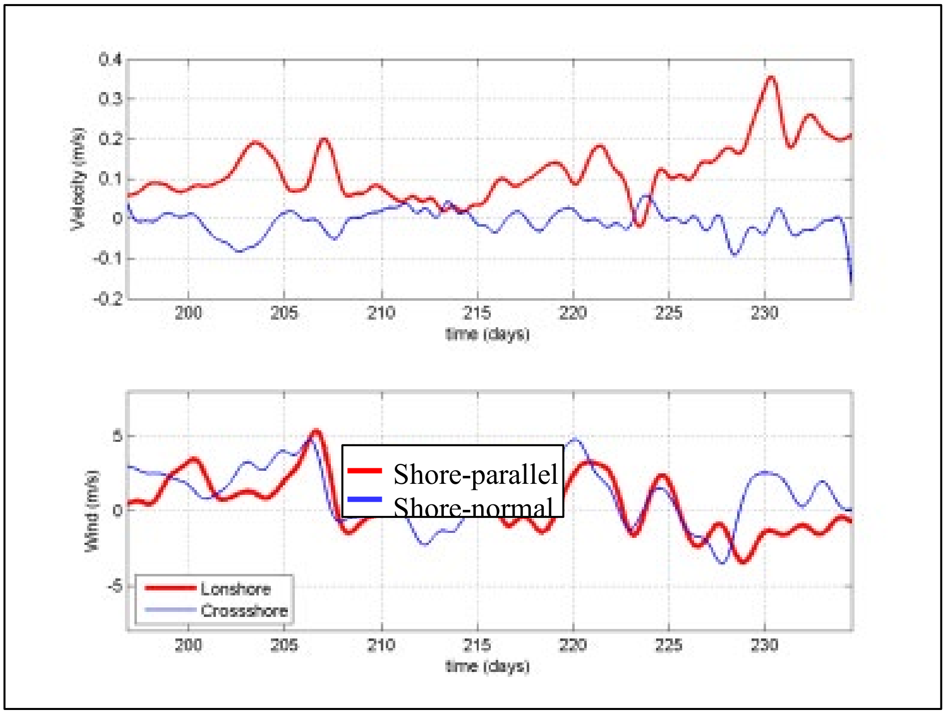

Figure 24. Low pass filtered flow velocity (upper panel) at station T2 inside the Sandy Point dredge pit in summer 2015 and wind components (lower panel)

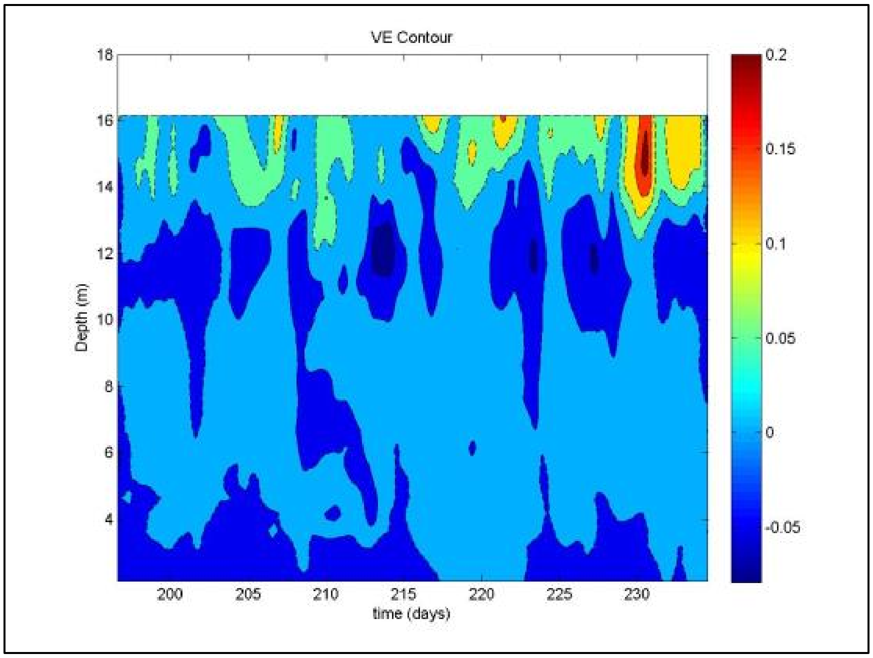

Figure 25. Low pass filtered east velocity (VE) vertical structure time series at station T2 inside the Sandy Point dredge pit in summer 2015

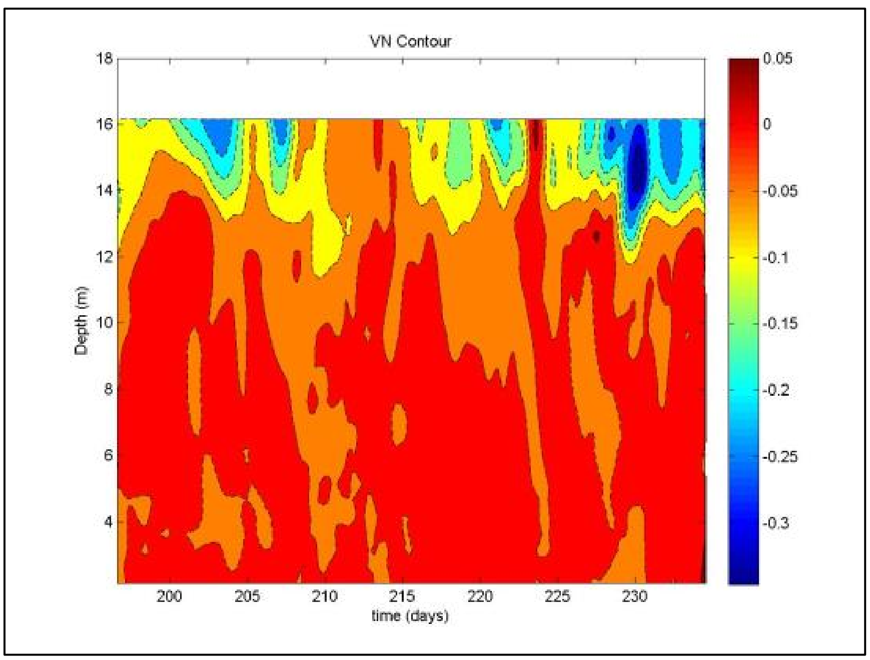

Figure 26. Low pass filtered north velocity (VN) vertical structure time series at station T2 inside the Sandy Point dredge pit in summer 2015

Coherence analysis

The magnitude squared coherence (MSC) between the shore-parallel wind and shore-parallel current, and that between the shore-normal wind and shore-parallel current (Figure 27) shows some differences. The former has relatively higher values at higher frequency band and the latter has relatively higher values at lower frequencies.

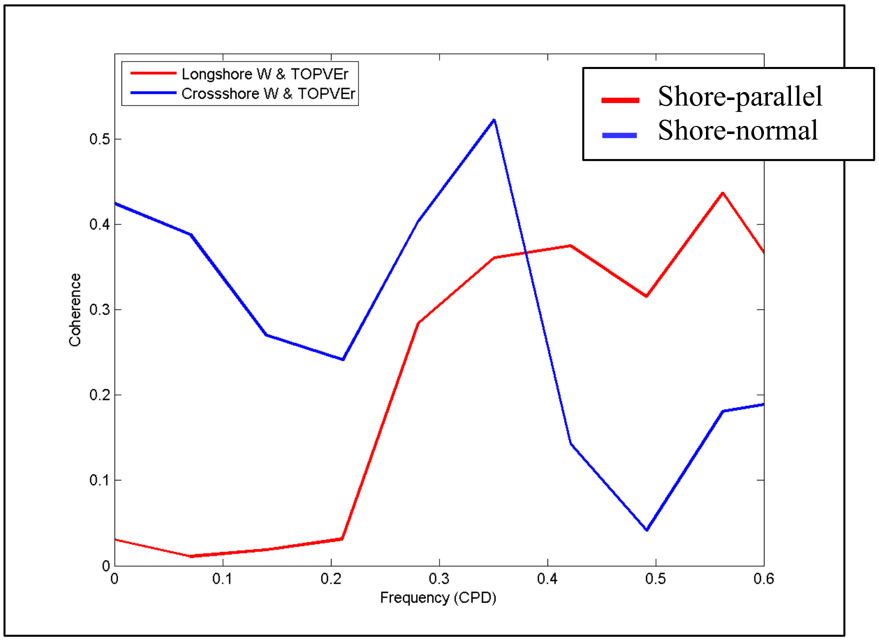

Figure 27. Coherence for shore-parallel wind with southeast flow (red) and that for shore-normal wind with the southeast flow (blue) at station T2 inside the Sandy Point dredge pit in summer 2015

In summer 2015 BBL data were collected at station T1 outside the Sandy Point dredge pit (Figure 19) and they were compared with river and wind data from nearby locations. The river discharge at Belle Chasse, Louisiana was declining during July-August 2015 (Figure 28A). The wind speeds at East Pilot Station, Louisiana were higher than 3 m/s most of the time during the deployment period, with no dominant wind directions (Figure 28B). The wave heights at station T1 were as high as 0.8 m during the observation period (Figure 28C). Wave heights generally are related to the wind speed, fetch (related to wind direction), and duration. It seems that wave heights did not correlate well with the wind speeds (Figs. 28B &C). The discrepancies between the wave heights and wind speeds are probably caused by the wind directions, which could influence the fetch greatly at this location. The currents were generally less than 8 cm/s and southward (between 90 and 270 degrees from north) during the observation (Figure 28D). The shear velocities at station T1 outside the Sandy Point dredge pit caused by the waves and currents were around 1 cm/s, and went up to 3 cm/s when the wave heights increased to 0.8 m (Figure 28E).

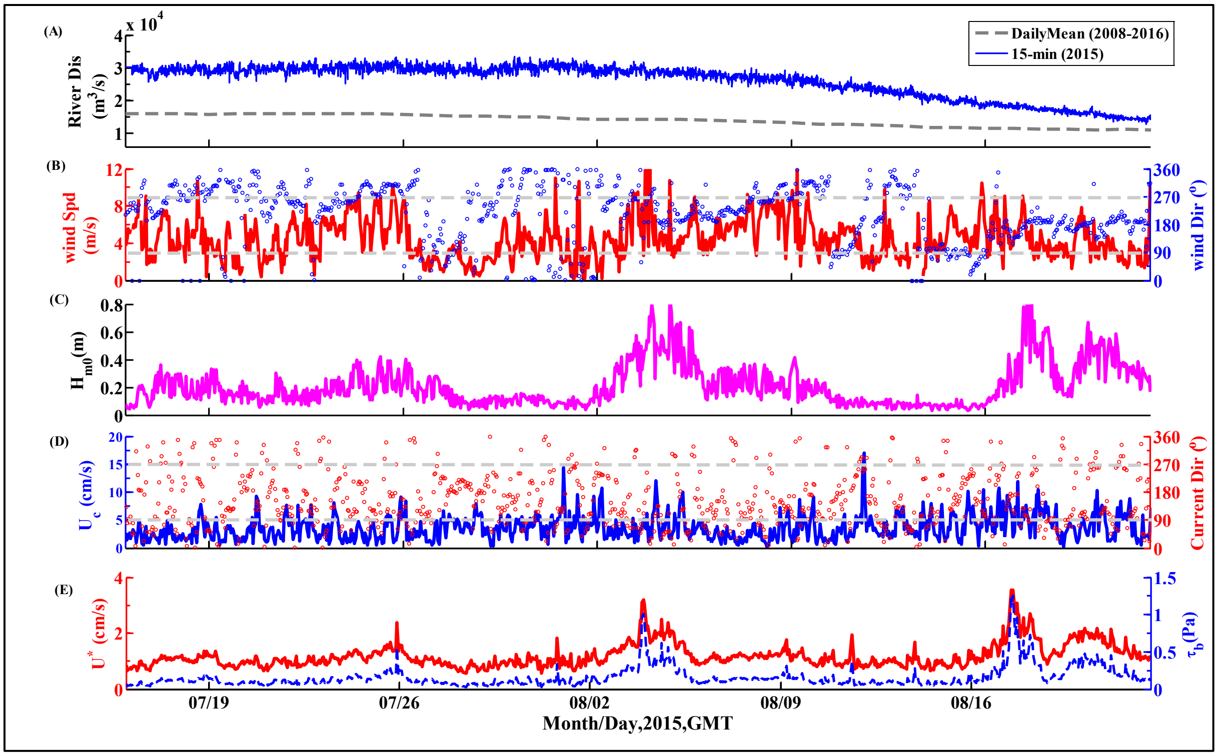

Figure 28. (A) River discharge at USGS station, Belle Chasse, Louisiana: daily mean is from 2008 to 2016; (B) Hourly wind data from NOAA East Pilot Station, Louisiana.

Dashed light grey lines separate the northerly and southerly winds. Time series results at station T1 outside Sandy Point dredge pit in summer 2015: (C) Zero moment wave heights; (D) Current speeds and directions: the dashed light grey lines indicate the northern and southern directions domain; (E) Near-bed wave-current combined shear velocity (red line) and bed shear stress (blue dashed line). From Wang et al. 2018.

Time series data were also collected at station T2 which is inside the Sandy Point dredge pit (Figure 19). The currents inside the Sandy Point dredge pit are characterized by a two-layer structure (Figure 29). The wave heights at station T2 were much lower than those at T1 station (Figure 29C). One possible reason is that the short period waves could not penetrate into the deep water. Another possible reason is that a high turbidity layer caused wave damping at the pit bottom (Kranenburg, 2008). The sub-bottom seismic data, described later, will show that a 0.5–1 m thick acoustically transparent package overlies the entire pit floor, which is interpreted as a high-turbidity layer. The near bottom suspended sediments concentration was around 4 g/l, with little variations (Figure 29D). This 4 g/L concentration is much higher than the suspended sediment concentration from the Mississippi River plume which is only about 0.1 to 0.3 g/L.

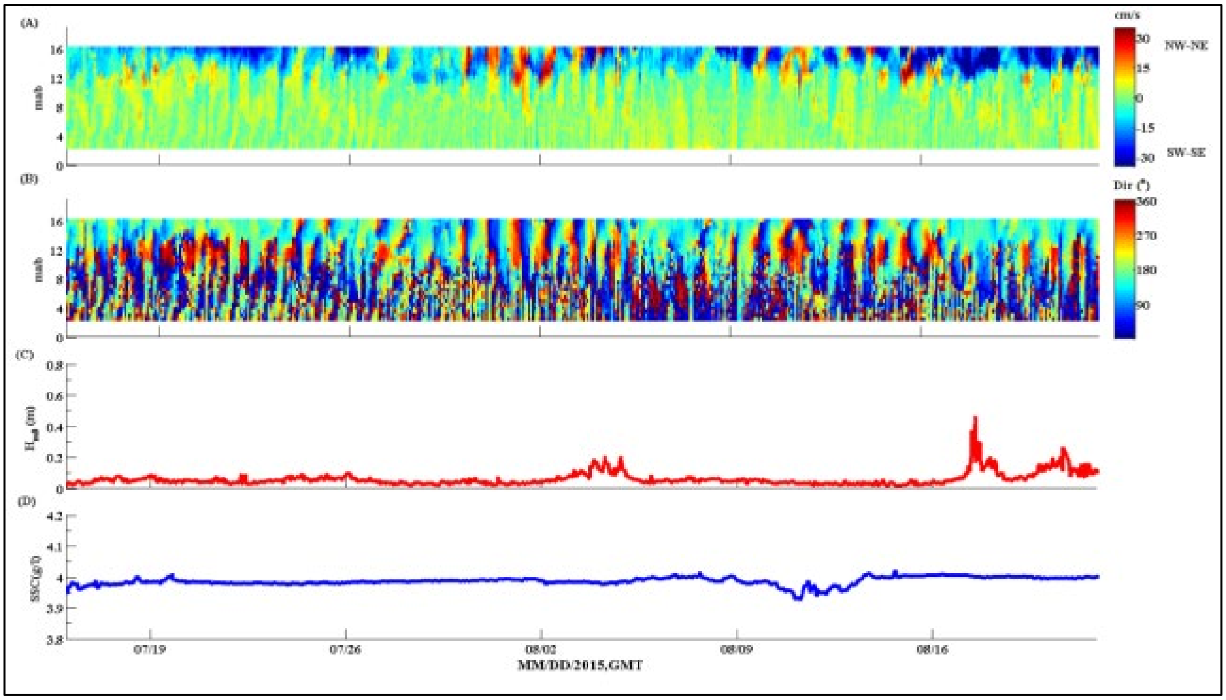

Figure 29. Observational results at station T2 inside Sandy Point dredge pit in summer 2015.

(A) Current speed within the pit; (B) Current direction within the pit; (C) zero moment wave height; (D) Near-bed suspended sediment concentration, calibrated from turbidity data.

During the deployments and retrievals of two tripods at stations T1 and T2, water samples were collected at sea surface and these samples were filtered and dried to calculate total suspended solids (TSS). TSS data were then used in the Nairn et al. (2005) sediment infilling model in Chapter 3 of this report. In addition, grab samples were collected at seabed surface near tripods at stations T1 and T2, and laser diffraction and loss-on-ignition methods were used to analyze these samples. Grab samples were used as "local sediment" in the lab for the calibrations of OBS sensors.

The grab samples collected at seabed surface at station T1 had more sand than those at station T2 (Table 3). However, the organic matter content at T1 was lower than T2. The total suspended solid (TSS) at T1 station showed slight decrease with the river discharge drop from July to August, 2015 (Table 3).

Table. 3 TSS, grain size and organic matter content at station T1 and T2 in the Sandy Point dredge pit

Stations		T1(outside pit)	T2(inside pit)
Grain size	Clay	26.21%	49.85%
	Silt	43.14%	45.84%
	Sand	30.65%	4.31%
Organic Matter Content		5.5%	9.2%
TSS (collection date)		26.2 mg/L (07/15/2015)	14.6 mg/L (07/15/2015)
		20.5 mg/L (08/22/2015)	16.33 mg/L (08/22/2015)

B. The Raccoon Island Dredge Pit

After the tripod work in Sandy Point dredge pit in summer 2015, there was a concern of rapid sediment burial of tripod inside the pit and interference of high-turbidity layer with tripod sensors. Instead of mounting sensors on two separate tripods, we deployed OBS3A, OBS5, ADV, Wave Gauge, ABS, one upward-looking and one downward-looking ADCP on one tripod outside the pit. This tripod was deployed at station R1 which was about 2 km north of Raccoon Island dredge pit (Figure 27). It was tethered to a leg of an oil platform using a pendent line. The sensors were deployed to collect waves, tides, currents, temperature, salinity and turbidity in the BBL. This tripod was deployed on May 23 of 2016 and retrieved on July 28 of 2016, collecting approximately two months of data.

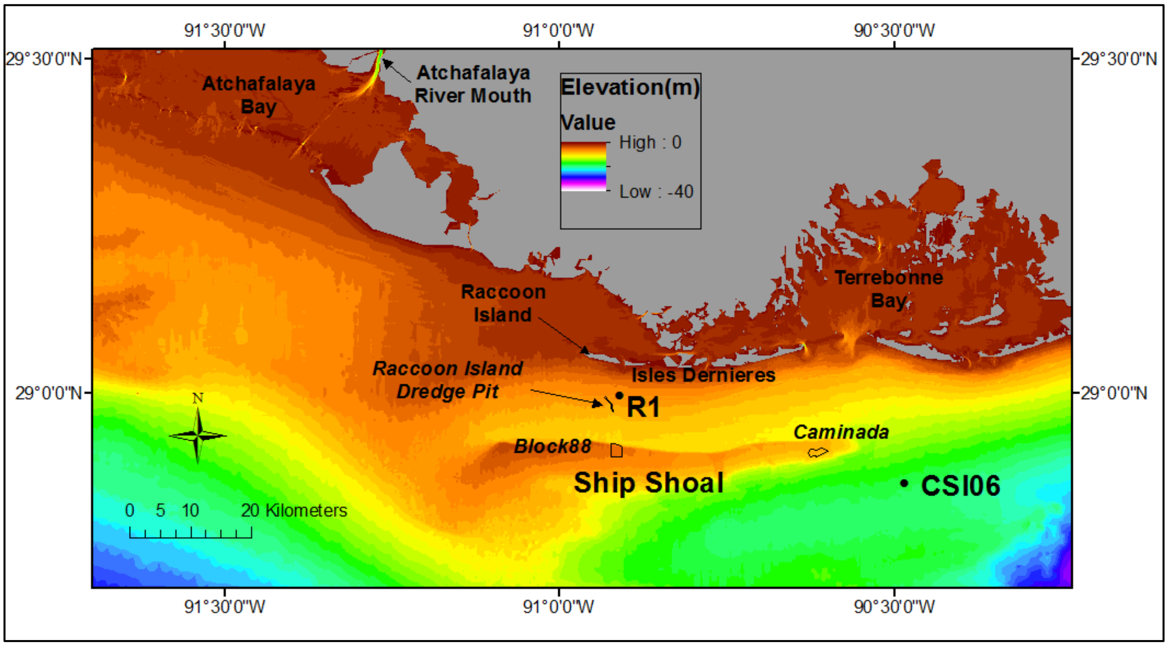

Figure 30. A map showing the location of Raccoon Island dredge pit, tripod station R1, Ship Shoal, and LSU WAVCIS station CSI06.

Beside data collected from R1, we also downloaded wind and ADCP data from LSU WAVCIS (wave-current information system) stations CSI06 which is about 40 km southeast of R1 (Figure 30). It should be noted that CSI06 is southeast of Ship Shoal whereas the Raccoon Island dredge pit and station R1 are north of and so generally sheltered by Ship Shoal.

During summer 2016, wind from CSI06 and wave data from R1 show that winds were somewhat correlated with wave heights and periods (Figure 31); Wave directions from R1 and CSI06 were similar, mainly between 100 and 200 degrees from the north (Figure 31). ADCP current data at R1 show that the velocities near the Raccoon Island dredge pit were mainly eastward and westward, with diurnal tidal velocities up to 50 cm/s; it is clear that easterly winds drove westward currents and vice versa at R1 (Figure 32). ADCP current data at CSI06 show typical diurnal tidal velocities up to 50 cm/s as well (Figure 33). When tidal current directions are compared, there seems to be a strong topographic control of the “trough” between Isles Dernieres and Ship Shoal on the shore-parallel current direction at R1 (Figure 34). In contrast, currents of CSI06 are more variable (Figure 34). Figure 35 shows the sediment concentration proxies collected using OBS3, OBS5, ADV and two ADCPs.

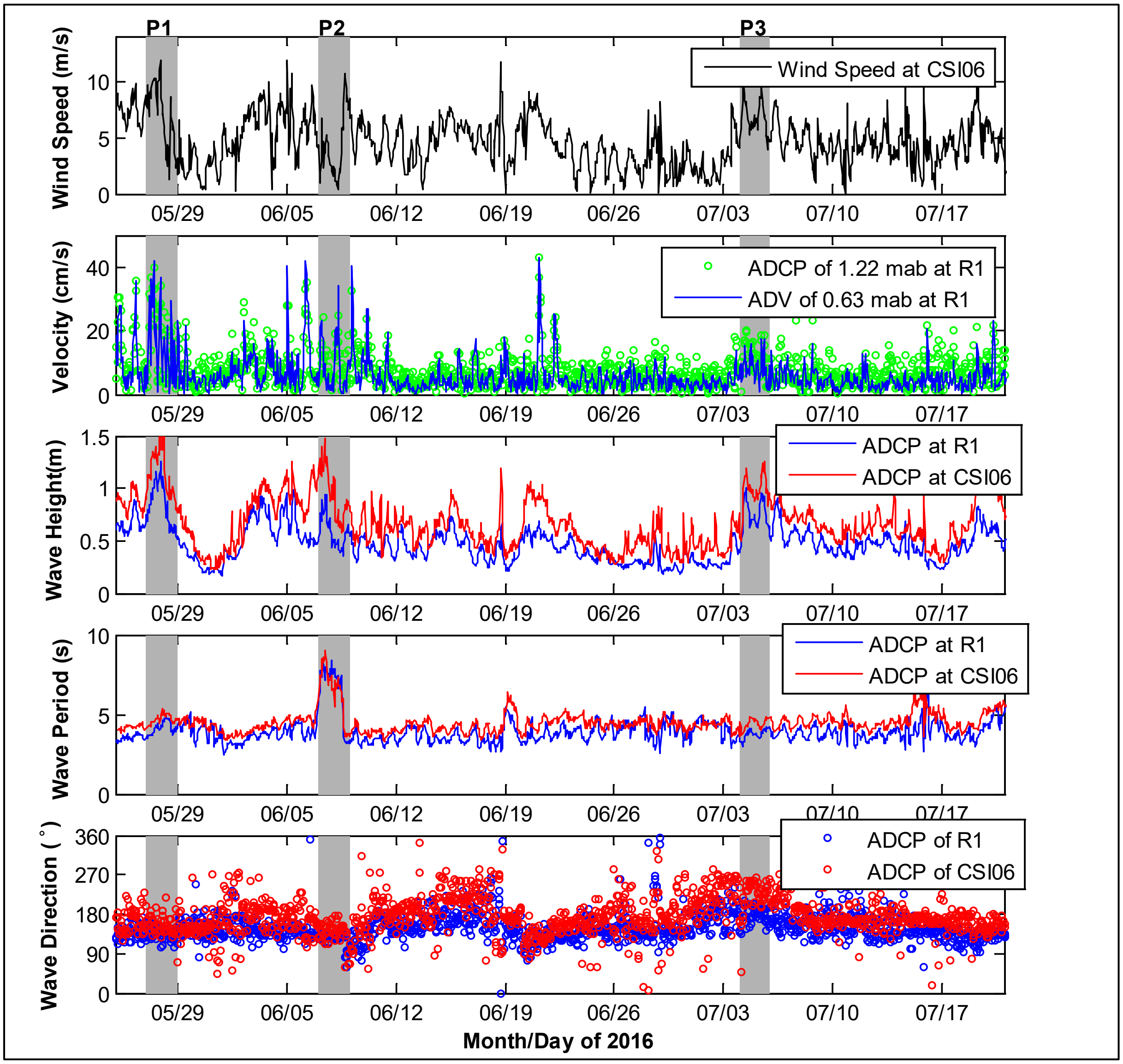

Figure 31. Time series of wind speeds at CSI06, horizontal velocities of ADCP and ADV at different elevations of station R1 north of the Raccoon Island dredge pit, significant wave heights, significant wave periods and directions at both R1 and CSI06.

P1, P2 and P3 are three comparing periods. Mab = meter above bed. See Figure 30 for the locations of tripod and other stations. From Xu et al. 2021.

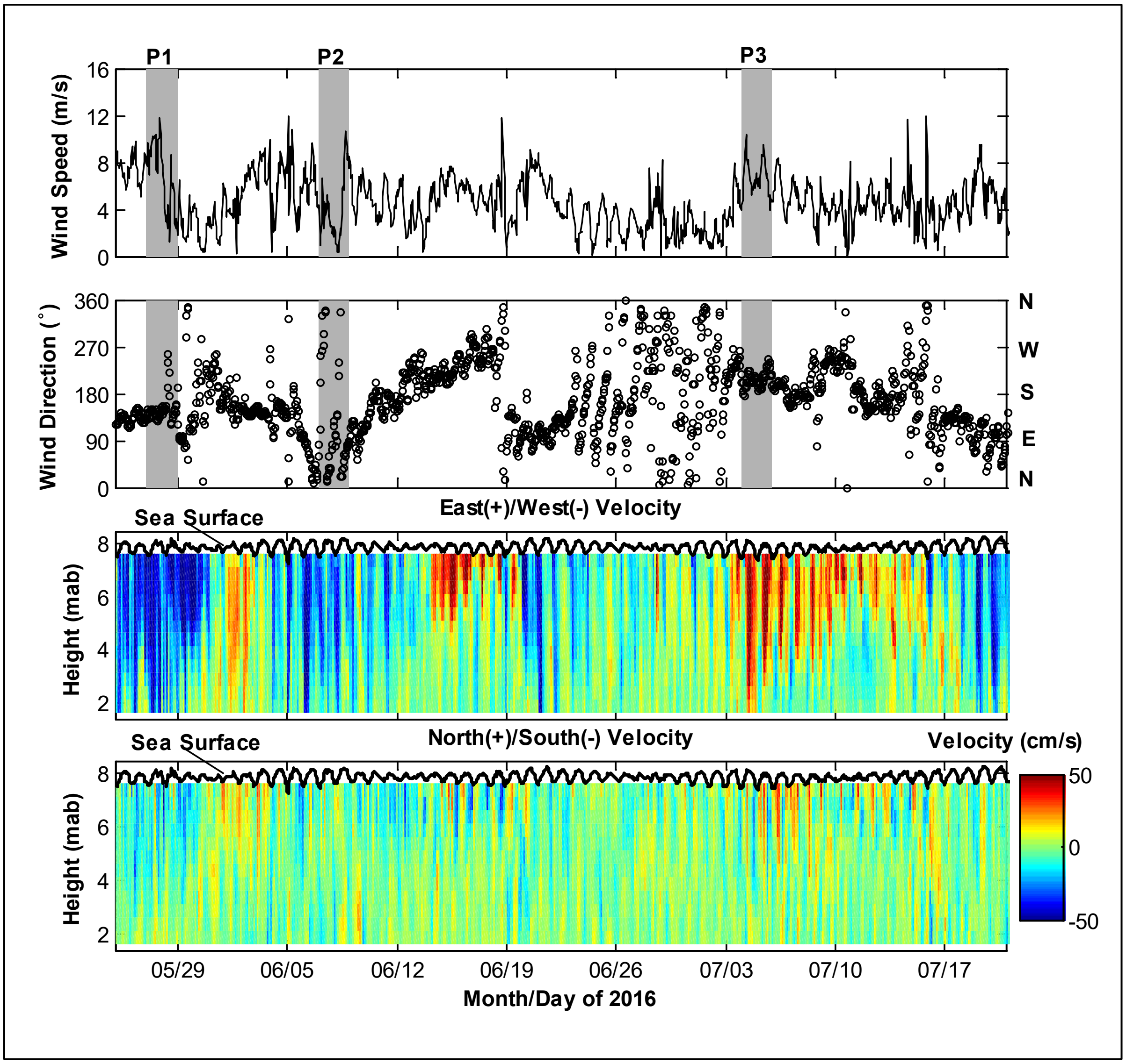

Figure 32. Wind speed and direction at CSI06 and east and north current profiles (m/s) at station R1 north of the Raccoon Island dredge pit.

P1, P2, and P3 are three comparing periods. See Figure 30 for the locations. From Xu et al. 2021.

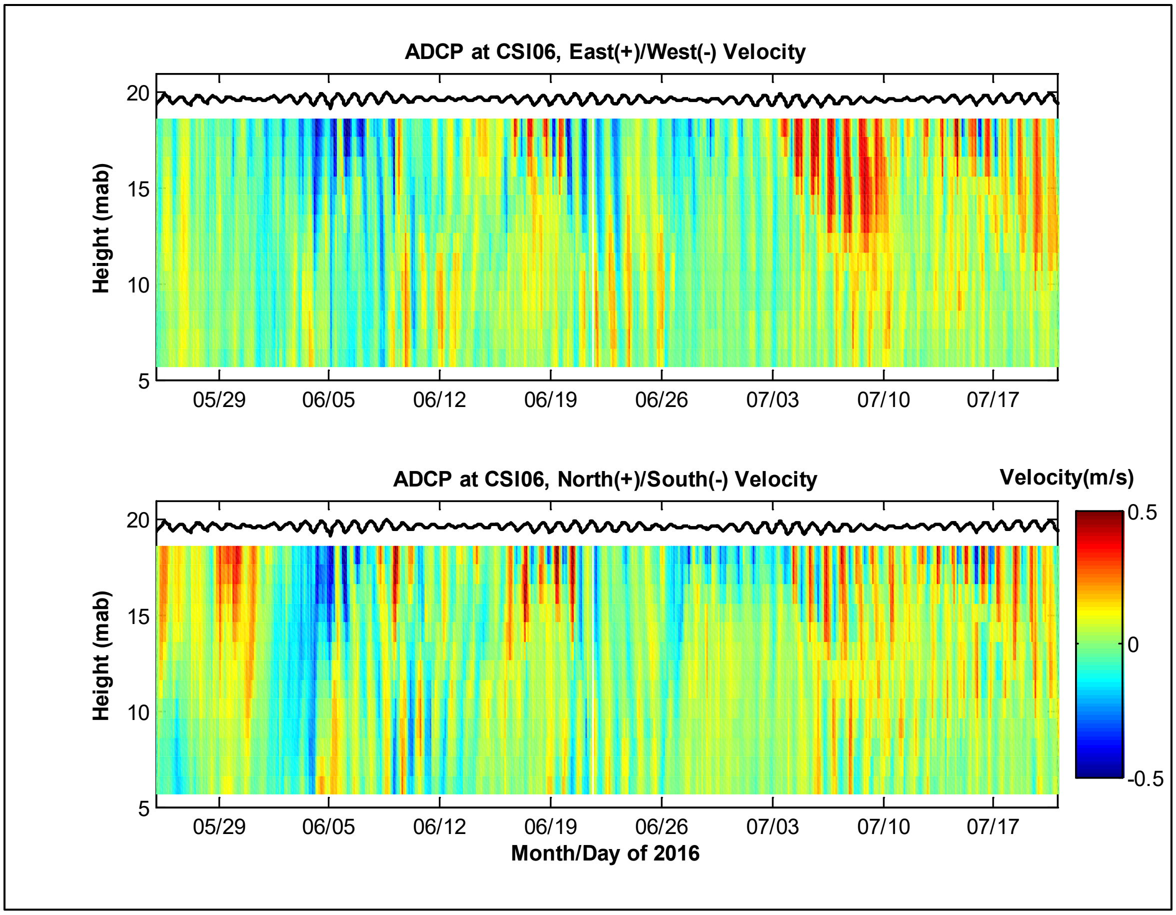

Figure 33. Time series of east(+)/west(-) and north(+)/south(-) velocities from an upward looking ADCP at station CSI06. mab = meters above bed.

From Xu et al. 2021.

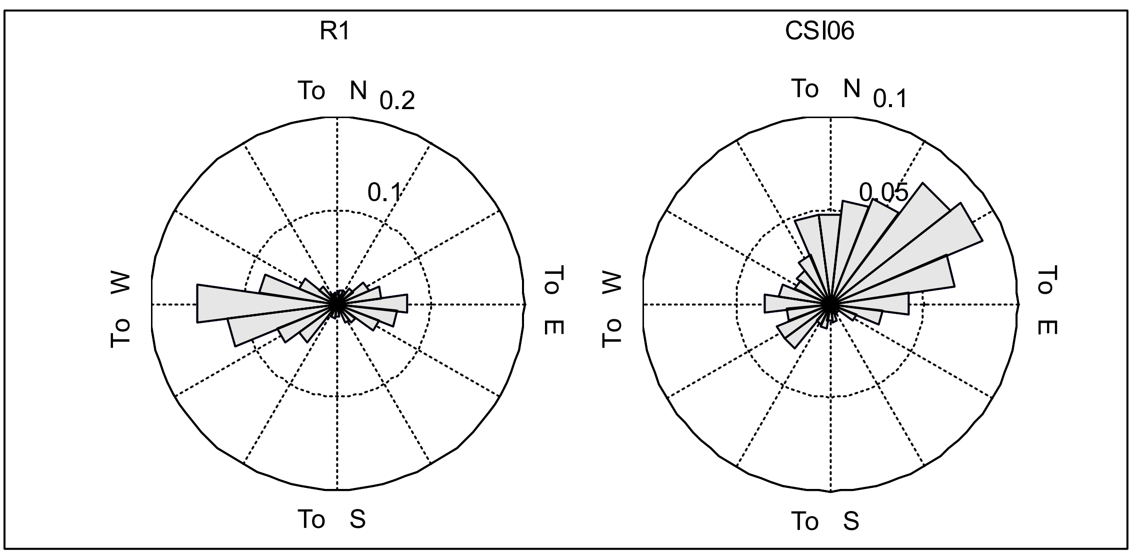

Figure 34. The frequencies of directions of depth-averaged currents in station R1 (north of the Raccoon Island dredge pit) and CSI06 in summer 2016.

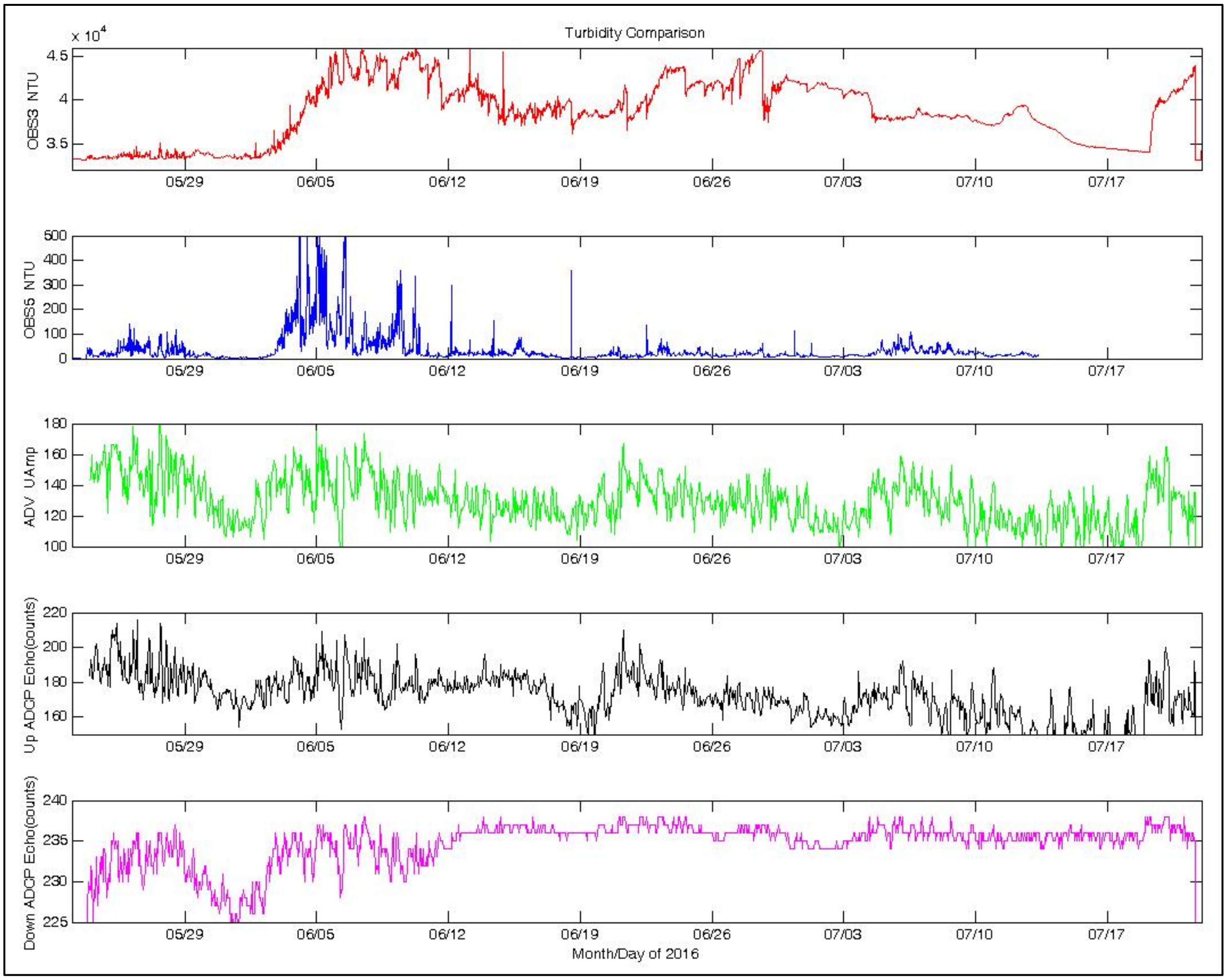

Figure 35. Sediment concentration proxies from OBS3, OBS5, ADV, and two ADCPs at station R1 north of the Raccoon Island dredge pit.

See Figure 30 for the locations.

2.2.3 Geophysical Survey Results

A. The Sandy Point Dredge Pit

Figure 36 shows the bathymetric map of Sandy Point dredge pit. The difference of depth (DoD) between 2012 and 2015 surveys indicates up to ~3 m of sediment vertical accretion in the pit and some localized erosion along the pit walls. The latitudinal and longitudinal bathymetric transects further confirm this type of erosional and depositional pattern (Figure 37). After dredging, the eastern wall of Sandy Point dredge pit is not only steeper than the western wall, but it also maintains the original cut geometry three years after construction (Figure 38). This is different from the western wall, which, since construction, has lost some of its steepness. Volumetric calculations in Table 4 show that about 616,550 ± 87,204 m^3 of total sediment infilling-deposition occurred inside this pit from 2012 to 2015. Comparing with this total infilling sediment, erosional volume from east and west pit walls are only -29,137 ± 9,433 and -19,140 ± 9,924 m^3, respectively.

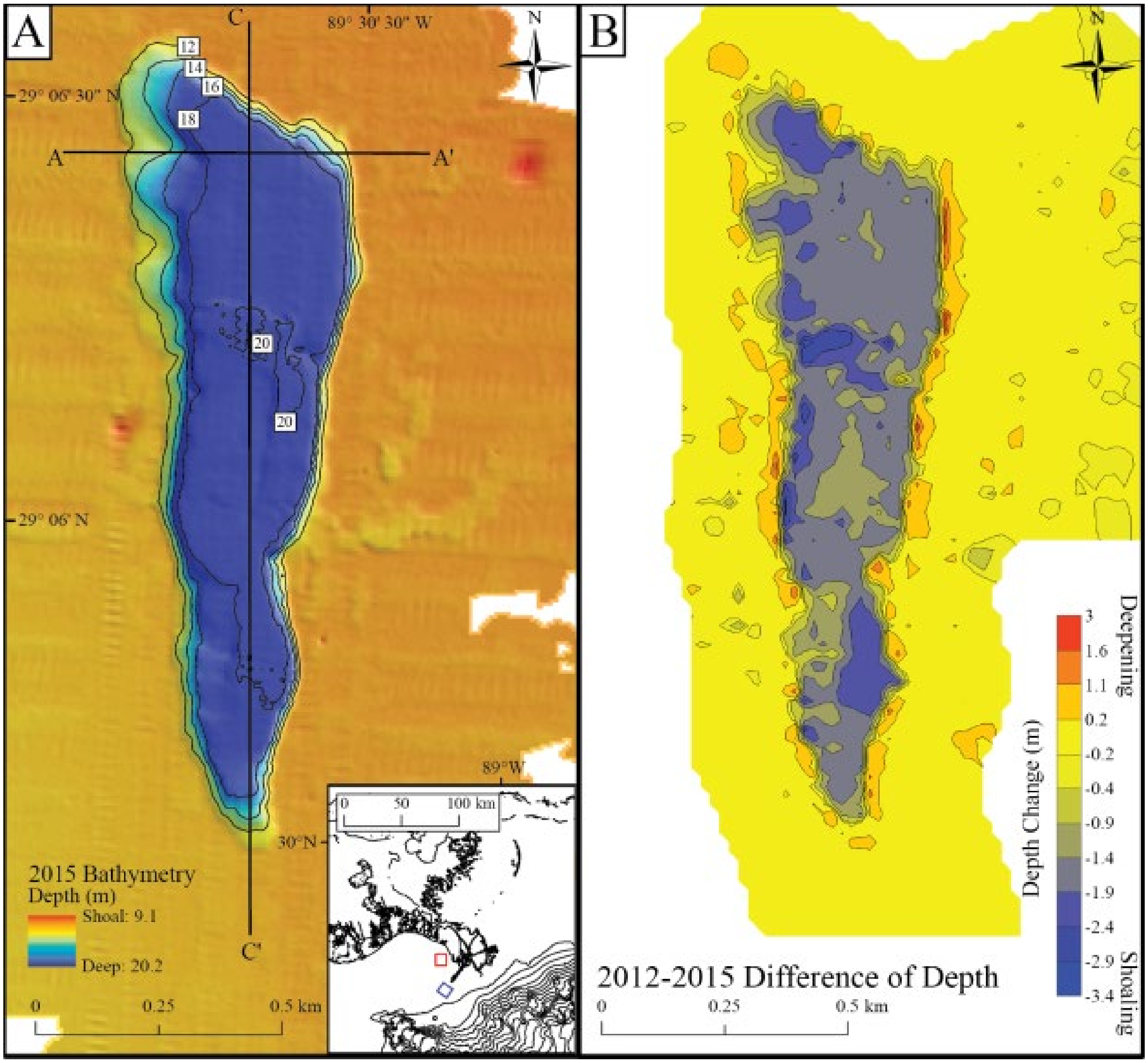

Figure 36. Isopach map showing thickness of acoustically transparent layer mantling the Sandy Point pit floor.

(A) Base map with 2015 hill-shaded bathymetry in the Sandy Point dredge pit. Contours are in 2 m intervals. Cross-sections correspond to Figure 37. Inset shows locations of Sandy Point (red square). (B) Difference of Depth between 2012 and 2015 surveys. Red values indicate deepening, blue values indicate shoaling. Yellow values are within the 2σ range of uncertainty (~0.5 m) and are therefore considered to be no significant change. Data of 2012 were collected using a multibeam system during a post-dredge survey. From Obelcz et al. 2018.

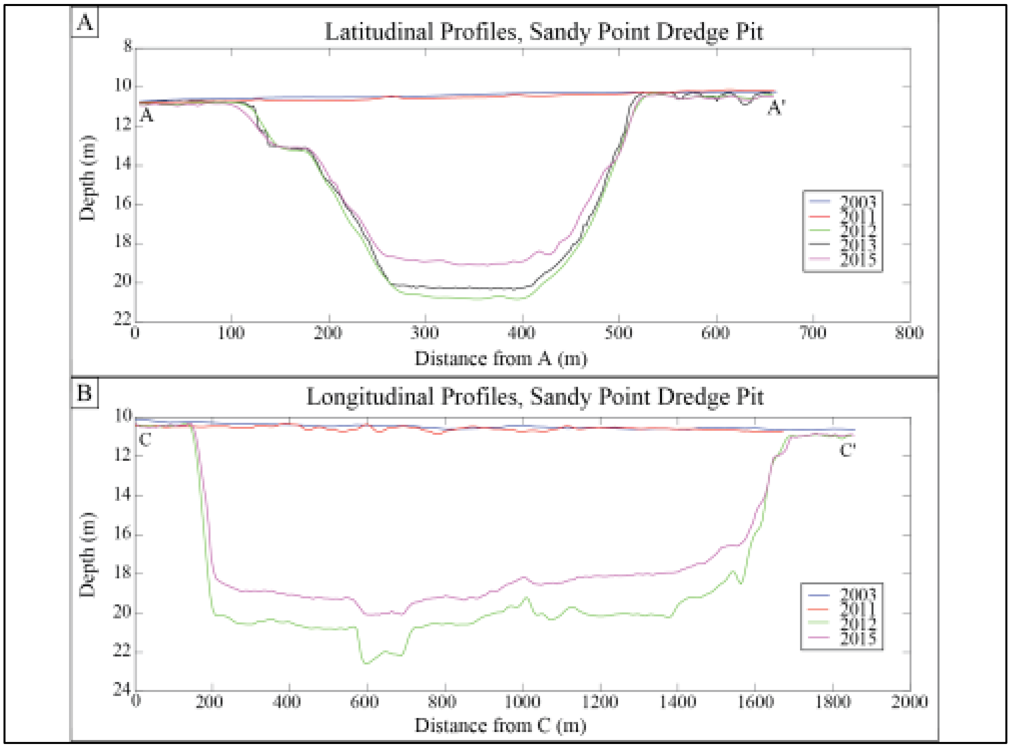

Figure 37. Preliminary bathymetry data of the Raccoon Island dredge pit.

(A) Latitudinal bathymetric transects before and after dredging in Sandy Point dredge pit. (B) Longitudinal transects before and after dredging. Note only four surveys are available instead of 5 for (A) due to lack of 2013 longitudinal survey coverage. From Obelcz et al. 2018.

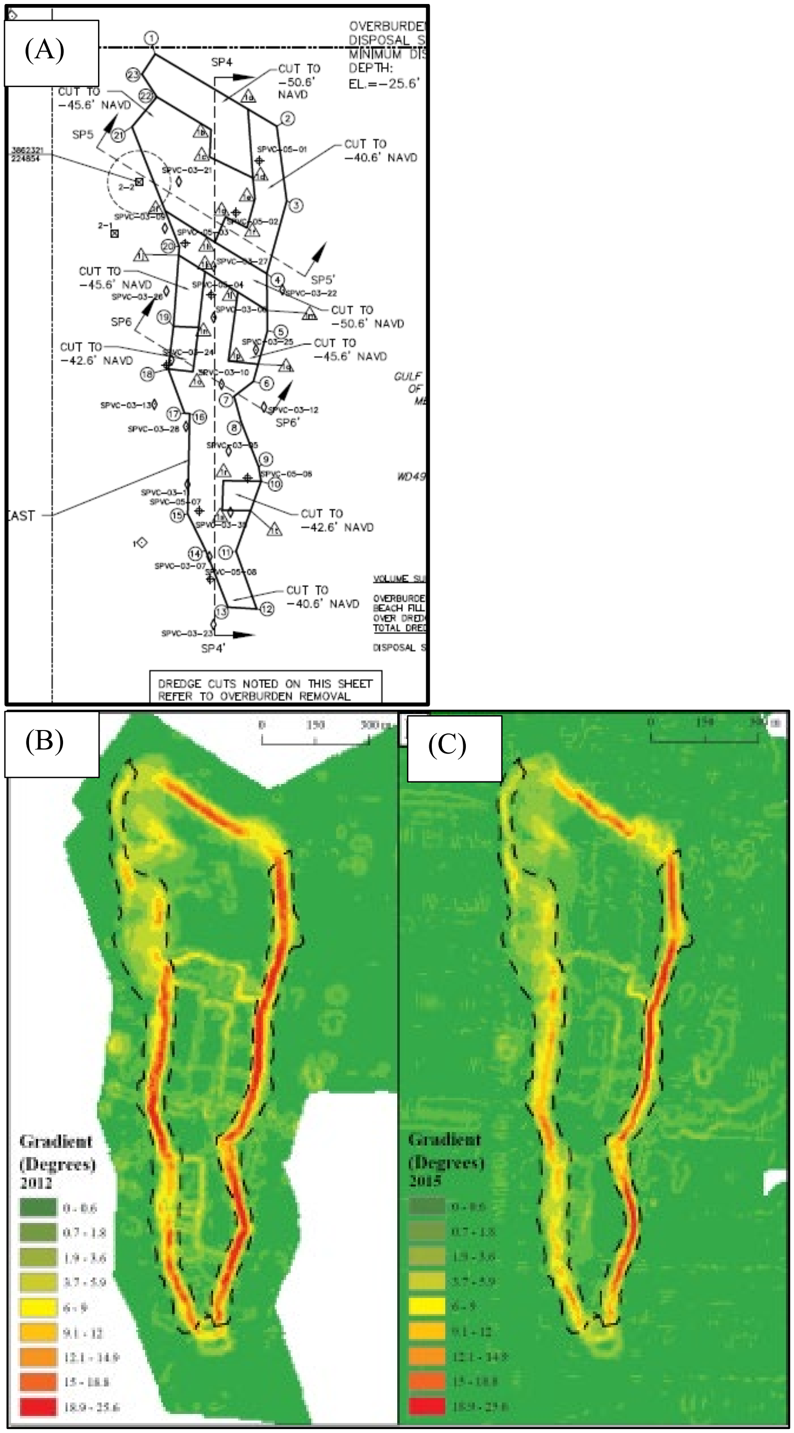

Figure 38. Interpolated bathymetry data collected in Jan 2013 and Mar 2013 at the Raccoon Island dredge pit and the differences in depths.

(A) Design plates for Sandy Point dredge pit; (B) Slope map of the Sandy Point dredge pit derived from 2012 bathymetry. Green colors represent flatter surfaces, while red colors indicate steeper surfaces. Dashed polygons are extents of western and eastern wall used for wall gradient analysis. (C) Slope map derived from 2015 bathymetry. From Obelcz et al. 2018.

Table 4. Sandy Point dredge pit volume calculations, 2012–2015

Location	Area (m^2)	Volume Change (m^3)
Entire Pit	436,020	616,550 ± 87,204
Eastern Wall	47,165	-29,137 ± 9,433
Western Wall	49,618	-19,140 ± 9,924

The sidescan sonar data highlight the collapse features along the western wall of the Sandy Point dredge pit (Figure 39); these features include stair-stepped retrogressive failures and collapse depressions, typical of the Mississippi River Delta Front (Coleman et al., 1980). This presumably indicates the veneer of mud on top of the sandy substrate behaves similarly to the predominantly muddy delta front sediments.

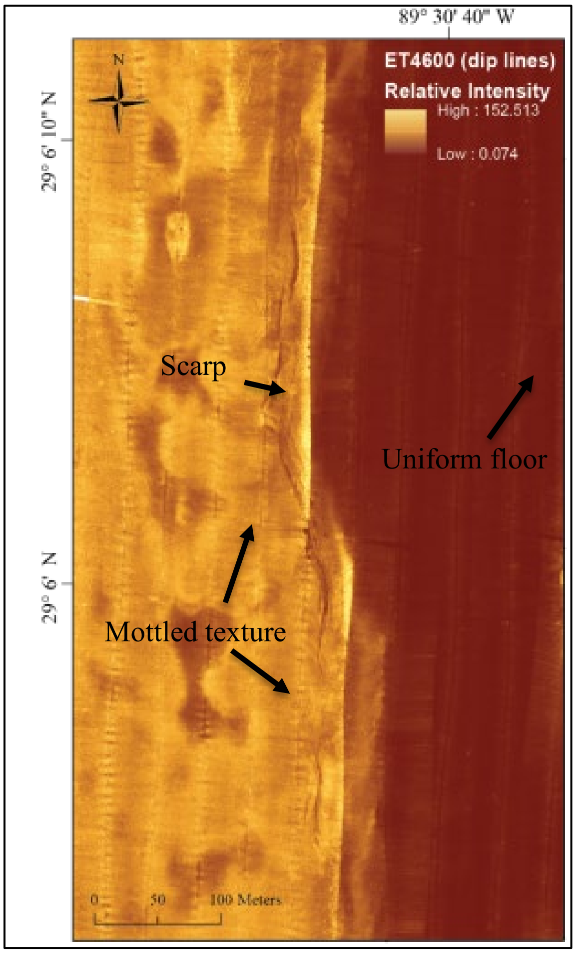

Figure 39. Sidescan sonograph showing the western wall of the Sandy Point dredge pit, 2015 survey.

Gold indicates high backscatter, and brown indicates low backscatter. Note mottled texture of continental shelf (left) and uniform low reflectance of dredge pit floor (right). Also note stair-stepped failure scarps.

Subbottom profiles of the Sandy Point dredge pit shows a substantial degree (1–3 m) of infill since the 2012 bathymetric survey, as well as a thin veneer of what appears to be a high turbidity layer (Figure 40). The isopach of high turbidity (acoustically transparent) indicates that this high turbidity is mainly located in the central part of the pit and follows the bathymetry of pit (Figure 41).

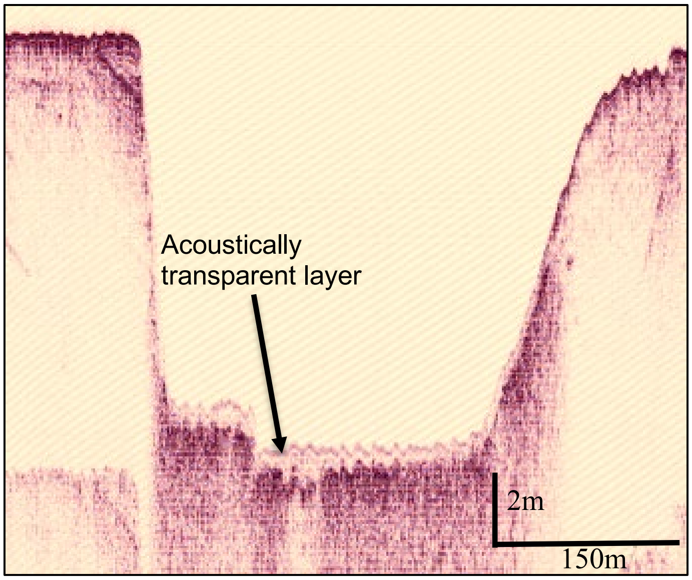

Figure 40. An E-W chirp subbottom profile going through the middle of the Sandy Point dredge pit, with an acoustically transparent layer siting on the pit bed.

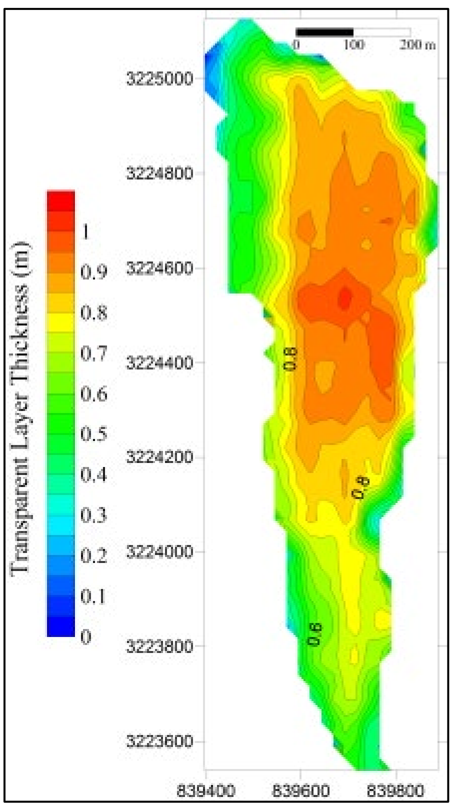

Figure 41. Isopach map showing thickness of acoustically transparent layer covering the Sandy Point pit floor.

Data are derived from chirp subbottom profiles, which demonstrate an acoustic impedance contrast above the hard reflector of the water bottom. Contours are in 0.1 m intervals. Horizontal and vertical axes are easting and northing of UTM zone.

B. The Raccoon Island Dredge Pit

Interferometric bathymetric data were collected at Raccoon Island dredge pit in June 2015 (Figure 42). The data underwent uncertainty analysis and removal of errant points, and a DEM surface was generated for this suvey. Single beam bathymetric data collected in January 2013 (pre-dredge) and March 2013 (post-dredge) were interpolated and compared with June 2015 data. Two differences of depths (DoDs) were calculated (Figs. 43 and 44).

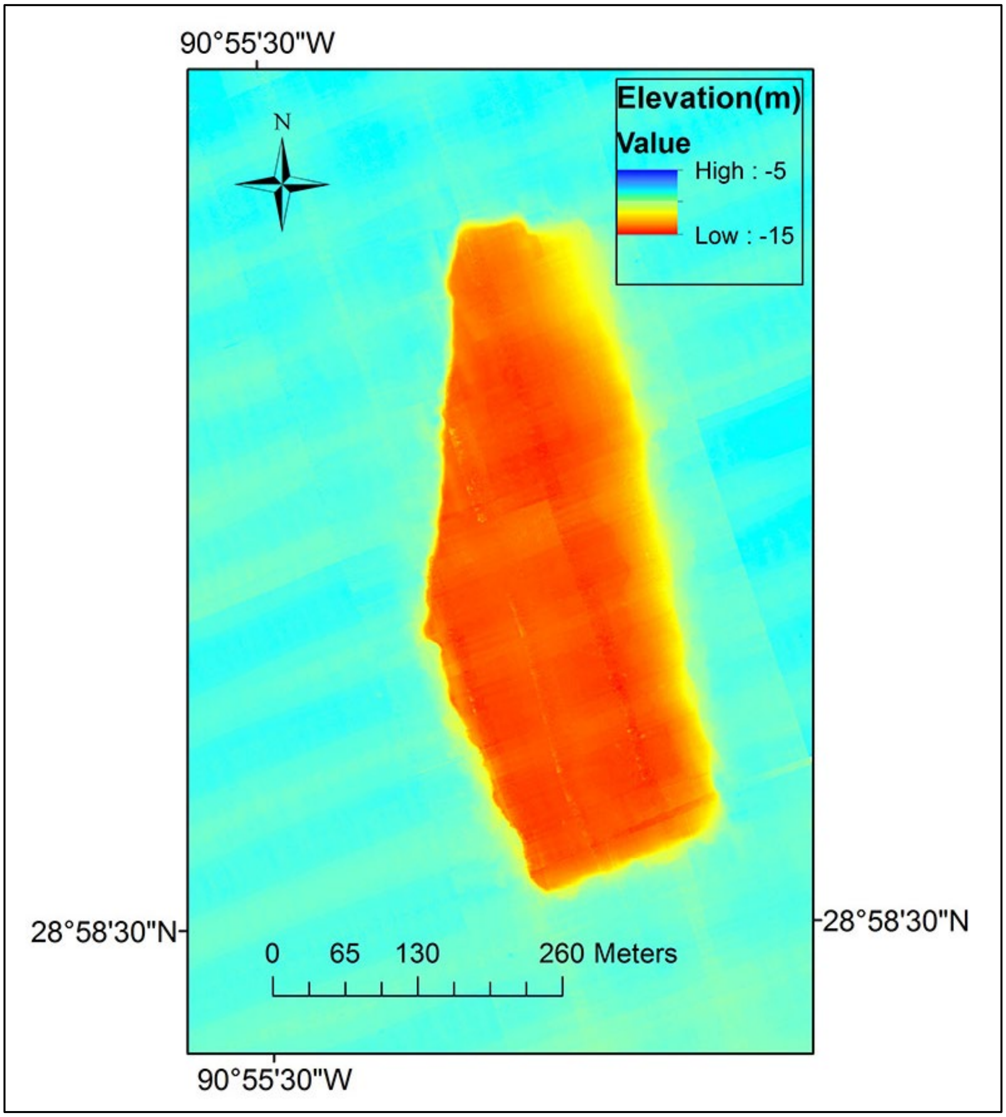

Figure 42. Bathymetry map of the Raccoon Island dredge pit based on June 2015 data.

This pit is about 200 m wide and 800 m long.

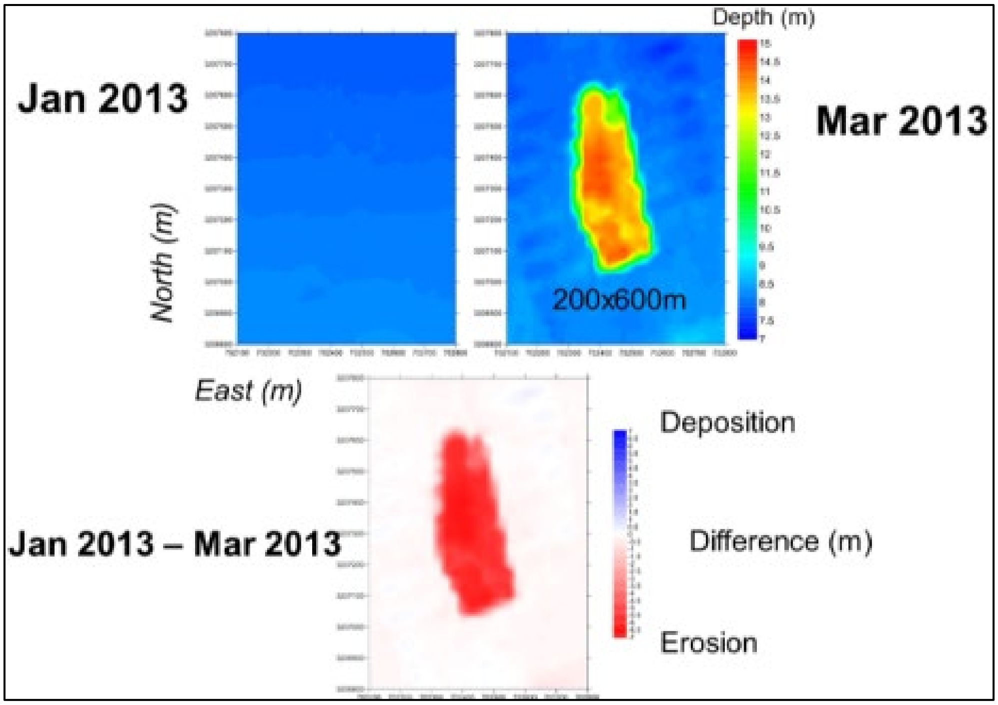

Figure 43. Interpolated bathymetry data collected in Jan 2013 and Mar 2013 at the Raccoon Island dredge pit and the differences in depths.

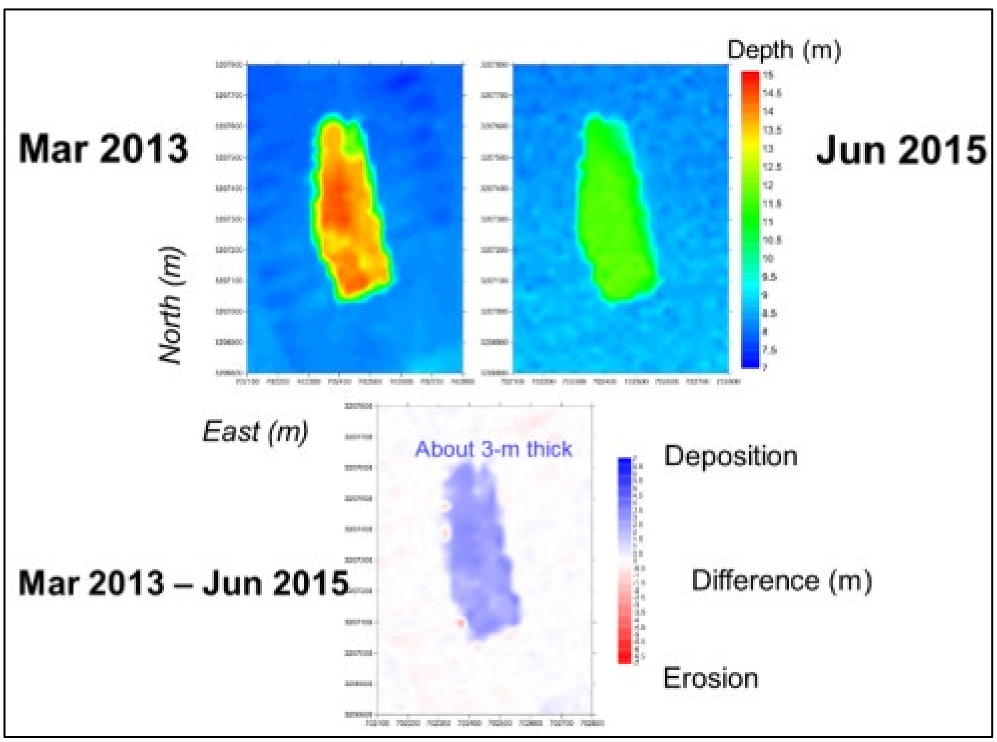

Figure 44. Interpolated bathymetry data collected in Mar 2013 and Jun 2015 at the Raccoon Island dredge pit and the differences in depths.

From Liu et al. 2020.

The Raccoon Island dredge pit seems to be an efficient sediment trap. It accumulated about 3 m thick of sediment from 2013 to 2015 (Figure 44). Below are mosaic maps showing the sidescan data of the entire Raccoon Island dredge pit (Figure 45).

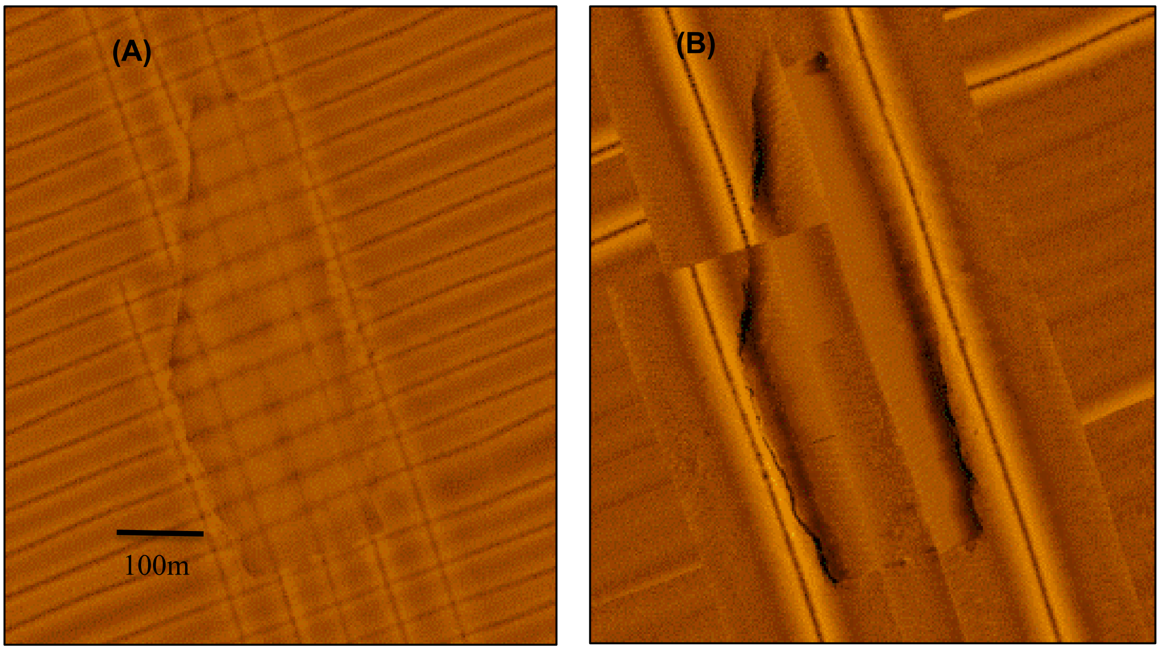

Figure 45. The averaging (A) and cover-up (B) sidescan mosaic map of the Raccoon Island dredge pit.

Morphological features inside and outside the borrow pits were examined in more detail on sidescan data. It was found that the edge of southwest corner of the Raccoon Island dredge pit was irregular and rough, as shown in Figure 46A. Small depressions were found outside of the pit, as shown in Figure 46B. A pile of sediment was deposited in the southwest corner of the Raccoon Island dredge pit (Figure 46B).

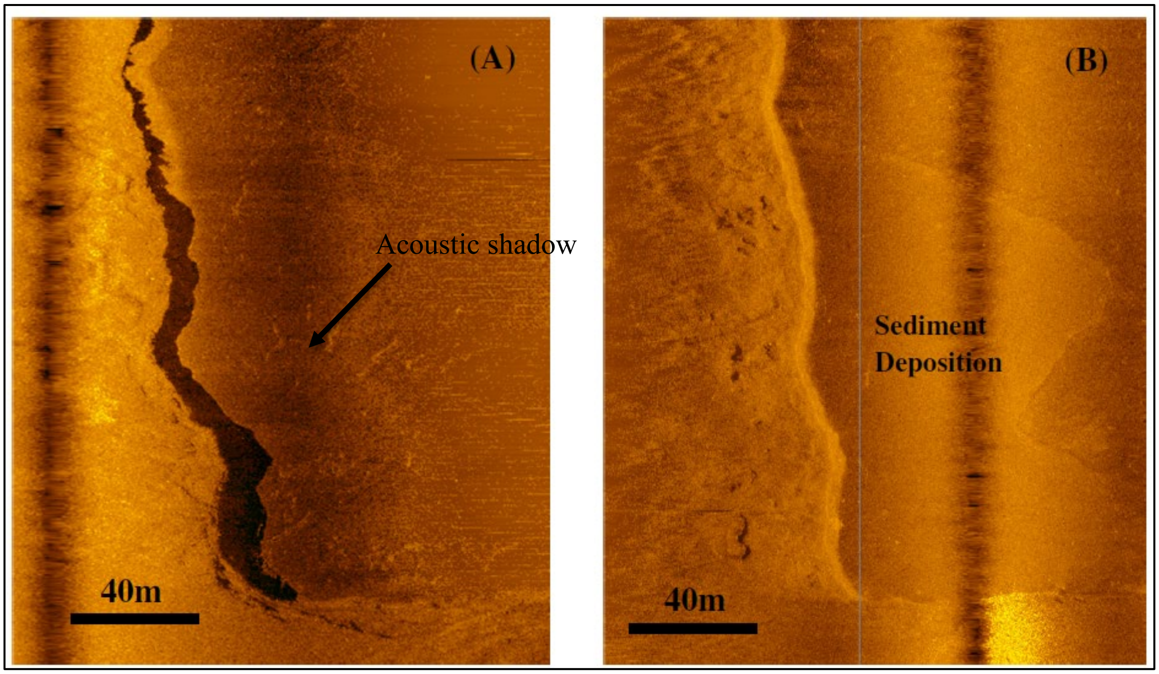

Figure 46. Sidescan sonar images collected in the southwest corner of the Raccoon Island dredge pit.

Acoustic shadows show the clear pit wall edge on left (A). An accumulation of sediment is found on the right (B). Two sidescan images cover the exact same spatial extent but were collected along different track lines.

Chirp subbottom profiles were collected using both Edgetech 0512i and 2000 (with a 216 sonar) systems. Figure 47 shows the stratigraphy and the comparison of penetration depths and resolutions of both systems.

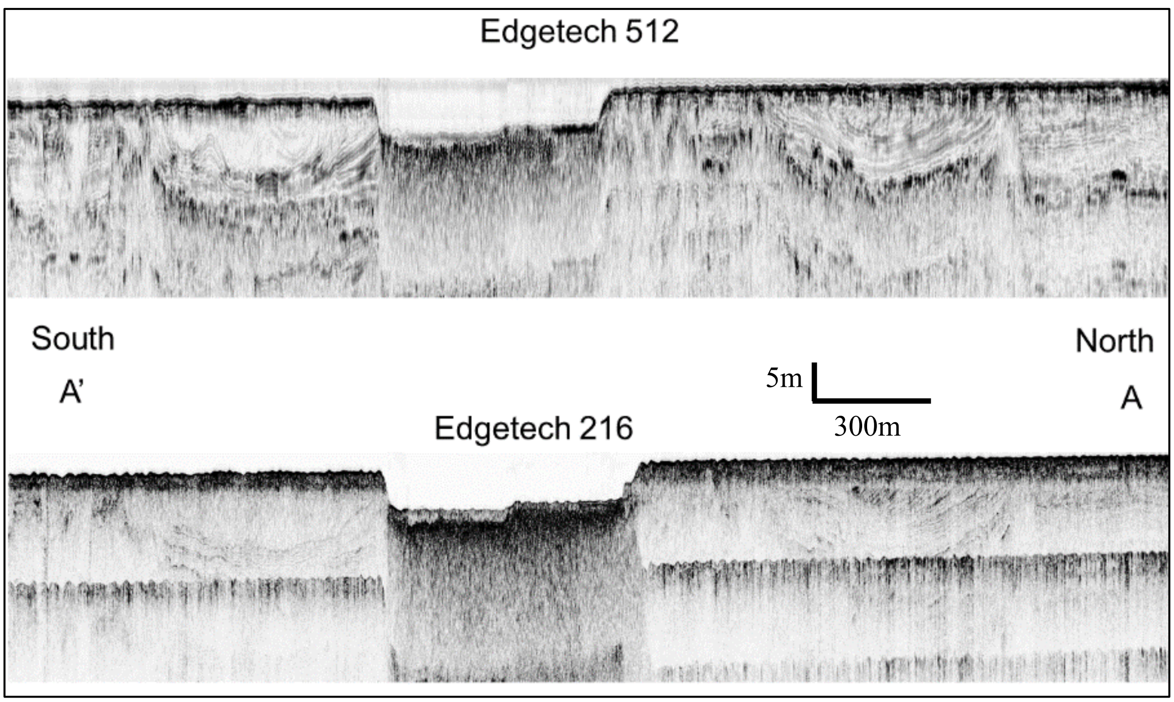

Figure 47. Comparison of a N-S subbottom profile collected at the Raccoon Island dredge pit using Edgetech 0512i and Edgetech 216 (a component of Edgetech 2000).

C. The Peveto Channel Dredge Pit

Figure 48 shows bathemetric maps of the Peveto Channel dredge pit in 2003 and 2016, and the difference of depths.

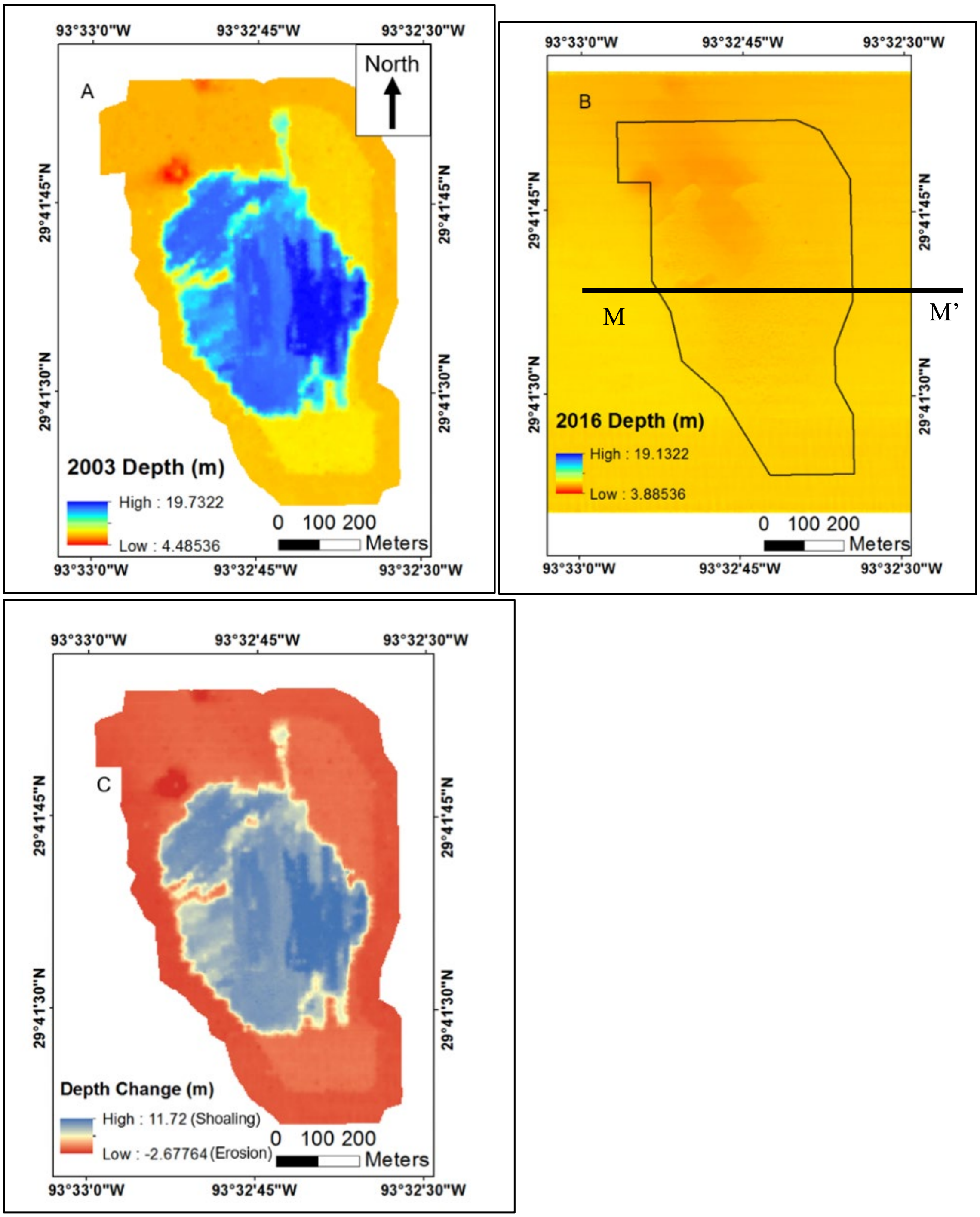

Figure 48. Bathymetric data from the Peveto Channel dredge pit in 2003 and 2016, and the difference of depth. From Robichaux et al. 2020.

Bathymetric data of 2016 show that the entire pit is 100% filled up, with some regional topographic highs in the NW portion of survey areas (Figure 48). Although the surface of sea floor generally has low gradients, some “seafloor instability features” were observed. These features resemble numerous small “mud volcanoes” in morphology (Figure 49) and are about 0.5 m tall and several meters apart. Although identifying the processes forming these morphological features requires further work, it is possible that the processes might be associated with consolidation and/or wave-induced dewatering or degassing processes.

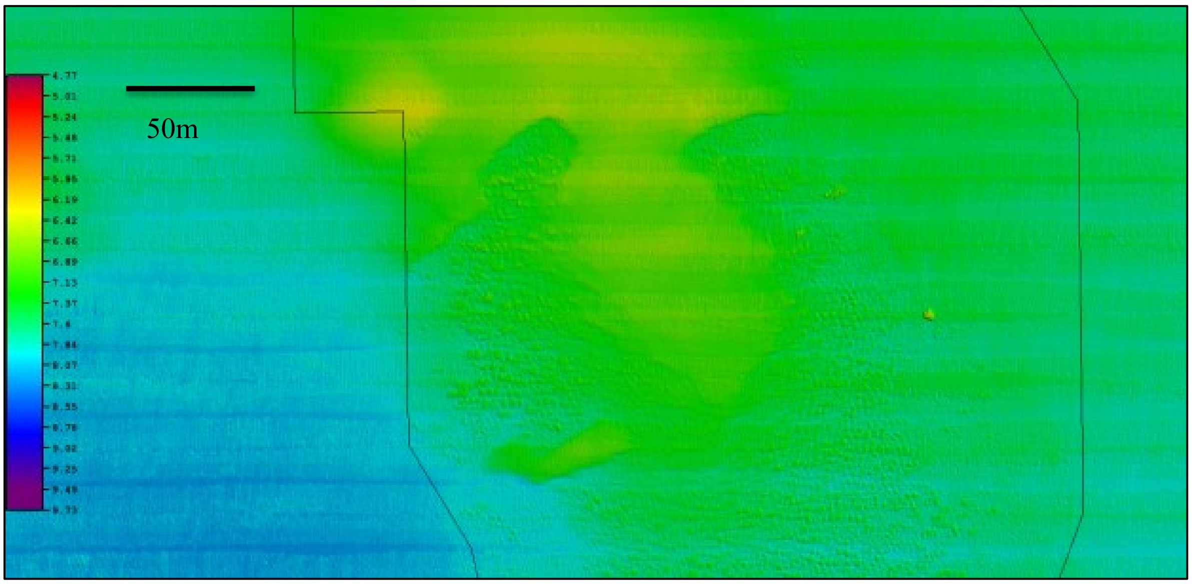

Figure 49. Detail of filled dredge pit bathymetry (vertical scale in meters).

Seafloor instability features associated with dewatering and possible gas release can be seen on surface.

Three categories of sediment are observed in side scan sonar mosaics (Figure 50): ambient seafloor, high intensity reflectance dredge side-cast material, and low intensity reflectance newly-deposited material. Sidescan data reveal dredge side-cast areas that are easily identified as high intensity reflectance patches (white in Figure 50), due to possible coarser grain-size of the sediments deposited during the dredging activities. Dredge side-cast deposits can be seen on southeast and northwest sides of the pit, as well as in the northwest corner of the pit. Trawl scars from fishing boats can be seen in Figure 50, as well.

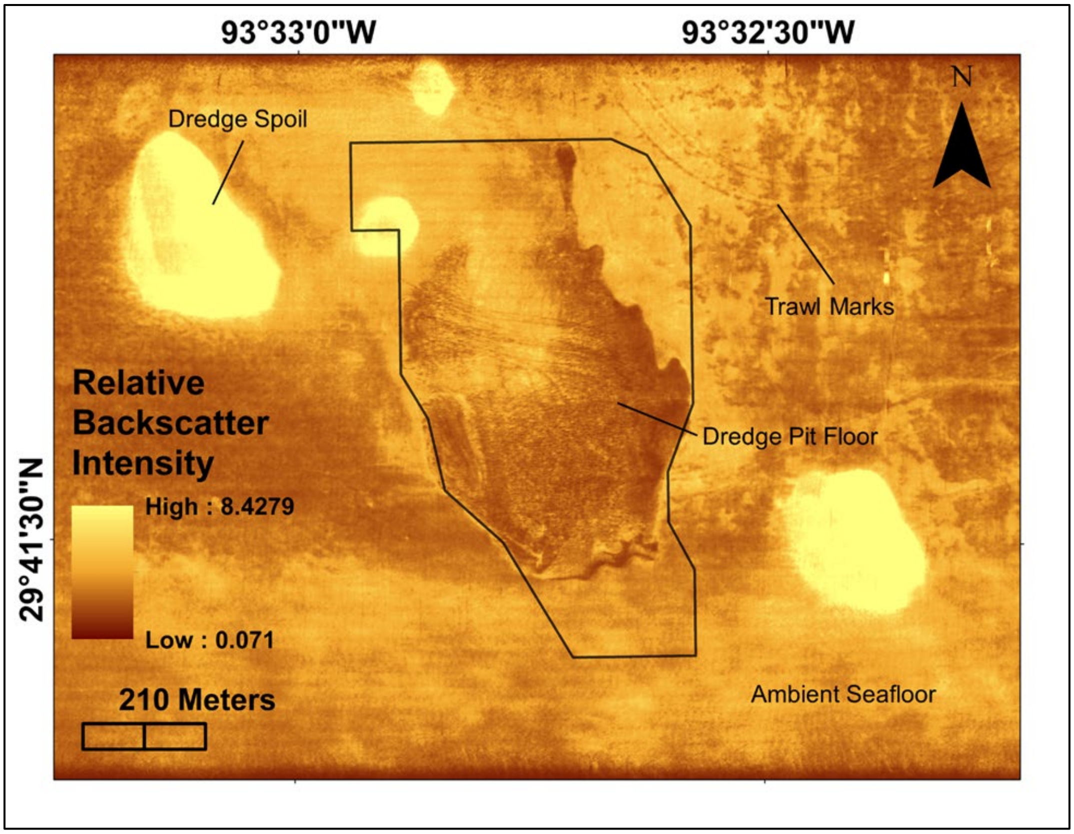

Figure 50. Sidescan mosaic of the Peveto Channel dredge pit (completely filled).

Note the differing sedimentary environments and boundary between newly deposited sediment and undisturbed seafloor. Yellow indicates high reflectivity. From Robichaux et al. 2020.

Both Edgetech 0512i and 2000 systems were used in subbottom data acquisition. Subbottom profiles outline the shape of the pit and also provide evidence of paleochannels near the pit (Figure 51). It is clear that the pit was 100% infilled in 2016 and that the fill was characterized by acoustically opaque seismic facies, relative to the undisturbed deposits where seismic reflectors representing natural stratigraphic contacts can be resolved. The acoustically opaque seismic facies is probably indicative of sediment with high biogenic gas content (Figure 51).

The source of the gas may be from higher organic content in the newly-deposited sediment. Although no cores were collected from the Peveto Channel pit due to the construction of a new pipeline, LOI results from cores collected at the Sandy Point dredge pit reveals 9.2% of organic matter by weight (Table 3). Over time, organic matter degrades, and the resultant gas products are forced out as the sediments consolidate. The degassing process is facilitated by wave-induced pressure loading on the seafloor, as described by Bea (1983) and Wright (1972). The increased water mass caused by a wave-front propagation increases pressure on the seafloor, and in an area of loosely consolidated, gas-charged sediment, this could force out any gaseous or liquid materials as the unconsolidated sediment is compressed.

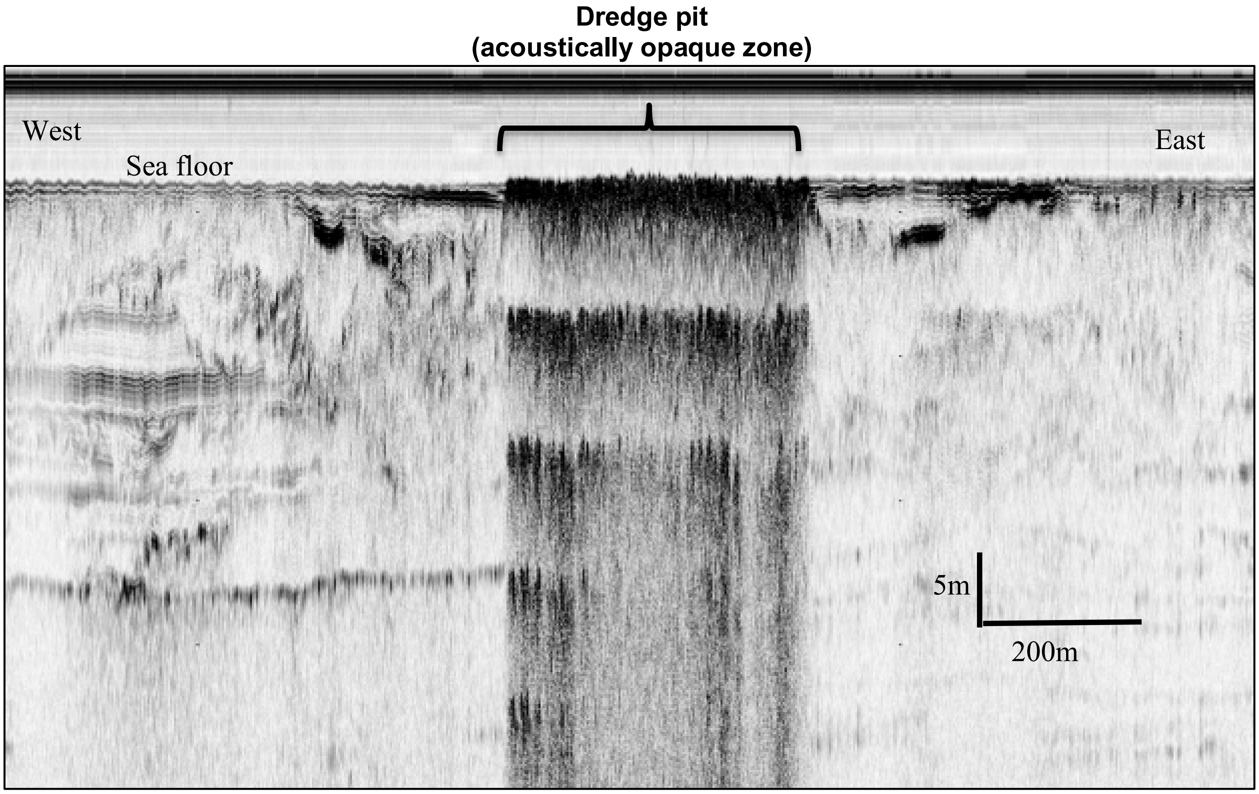

Figure 51. East-West subbottom profile from Peveto Channel.

Paleochannels are visible on either side of the pit. The pit itself is marked by a thick black band of acoustically opaque, gaseous sediment. Location of part of this profile is M-M' in Figure 48. From Robichaux et al. 2020.

A Geometrics Magnetometer G882 System was used to collect magnetometer data through the entire survey in the Peveto Channel dredge pit. The primary purpose of including the magnetometer was pipeline detection because a pipeline had been constructed in the middle of the pit since the previous survey had been conducted in 2007. Results of the interpolated magnetic anomaly map are in Figure 52. It is clear that a new pipeline was constructed through the middle of the Peveto Channel dredge pit.

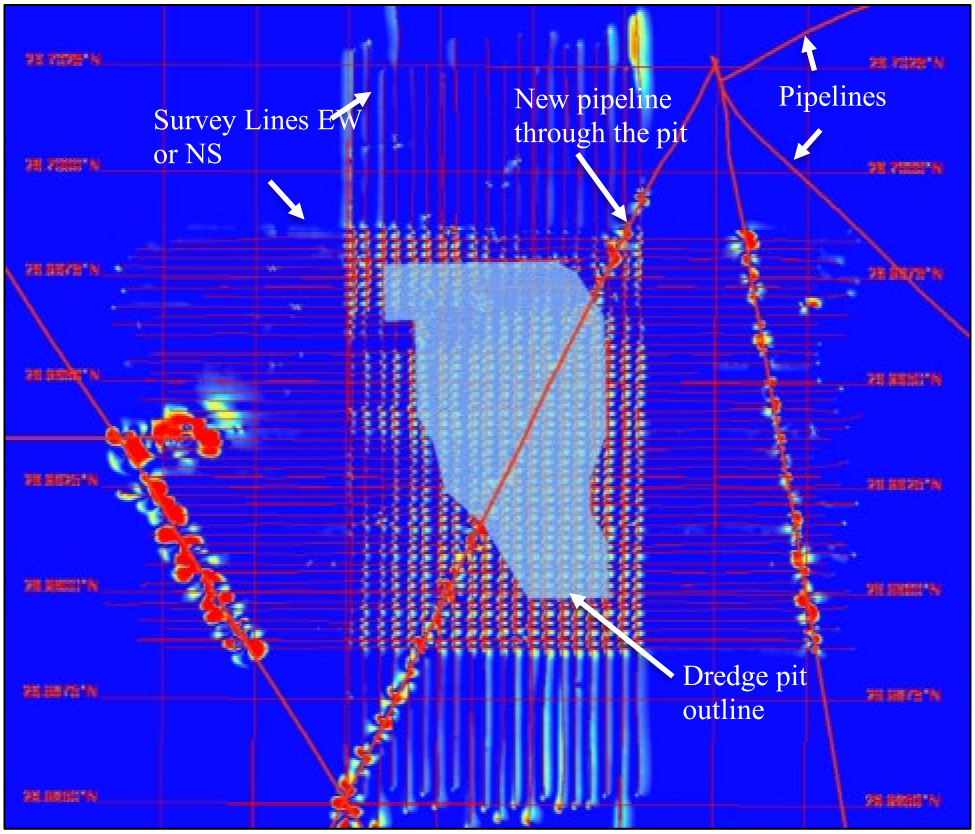

Figure 52. Overlay map of magnetic anomalies, dredge pit outline (light blue), and previously compiled pipeline data (thick red lines) provided by BOEM.

The anomalous signals have a high degree of correlation with the BOEM pipeline archive.

2.2.4 Sediment Cores

Multicores were collected at five stations in the Sandy Point (SP) dredge pit and five stations in the Raccoon Island (RI) dredge pit (Figure 53). No cores were collected at Peveto Channel due to the construction of a new pipeline (Figure 52). These multi-cores were mainly used for imaging, x-radiograph, grain size, and radionuclide analyses. Vibracores were collected at these stations, as well, and used for core logger and imaging analyses.

Figure 54 shows the images of three sections of core RI1 in the Raccoon Island vibracore, with a clear shift from recent fluvial mud deposition to sandy paleochannel sediment. Core logger data in Figure 55 further confirm that there are two contrasting layers in the deposited sediment at the Raccoon Island core RI1: a less dense muddy package on top and a denser sandy package on the bottom.

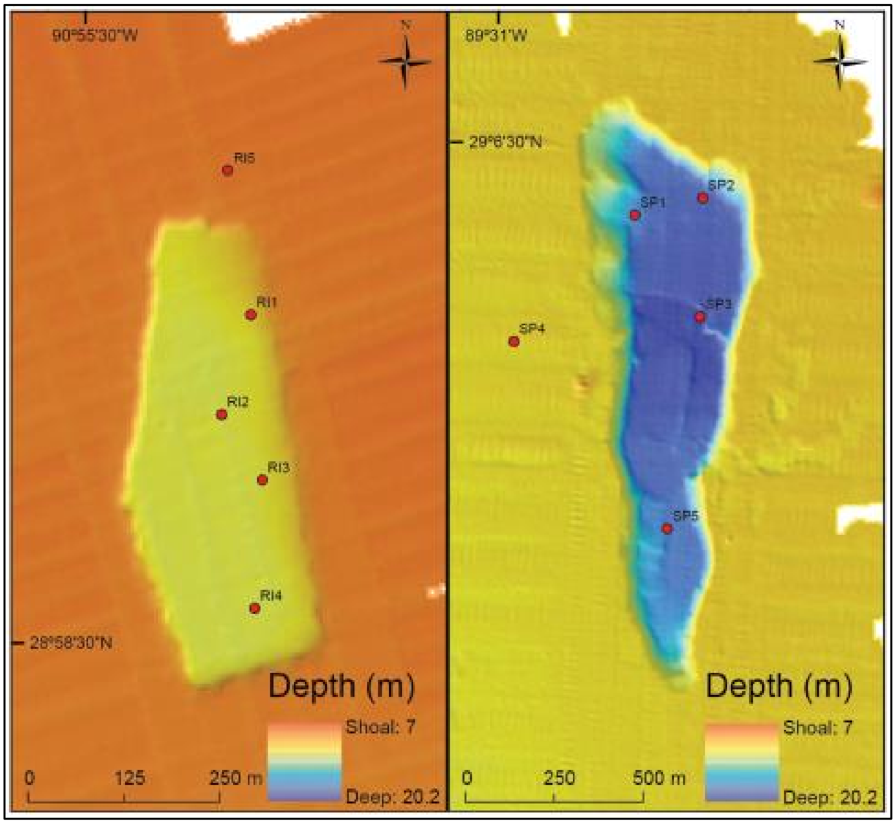

Figure 53. Coring locations of both the Raccoon Island (left) and Sandy Point (right) dredge pits.

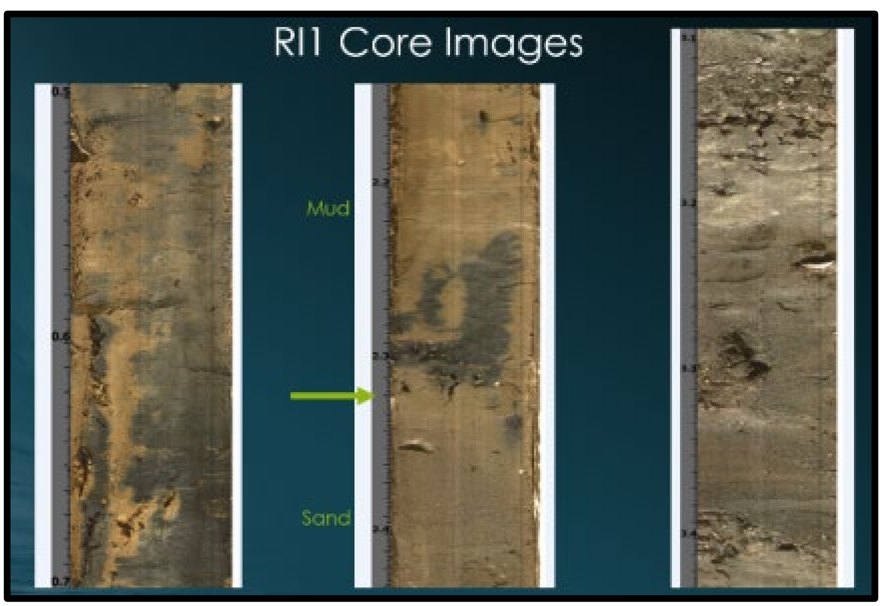

Figure 54. Three sections of a split Raccoon Island vibracore RI1.

From left to right: 0.5–0.7 m; 1.15–2.43 m; 3.1–3.43 m, from left to right. The green arrow in the middle section shows the shift from recent fluvial mud deposition to sandy paleochannel sediment.

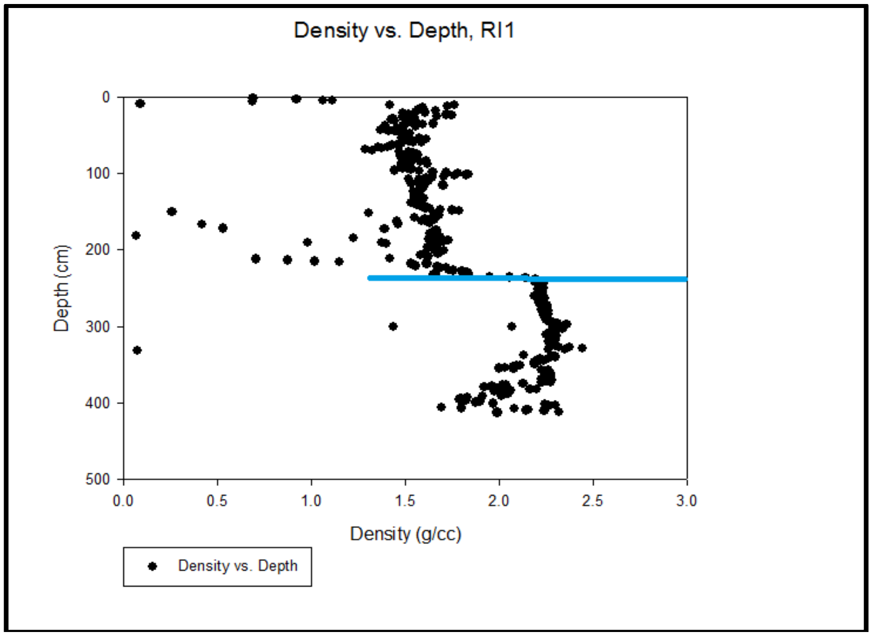

Figure 55. Data from the whole-core logger show the density over depth in the Raccoon Island RI1 vibracore.

Two distinct sediment packages can be seen: a less dense, muddy package overlaying a sandy substratum. The boundary between these two packages is indicated by the blue line.

Sandy Point x-radiographs reveal two bedding surfaces, identified as linear planes of higher density (white) sediment at the top of each of the four within-pit cores (Figure 56). The surfaces are located at about 5 and 10 cm depth. In SP1 and SP2, the top two bedding planes dip down from the left to the right. The same surfaces lie flat and parallel to each other in SP3, and are parallel to the surface but somewhat undulatory in SP5. SP1 reveals the highest number of muddy deposits or clasts scattered throughout the x-ray between 5 and 30 cm. This corresponds with a relatively low amount of bioturbation, though a few thin but long burrows appear. SP2 and SP3 contain tightly packed, thin burrows between 5 and 40 cm. Between 40 and 60 cm, both SP2 and 3 contain large burrows. SP2 exhibits a layer of bioturbated sediment at 50 cm lying immediately above a muddy deposit and 5 cm of mm-scale laminations. Millimeter-scale laminations are also evident in the following locations: between the two bedding planes at 5 and 10 cm (SP3 and SP5) and between 25 and 40 cm (SP5).

The Raccoon Island x-radiographs contain large muddy clasts up to 8 cm wide and 2 cm tall (Figure 56). These deposits occur in all RI x-radiographs but appear largest and most prominent in RI3 at a depth of 40-55 cm. Burrows in RI3 and RI4 terminate at 10 cm. Following the abatement of burrows in RI3 are several cm of mm-scale laminations. RI2 captures the most extensive burrows, from 10–30 cm.

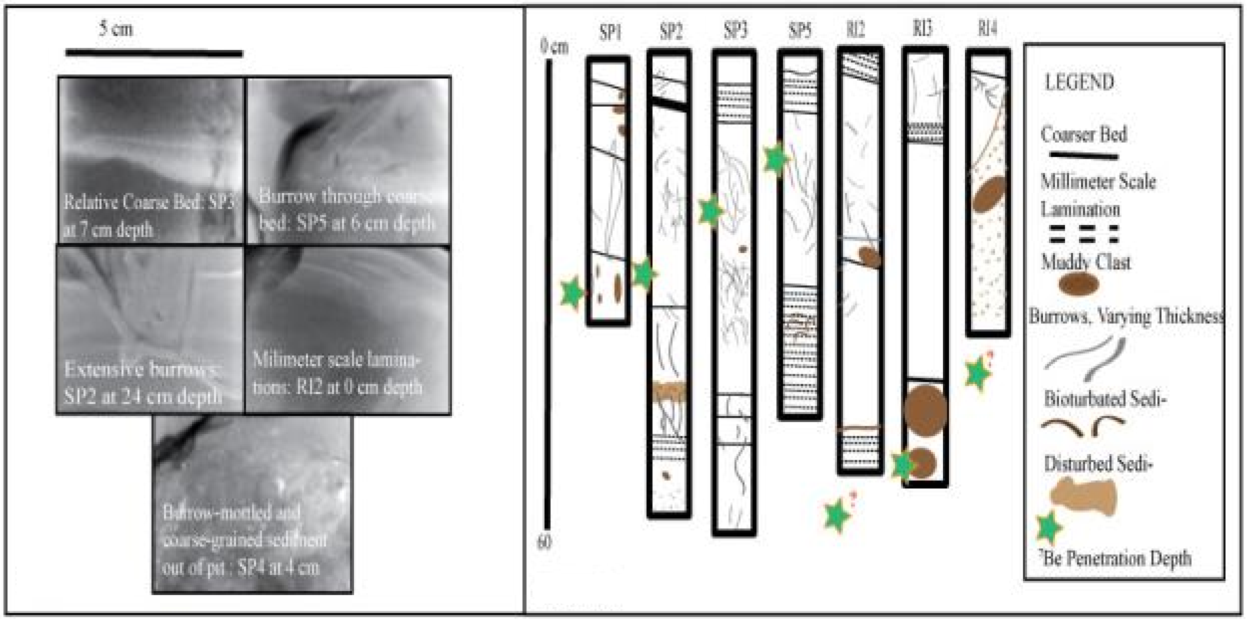

Figure 56. Examples of bedding features from various x-radiographs; sketched x-radiographs.

Left panel: Examples of bedding features from various x-radiographs; lighter colors denote higher-density material.

Right panel: Sketched x-radiographs show depths and locations of relatively coarse beds, laminations, muddy clasts, burrows, and bioturbated or disturbed sediment throughout select cores. Two bedding planes are evident in all Sandy Point multicore x-radiographs, one at ~4 cm depth and the other at ~6 cm depth as well as burrows throughout. Raccoon Island contains larger muddy clasts and bioturbation only above 30 cm. Green stars represent the depth of ^{7}Be penetration.

All multicores from inside the dredge pits contain activity of ^{7}Be to depths well below the sediment surface (Figure 57). In Sandy Point multicores SP1, SP2, SP3, and SP5, ^{7}Be is evident in each core from the surface to a depth of 14-28 cm. The peak activity ranges from 1.28 +/- 0.38 dpm/g (disintegration per minute per gram) to 5.7 +/- 0.57 dpm/g. The cores generally exhibit a decreasing trend in activity from surface to depth, with intermittent peaks. In contrast, SP4, a core collected outside the SP pit (Figure 53), contains ^{7}Be in only the surface sample, 0-2 cm. The activity in SP4 0-2 cm has the lowest recorded peak, at 0.94 +/- 0.60 dpm/g.

In Raccoon Island cores RI1-4 (all collected inside the pit), all multicores contain ^{7}Be at considerable depth (Figure 58). In fact, the ^{7}Be penetrates to such depth that multicores RI1, RI2, and RI4 are not long enough to capture the base of penetration; ^{7}Be is present throughout the entirety of the ~50 cm cores. Only RI3 captures a base (dpm/g= 0) of ^{7}Be, at 40 cm. RI5, from outside of the pit, contains no ^{7}Be.

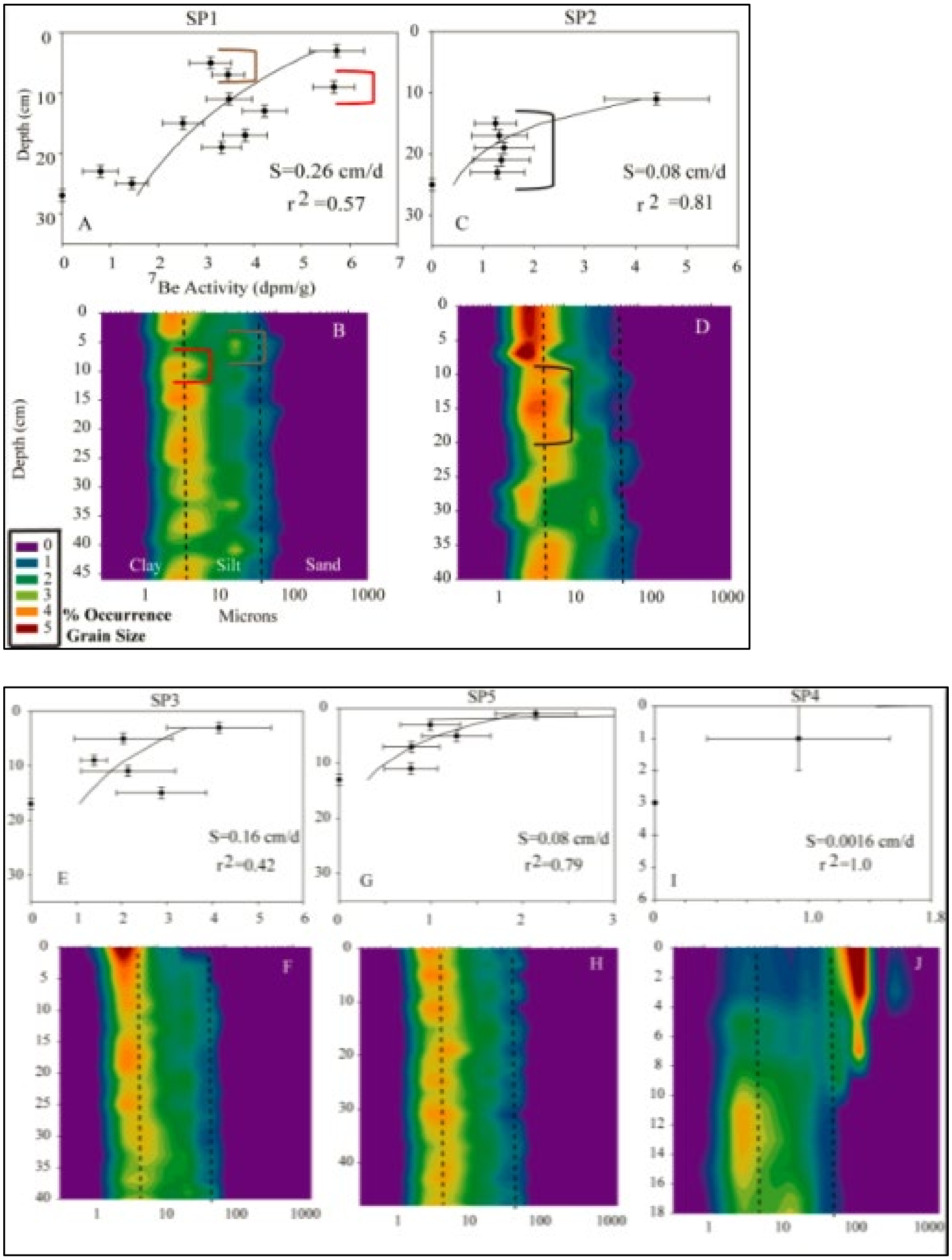

Figure 57. Grain size distribution and 7Be profiles of Sandy Point (SP) multicores.

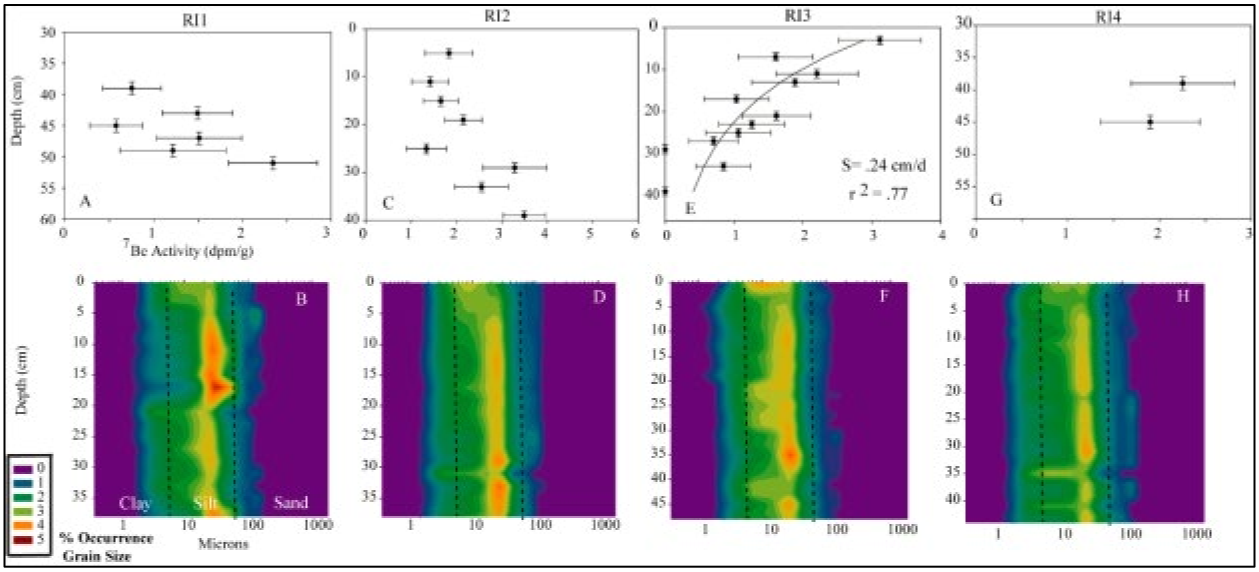

Figure 58. Grain size distribution and 7Be profiles of Raccoon Island (RI) multicores.

^{7}Be profiles of Raccoon Island accumulation rates exceed an average of .24 cm/day in RI3.

Sandy Point multicores SP1, SP2, SP3, and SP5 (within the pit) contain predominantly coarse clay and fine silt (2–10 microns). SP1 and SP2, the northernmost sites, contain zones enriched in medium-coarse silt (20–30 microns). SP1 captures three of these occurrences at the following depths: 3–8 cm, 31–35 cm, and 39–45 cm. SP2 captures one silt deposit from 26–33 cm. SP3 contains two silt-rich zones, which are less distinct and identified at 32–36 cm and 37-–9 cm. SP5 proves the most homogenous, with no significant deviations from the 2–10 micron grain size throughout the core (Figure 57). SP4, from outside the pit, shows two distinct packages of sediment with different grain sizes. Sand (63–200 microns) is dominant from the surface to a depth of 8 cm. From 8 cm to the bottom of the core at 18 cm, the grain size is medium clay- medium silt (1–20 microns), which coarsens downward (Figure 57).

Raccoon Island multicores 1–4 (within the pit) contain almost entirely silt (Figure 58). In all four cores, the top 5–10 centimeters contain a wider range of grain sizes, from 3 to 30 microns (coarse clay to coarse silt). Moving down core, all four cores have a modal grain size of 20 microns are relatively homogenous vertically. Occasional excursions towards finer grains occur and demonstrate that the mode grain size for discrete intervals can be as fine as 2 microns. These intervals occur as follows: in RI1, fine intervals are recorded at 0–4 cm, 21–22 cm, 26–28 cm, and 32–36 cm; in RI2, the intervals are recorded at 0–10 cm, 16–18 cm, and 31–32 cm; in RI3, the intervals are 0–4 cm, 14–19 cm, 20–31 cm, and 40–43 cm; in RI4, the intervals are 0–8 cm, 9–13 cm, 33–36 cm, and 40–42 cm (Figure 58).

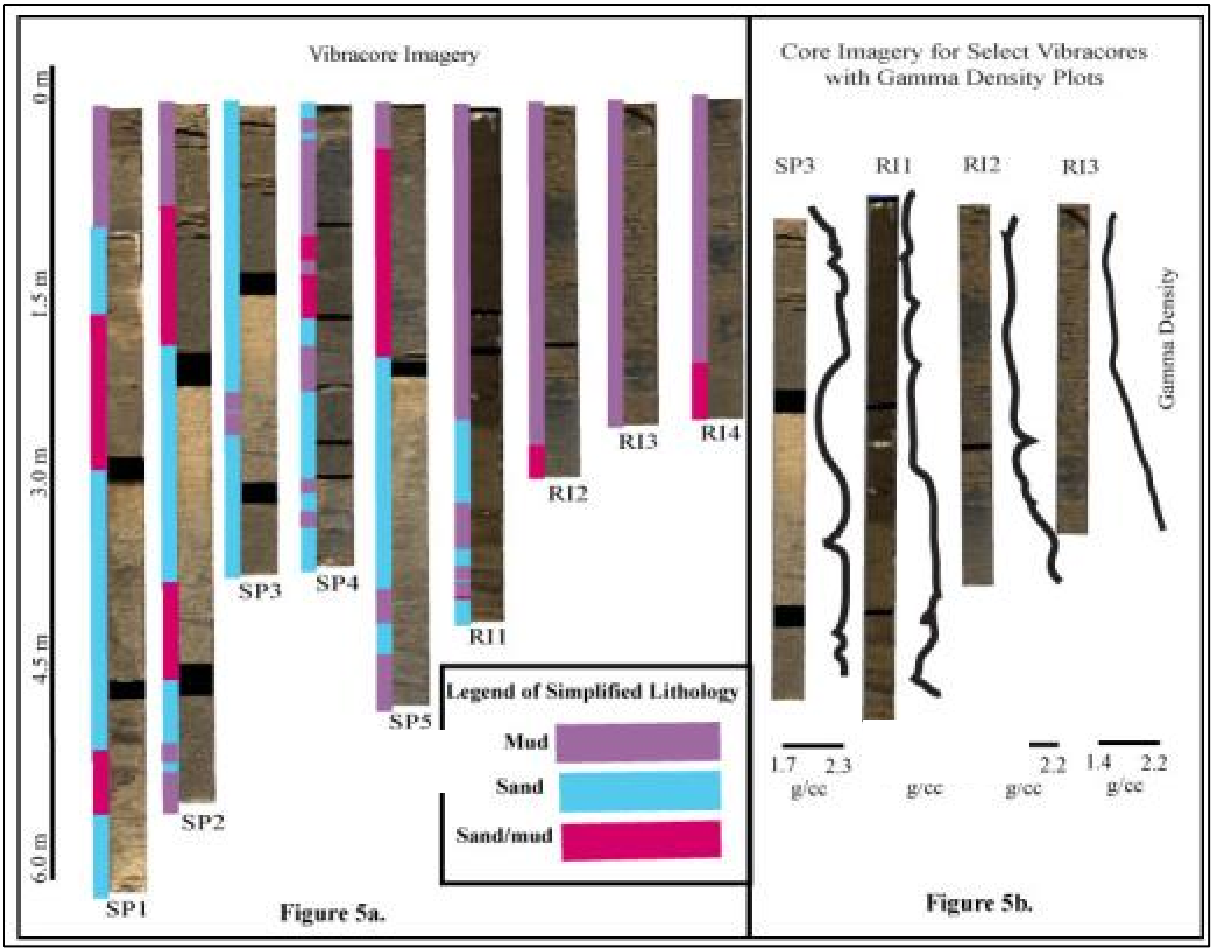

Figure 59.Model results of pit infilling in the Sandy Point dredge pit.

In left panel, high resolution core imagery from the Sandy Point and Raccoon Island pits with color bands corresponding to one of three lithologic types found in cores: mud, sand, or sandy mud-silt (mixed sediment). Cores are stretched vertically to show lithology more clearly. Due to potential non-recovery of sediment at surface, 0 cm depth may not represent the sediment-water interface.

The right panel: select core imagery from SP and RI vibracores and gamma density plots. SP cores exhibit alternating packages of high and low sediment, while RI cores contain low density (~1.4 g/cc) that gradually increases to ~2.2 g/cc at the base. Black gaps on pictures are due to post-collection consolidation.

The images of vibracores demonstrate zones of sand, mud, and mixed sand and mud (Figure 59). These sections correlate highly with bulk density values. Sections with bulk densities in the 1.5–1.8 g/cc range appear dark, often black. Bulk densities ranging from 1.9–2.4 g/cc appear as lighter-colored sandy sediment. The cores have occasional gaps mid-core, likely due to post-collection dewatering and consolidation. Some packages contain mixed sand and mud. RI cores contain discrete muddy layers and muddy clasts up to 5 cm tall and wide.

Based on sediment accumulation rates, bulk density, the dimensions of the pits, sediment transport rates can be calculated. Minimum and maximum sediment transport rate estimates (assuming 100% capture of sediment by pits) indicate:

- Sandy Point:
  - Min: 58,019.80 tons/~100 days/1460 m (pit length)= .40 tons/(m d)
  - Max: 58,019.80 tons/~100 days/670 m (pit width)= .87 tons/(m d)
- Raccoon Island:
  - Min: 31,801.00 tons/~100 days/575 m (pit length)= .55 tons/(m d)
  - Max: 31,801.00 tons/~100 days/435 m (pit width)= .73 tons/(m d)

3. Modeling Methods and Results

3.1 Modeling Methods

Three types of models were used to predict the long term morphology evolution and sediment transport processes in the pits: (1) pit infilling and margin evolution model from Nairn et al. (2005) and Lu and Nairn (2010), (2) sediments resuspension bottom boundary layer (BBL) model from Styles & Glenn (2000); (3) wave induced pit margin collapse model from Henkel (1970).

3.1.1 Nairn Model

The pit infilling and margin evolution models were reported in Nairn et al. (2005). This model was employed by Nairn (2005) and Lu and Nairn (2010) in the Peveto Channel and Sandy Point dredge pits, but not in the Raccoon Island dredge pit.

3.1.2 Henkel Model

In shallow water, the largest shear stresses exerted on the seabed may be induced by the passage of storm waves (Lee and Edwards 1986), which are likely the primary triggering mechanism for most submarine landslides globally (Henkel 1970). As waves pass, the seafloor is subject to travelling pressure waves (increased pressure under wave crests and decreased pressure under troughs) which can induce cyclic stresses within the pore systems of the seabed, leading to the progressive buildup of pore pressure. In this study we used Henkel (1970) to access pit wall slope stability under the loading of various wave conditions observed near the pits.

3.1.3 Styles and Glenn model

To better understand the pit infilling and sediment resuspension for seabed, Styles and Glenn (2000) BBL model was applied to calculate the BBL resuspended sediment concentration within the water column outside Sandy Point dredge pit and to simulate the resuspension processes in the ambient seabed (Styles and Glenn 2000).

3.1.4 DELFT-3D model

A numerical model, Delft3D, was used to simulate ocean circulation and sediment transport at Sandy Point dredge pit. The core module in Deflt3D-FLOW provides knowledge about the 3-D hydrodynamics and sediment transport. The model domain encloses the Louisiana inner shelf from west of Terrebonne Bay to east of Mobile Bay. The mesh comprises a 347 x 269 curvilinear orthogonal model grid cells with resolution from 2 m to 2 km. The hydrodynamic module Delft3D-FLOW and Delft3D-WAVE module (SWAN) were coupled, and the hydrodynamic 'background' calculated by Delft3D-FLOW was available upon each call for Delft3D-WAVE. In a communication file, the readable results by both modules were saved. To set up the FLOW module wind data were obtained from observations at WAVCIS, CSI-06 (Figure 3) and the wind speeds were corrected for U_{10}, and nine tidal constituents ($O1$, $K1$, $Q1$, $M2$, $S2$, $N2$, $K2$, $M4$ and $M6$) computed by ADCIRC were applied to the model's open boundary. The vertical discretization of model was based on sigma coordinate including 10 layers. The Mississippi River discharge at Tarbert Landing, Mississippi was added to the model. To set up the WAVE module, wave boundary conditions for three open boundaries (south, east, and west) were obtained from WAVEWATCH III (WWIII) model results. The data including significant wave height (H_s), wave peak period (T_p) and peak wave direction accounting for remote swell were downloaded from the National Weather Service Environmental Modeling Center website and were prescribed in time series to the open boundaries in WAVE module. In addition, wind-induced waves were generated through coupling of the WAVE and FLOW modules. The simulated H_s was compared with measured H_s at CSI-06, CSI-09, CSI-

16, and station LOPL1 (Louisiana Offshore Oil Port, Louisiana), and a mean wave period at CSI-06 and CSI-09 and water level variations at Southwest Pass station.

3.2 Modeling Results

3.2.1 Nairn Model

Bathymetric and radiometric data collected at Sandy Point dredge pit were used to compare with the predictions by Nairn et al. (2005). Our comparisons in Figs. 60 and 61 show over-predictions of Nairn et al. (2005) model in Sandy Point dredge pit, in terms of both pit in-filling rates and pit margin evolution. In the Peveto Channel dredge pit, four bathymetric datasets were collected; Figure 62 shows slight over-prediction of filling in rates there.

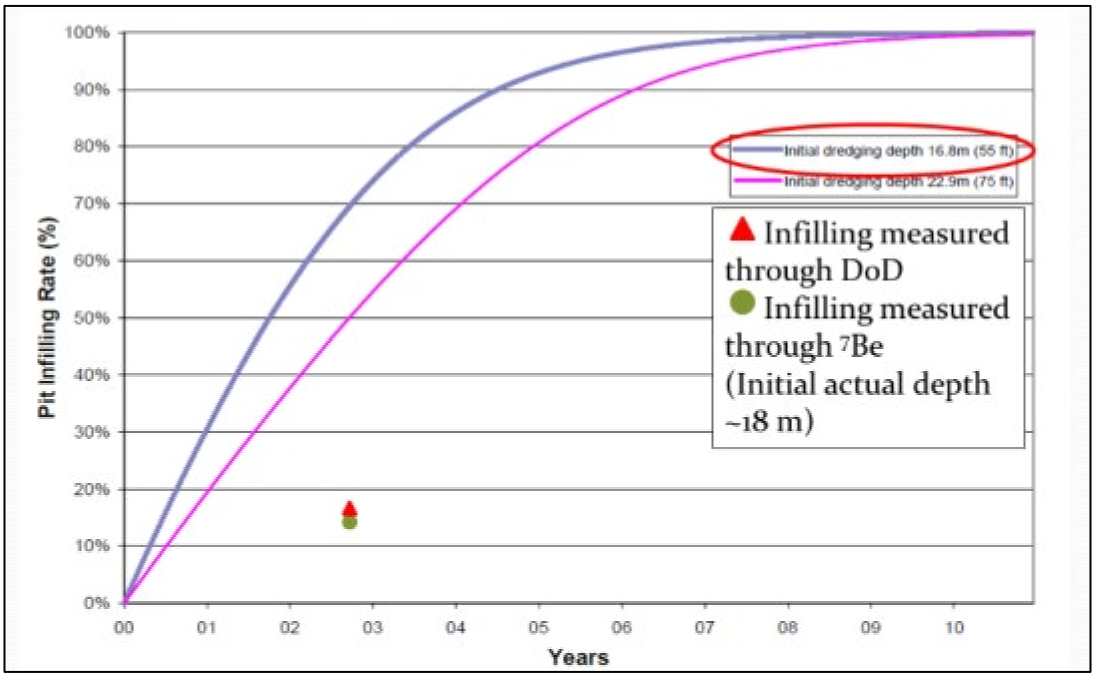

Figure 60. Comparison of Nairn et al. (2005) infill simple analytical modeling results with 2015 geophysical (red triangle) and seasonal-scale radiochemical ^{7}Be (green circle) data in the Sandy Point dredge pit.

Observational data indicate the Nairn model over predicts the infilling rate. Background figure is from Nairn et al. (2005).

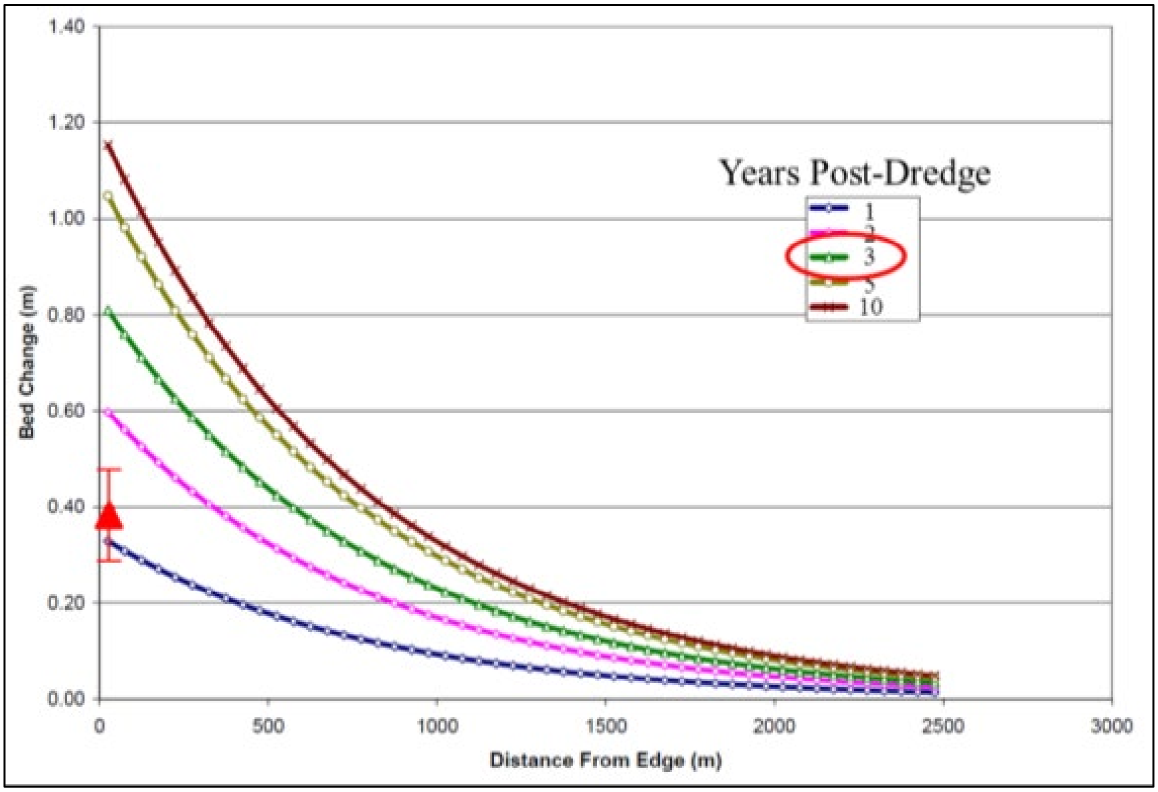

Figure 61. Comparison of Nairn (2005) pit margin erosion modeling with 2015 geophysical (red triangle) data in the Sandy Point dredge pit.

Green curve represents three years post-dredge, which is closest to the ~2.75 years the 2015 data represents. Observational data indicate vertical pit margin erosion was less than predicted by the Nairn model. Background figure is from Nairn et al. (2005).

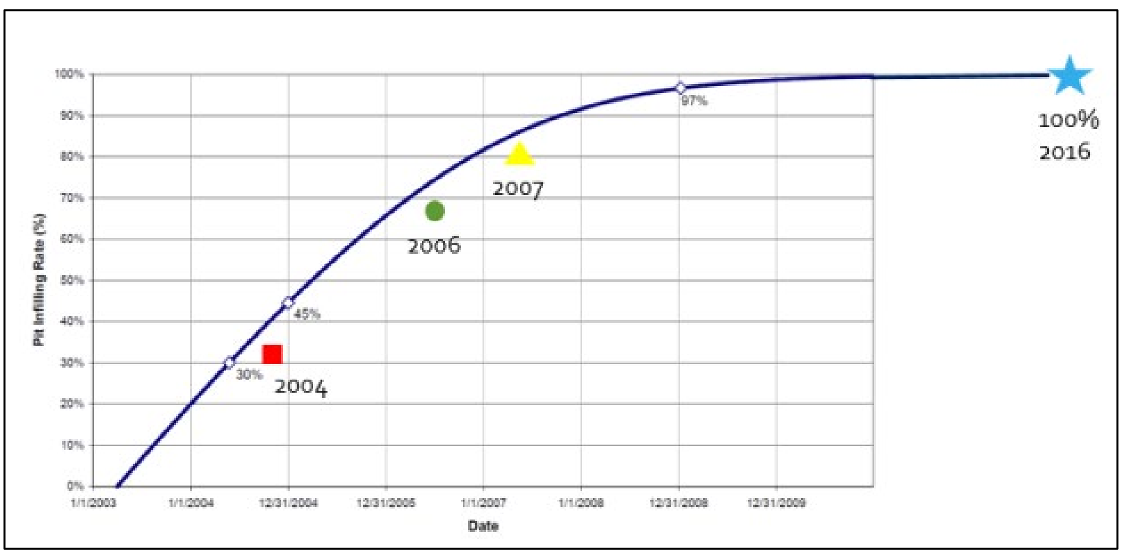

Figure 62. The pit infilling rate estimated by Nairn et al.(2005) and the observed rates of Peveto Channel in 2004, 2006, 2007, and 2016.

Background figure is from Nairn et al. (2005).

Using the measured TSS (Table 3) and current data as input parameters, the infilling model was applied along two profiles (E-W and N-S) of the Sandy Point dredge pit to predict the long term pit infilling and margin evolution. The settling velocity (0.0015 m/s) was chosen from the Nairn studies. The Lu and Nairn (2010) model was also used to study the sediment infilling process. Figure 63A shows that the prediction of this study (red dot) is close to the measured infilling depth. Based on this prediction, it will take more than 10 years to fill in the entire pit at Sandy Point. It should be noted that this model only considers sediments settling within the water column over the pit, which is either from the Mississippi River plume or ambient sea floor resuspension. No mass failure contribution from the pit walls is included in this model. Figure 63B indicates the pit margin erosion in the early stage and pit margin deposition in the later stage at the Sandy Point dredge pit. The pit margin erosion caused by the current adjustment at the N-S profile is greater than the E-W profile, which is related to the orientation of the pit.

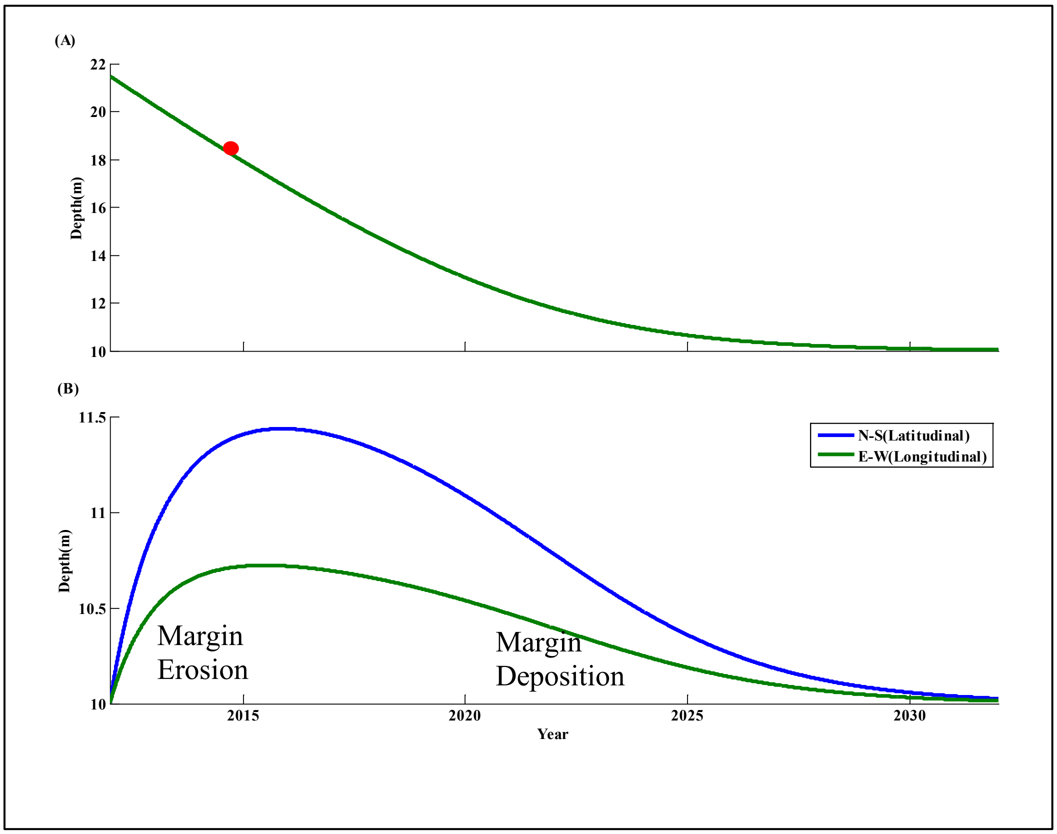

Figure 63. Model results of pit infilling in the Sandy Point dredge pit.

(A) Depth change in the pit with sediments infilling: the red dot is the measured pit depth at 2015; (B) Depth changes of the western (green) and southern pit margin (blue). From Wang et al. 2018.

3.2.2 Henkel Model

Waves can produce pressure changes between the crest and trough, as the waveform passes over the seafloor, which may mobilize the sediments on the sea floor (Henkel 1970). The pressure differences along two profiles are shown in Figure 64. It is clear that the pressure differences at the steep pit walls are much greater than the adjacent flat floor. The places with abrupt bathymetric change produce greater pressure differences and are the most likely places to collapse.

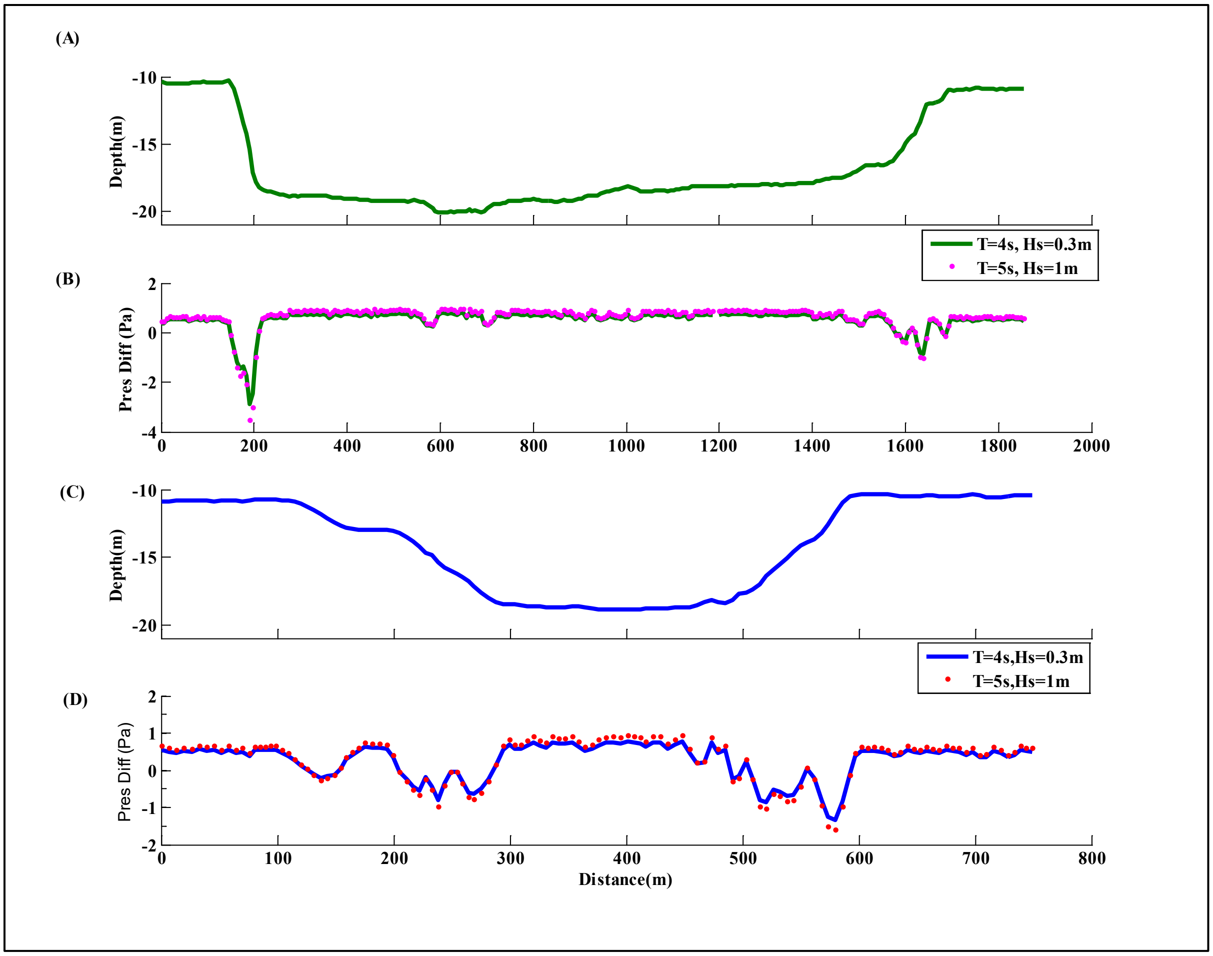

Figure 64. Wave induced pressure difference around the Sandy Point dredge pit.

(A) North-South bathymetric profile of the pit; (B) Pressure difference along the North-South profile; (C) East-West bathymetric profile of the pit; (D) Pressure difference along the East-West profile. From Wang et al. 2018.

3.2.3 Styles and Glenn model

The Nairn et al. (2005) infilling model predicts how much sediment accumulates in the dredge pits, but does not identify the sources of sediment. The sediment sources can be from (a) pit wall collapse, (b) resuspension from sea floor, and (c) settling from river plumes. In this project, the Styles and Glenn (2000) model is used to predict how much sediment is resuspended from the sea floor in Sandy Point dredge pit. The grain size groups of 0.005, 0.05, 0.1, 0.125, 0.25 mm in this model are based on sediment grab samples collected in the field.

The model results show that there was no strong resuspension near the sea floor at Sandy Point in fair-weather July and August of 2015. The resuspension only occasionally happened when the wave heights were almost 0.8 m and the near sea bed currents were around 20 cm/s (Figure 65). Thus it can be assumed that: 1) the sediment deposited on the sea floor could barely be resuspended under fair weather conditions in summer 2015, and 2) sediment deposited at Sandy Point dredge pit in summer 2015 should be from pit wall collapse and/or the Mississippi River plume.

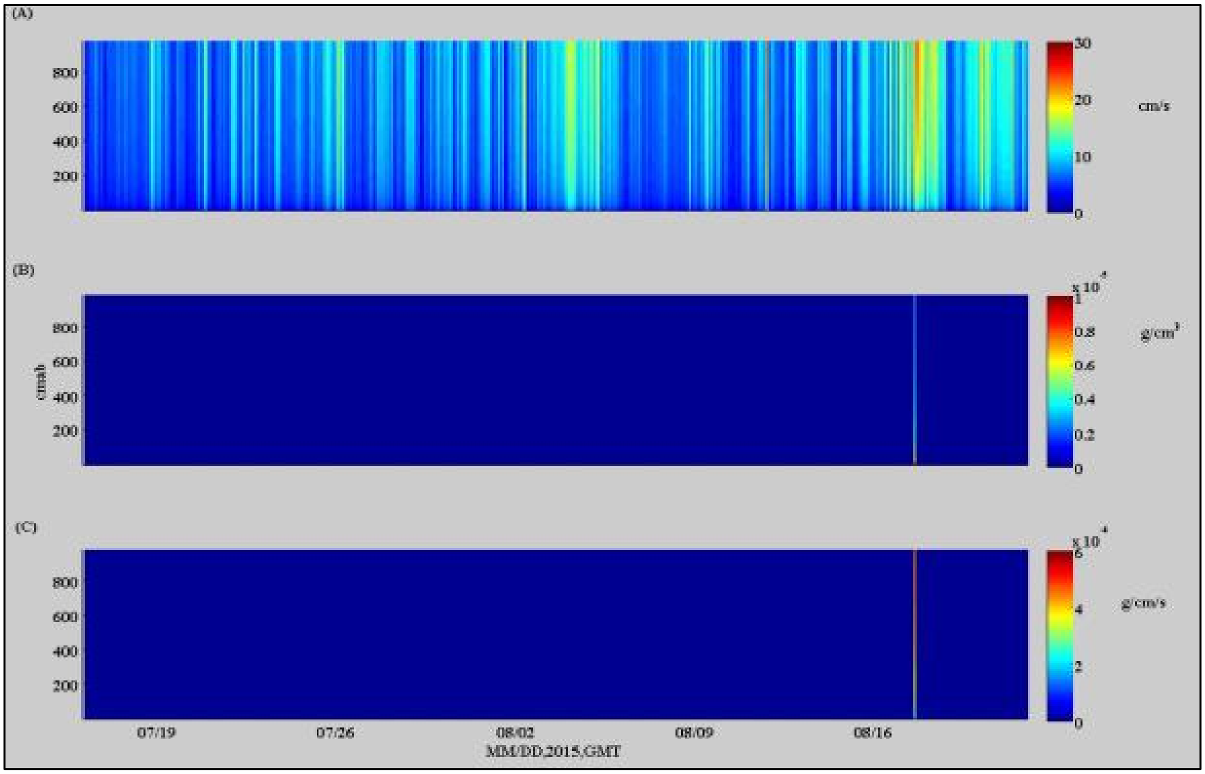

Figure 65. The model results of resuspended sediments concentration within the water column at station T1 inside the Sandy Point dredge pit.

(A) Current speed within the water column; (B) Resuspended sediments concentration of grain size 0.05mm within water column; (C) Sediment transport flux within the water column. From Wang et al. 2018.

3.2.4 DELFT-3D model

As previously discussed, the focus area of the DELFT-3D model for this study was the Sandy Point dredge pit. The simulated velocity (u and v components) of tidal currents were compared with tidal currents from the measurements at stations CSI06 and tripod station T2 inside the Sandy Point dredge pit at variable depths. Simulated water level variations were compared with NOAA stations at Southwest Pass and South Pass. Figs. 66 and 67 show the comparison between simulated u-velocity component (m/s) and observational values. Our results showed that there is a good agreement between numerical results and observations at these stations.

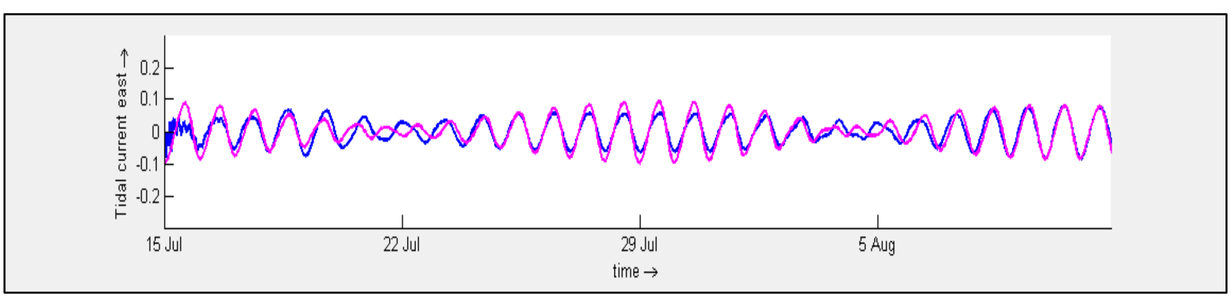

Figure 66. Comparison of u component of tidal current velocity derived from harmonically analyzed data and numerical model at CSI06 at 18m above seabed in July–August 2015.

Magenta line: from harmonically analyzed data. Blue line: from numerical model at CSI06 above seabed. From Chaichitehrani et al. 2019.

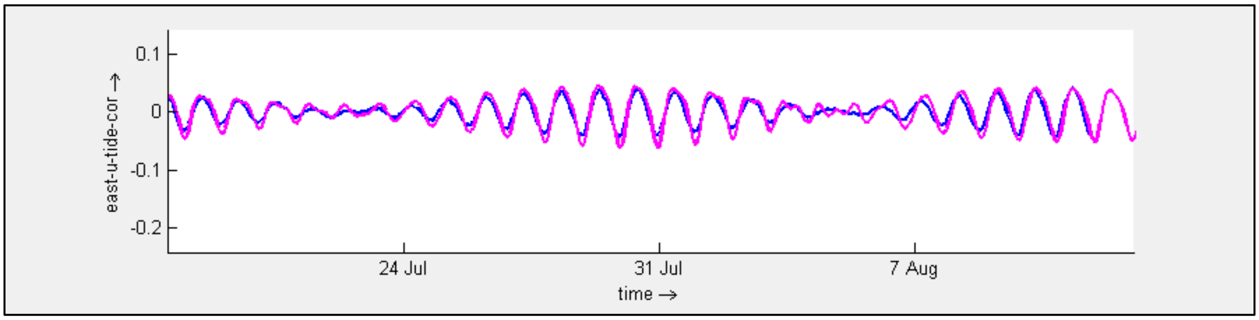

Figure 67. Comparison of u component of tidal current velocity derived from harmonically analyzed data and numerical model at tripod station T2 at the surface in July–August 2015.

Magenta line: from harmonically analyzed data. Blue line: from numerical model at tripod station T2 at the surface. From Chaichitehrani et al. 2019.

Simulated total current velocities were compared with the measurements at CSI06 and T2 during July 15–August 15, 2015. The simulation took all forces of wind, wave, tide, and river discharge into consideration. Comparisons were performed using the index presented in Willmot (1982).

The index is represented as:

$$d = 1 - \frac{\sum_{j=1}^{n}[y(j)-x(j)]^2}{\sum_{j=1}^{n}[|y(j)-\overline{y}|+|x(j)-\bar{x}|]^2} \quad (11)$$

where *x(j)* are measured values, *y(j)* are simulated values, and $\overline{x}$ and $\overline{y}$ represent the mean values of measurement and simulation, respectively. Index values vary between 0 for poor agreement and 1 for a perfect match. Index was calculated for each comparison, and results are in Table 5. Index values show an appropriate model performance, as indicated by Wang and Justić (2009).

Table 5. Comparison of observed and simulated current velocities (Willmot's index) for stations CSI06 and T2 at the Sandy Point dredge pit.

Station	u-velocity component	v-velocity component
CSI06 (Surface)	0.72	0.68
T2 (Surface)	0.69	0.70
T2 (4 m above seabed)	0.79	0.71

To validate the Delft3D-WAVE model, a comparison was made between the wave model results and the field measurements at CSI06, CSI09, and LPOL1(Louisiana Offshore Oil Port, Louisiana). Because there were no wave data available near the Sandy Point dredge pit during July and August 2015, the WAVE module was run for another time period, in March 2012, when observations were available. The simulated significant wave height H_s was compared with measured H_s at CSI06, CSI09, CSI16, and station LOPL1 (Figure 68). A good agreement was found between the modeled wave height and period with the measured data.

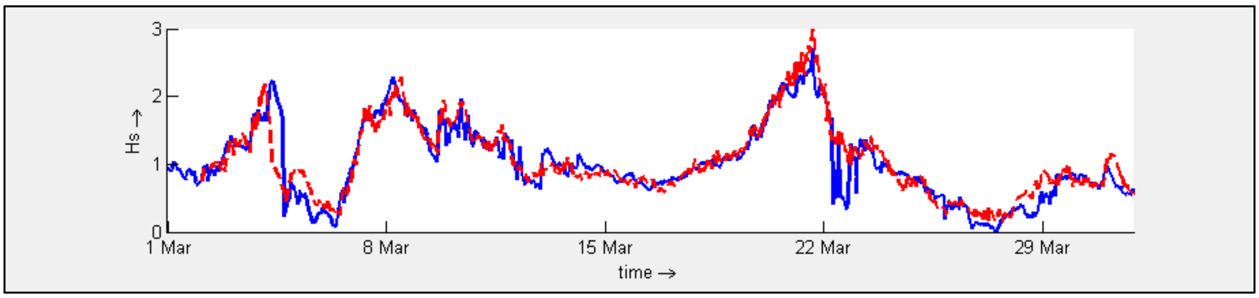

Figure 68. The comparison between simulated Hs (m) and measured Hs (m) at CSI-06 during March 2012.

Blue line: simulated Hs(m). Red line: measured Hs(m) at CSI-06.

Wave module was coupled with FLOW module to calculate bed shear stress. The results showed that the wave energy plays a critical role in resuspension of sediment in shallow region. Figure 69 shows the comparison of simulated bed shear stress for two different scenarios. Figure 69 (a) shows the simulated bed shear stress when the wave energy is not included in the simulation. Figure 69 (b) shows the simulated bed shear stress when the wave energy is included. Figure 70 presents the comparison between simulated sediment concentration (kg/m^3) and the suspended particle matter (SPM) map retrieved from LANDSAT-8, Operational Land Imager (OLI). In addition, simulated SPM values were compared with SPM field data (from Xu et al. 2016) in Table 6 to evaluate the performance of the model in estimation of SPM over our study area. These comparisons indicate that the model performs relatively well in estimation of sediment concentration over our study area.

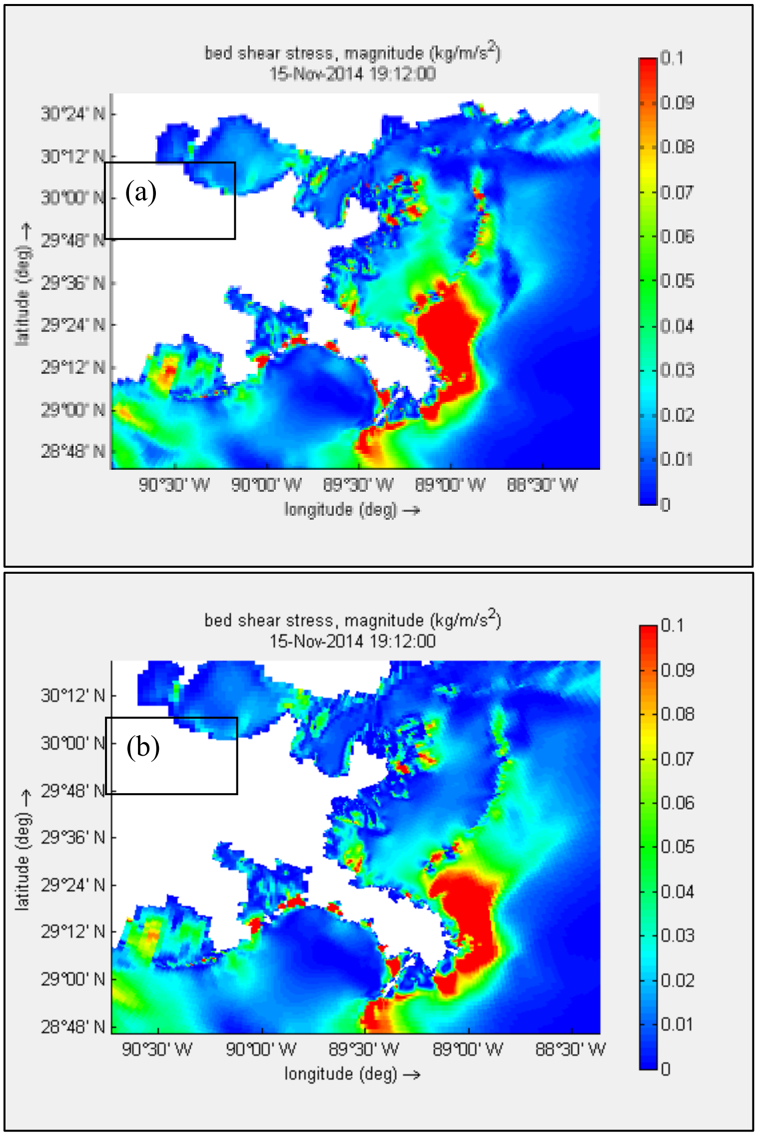

Figure 69. Simulated bed shear stress (a) excluding wave energy and (b) including wave energy.

Table 6. Comparison between modeled SPM and field data

(Xu et al. 2016)

Study Area	Station	Fieldtrip Date	Longitude	Latitude	SPM-Field (mg/L)	SPM-Model (mg/L)
West Bay	WB1	19 Nov 2014	89 18.962 °W	29 10.187 °N	12.95	11.45
	WB3	20 Nov 2014	89 19.962 °W	29 9.128 °N	11.25	11.02
	WB4	19 Nov 2014	89 17.821 °W	29 10.148 °N	17.10	14.35
	WB6	20 Nov 2014	89 18.458 °W	29 7.582 °N	10.75	10.10

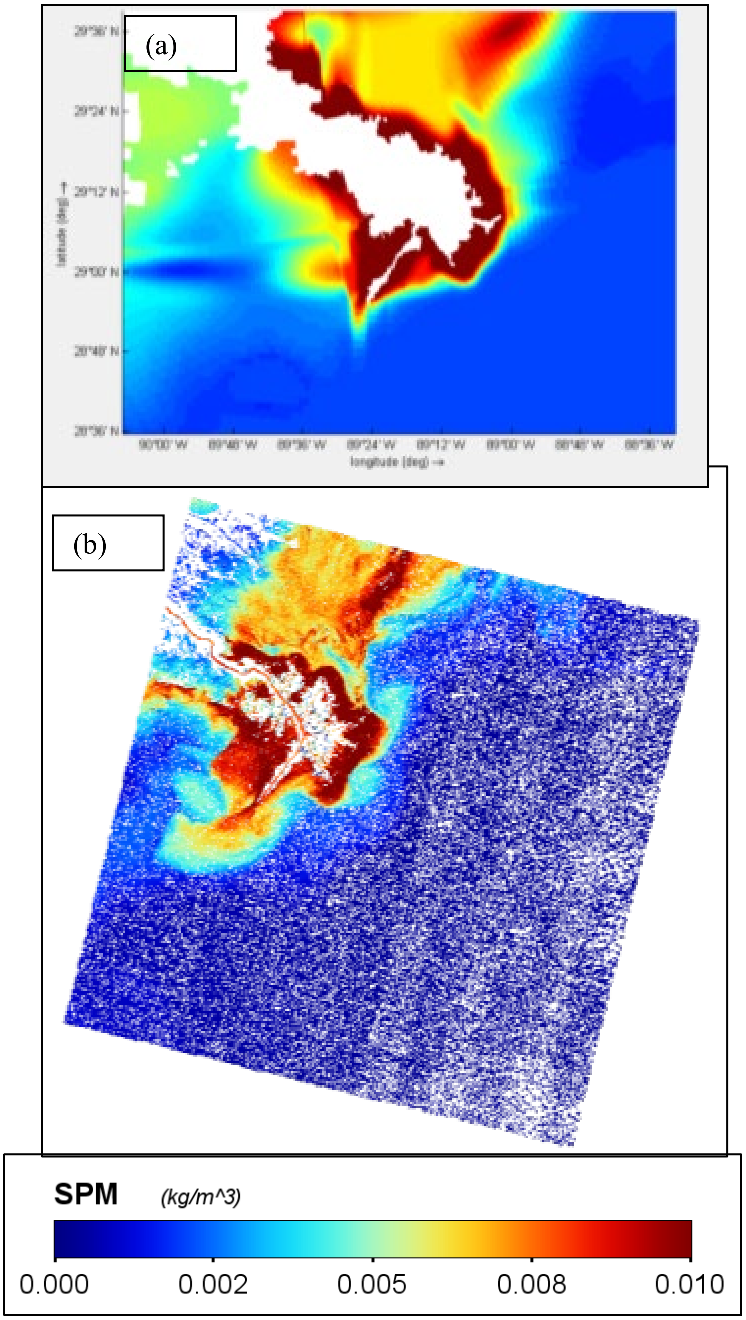

Figure 70. SPM concentration (kg/m^3) from (a) modeled (b) retrieved from LANDSAT-8.

Our tripod study at Sandy Point was performed in low energy summer of 2015, but sediment transport during energy events, such as cold fronts, can also be important to sediment infilling in Sandy Point. For comparison, the Delft3D model was used to study the conditions before, during, and after an energetic cold front passing the Sandy Point dredge pit in November 16–22, 2014.

Before this cold front breaks, the condition was characterized by mild wind speed and moderate wave heights. Bottom shear stress (BSS) over the entire Sandy Point dredge pit and other areas around the pit was about 0.05 Nm^{-2}, which was substantially below the critical shear stress for resuspension at 0.11 Nm^{-2} suggested by Wright et al. (1997) (Figure 71). Then cold front-induced wave and current increased BSS to the values of >0.2 Nm^{-2} over the shallower areas around the pit, especially on the east side (Figure 71). Inside the pit, BSS was all smaller (0.1 Nm^{-2} for the middle deepest part and 0.05 Nm^{2} for the northern part) than the critical value. After the passage of this cold front, BSS were lower than critical shear stress everywhere again.

Sediment erosion and depostion were simulated under three scenerios: (a) including wave force and river discharge, (b) including wave force and excluding river discharge, and (c) excluding wave force and including river discharge (Figure 72). The comparison of the results for these three scenarios suggests that the major bed level change inside the pit was associated with wave action (similar top and middle panels in Figure 72). When both river and waves were simulated in the model, it showed the larger sedimentation over the pit occurred in the northern part of the pit. Sedimentation decreased as approaching to the south of the pit. Based on our analysis, this was mainly due to sediment transport from the south to the north of the pit during this cold front as a result of northward near-bottom currents. The calculated average sedimentation over the entire pit was 4 mm during the cold front passage. Assuming that the Louisiana shelf is affected typically by 30–40 cold front passages per year (Roberts et al. 1987), the annual average sedimentation associated with cold front would be 12 cm to 16 cm at Sandy Point dredge pit. The annual sedimentation thickness over the Sandy Point dredge pit, calculated from 7Be radionuclide data varied from 50 cm to 100 cm. Therefore, cold front passages could contribute to the total annual sedimentation thickness over the Sandy Point dredge pit from 16% to 24%. Other factors like episodic pit wall collapse, year-long background river plume deposition, hurricanes in summer, and river floods in spring also can contribute to sediment infilling at the Sandy Point dredge pit.

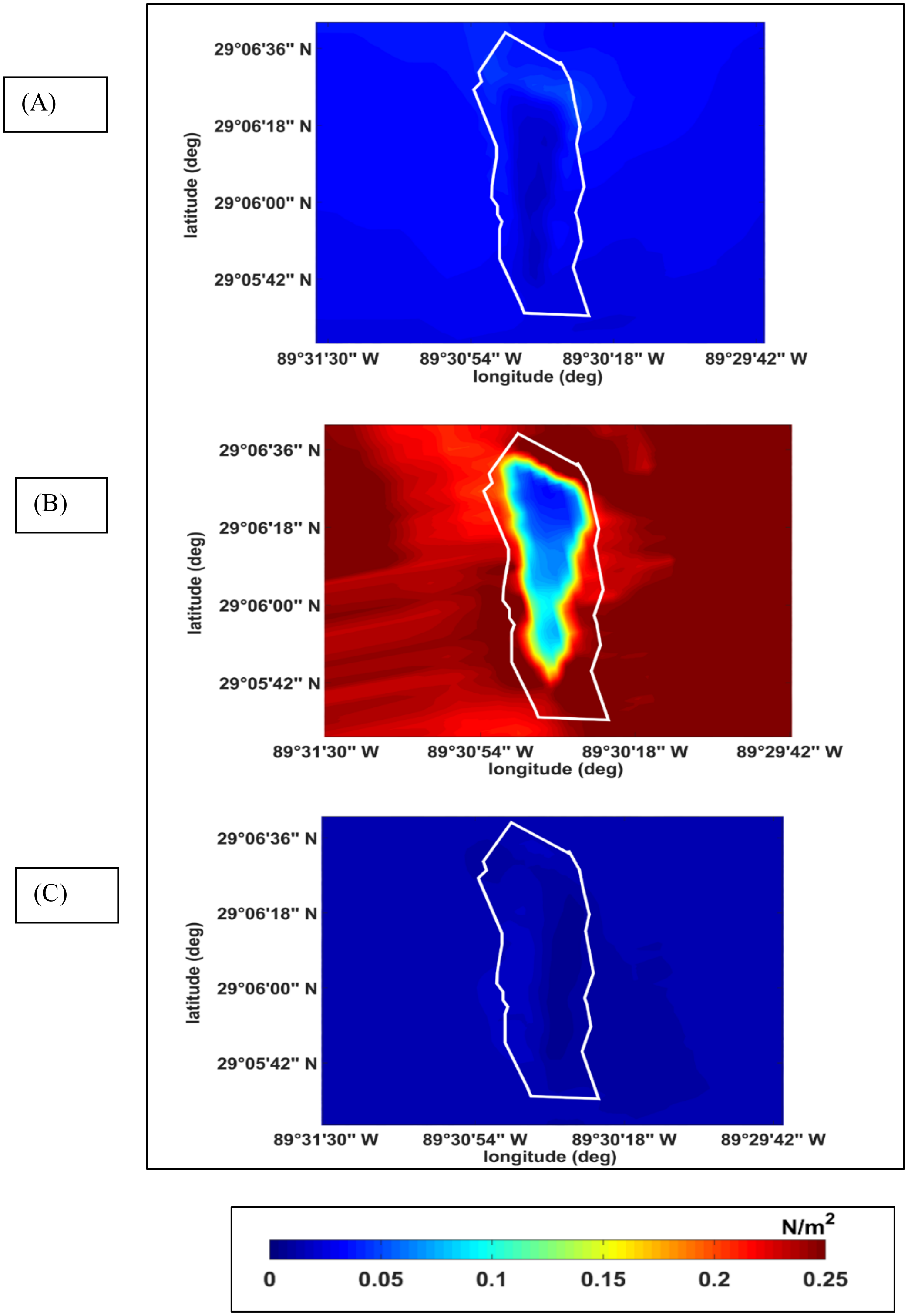

Figure 71. Bottom shear stress (Nm^{-2}) variations over the Sandy Point dredge pit when wave force was considered (top) before the cold front, (middle) during cold front passage, and (bottom) after the cold front.

White polygon is the design plate in the Sandy Point dredge pit. The modeling period is in November 16–22, 2014. From Chaichitehrani et al. 2019.

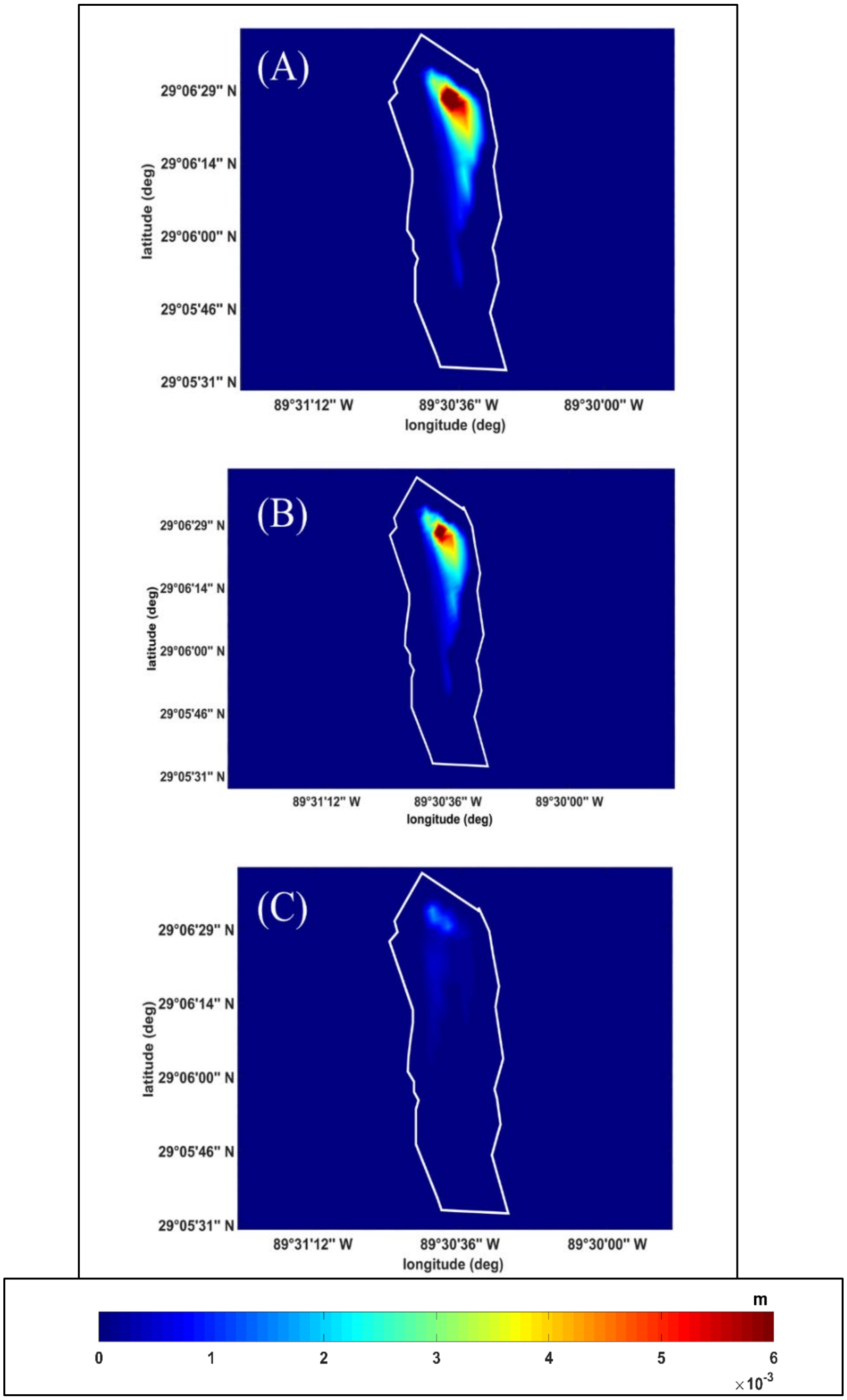

Figure 72. Thickness of sediment accumulation (m) (top) with including wave force and river discharge, (middle) with including wave force and excluding river discharge and (bottom) without wave force and including river discharge.

White polygon is the design plate in the Sandy Point dredge pit. The modeling period is in November 16–22, 2014. From Chaichitehrani et al. 2019.

4. Discussion and Conclusions

4.1 Hydrodynamics

Hydrodynamic processes are important drivers of sediment transport and morphological evolution of dredge pits. Vessel-based ADCP profiling data show that spatially there are generally two to three layers of flow over the dredge pits. For example, at the Sandy Point dredge pit, the sea surface flow is most rapid, the middle water column is at an intermediate speed and the flow inside pit is random and sluggish. This confirms the Nairn et al. (2005) conceptual model predictions that flow velocities in the pit are slower than outside of the pit (Figure 7), and indicates a low-energy environment prone to sediment trapping.

Tripod mounted ADCP data in station T2 at Sandy Point dredge pit and station R1 north of the Raccoon Island dredge pit show that the ocean circulation patterns in Sandy Point and Raccoon Island are controlled by winds, tides, rivers, and bathymetric relief. Diurnal tides are common in Louisiana shelf regions, with a tidal range of ~0.5 m. Among all diurnal tidal components at Sandy Point dredge pit, three of them (K1, S1, P1) are significant, but the other two (O1, M1) are negligible. Surface currents are highly influenced by winds, and strong correlations between winds and waves are found in the Raccoon Island dredge pit. The flow directions near the Raccoon Island dredge pit are mainly eastward and westward because the pit is located in a bathymetric trough defined by the Ship Shoal and Isles Dernieres bathymetric highs south and north of the pit, respectively. When compared to those at Raccoon Island, the waves at the Sandy Point dredge pit are less correlated with winds due to limited fetch associated the wind-sheltering effect of the adjacent bird-foot Mississippi River Delta landmass.

4.2 Sediment Transport and Infilling

Sediment delivered to the dredge pits can be sourced from: (1) the collapse of pit walls, (2) the resuspension of ambient seabed sediment, and (3) the settling of river plume sediment. Based on our results using the Styles & Glenn (2000) model, there seems to be little to no sediment resuspension during fair weather conditions in summer 2015 at the Sandy Point dredge pit. This is consistent with the conclusions of Wright et al. (1997) who reported that fair-weather conditions cannot suspend appreciable sediment on the inner continental shelf offshore Louisiana. On the other hand, our Delft3D modeling study of sediment transport during a cold front in winter 2014 at the Sandy Point dredge pit reveals large sediment resuspension from seabed due to waves generated by the cold front. Thus the contribution from resuspension of the ambient seabed probably occurs on a sub-annual basis but is highly variable seasonally.

Inside the Sandy Point dredge pit, there was a high turbidity layer of ~4 g/L found inside the pit. This turbid layer can be detected as an acoustically transparent layer on the subbottom seismic data. This layer was found at Sandy Point, but not in the Raccoon Island or Peveto Channel dredge pits.

Because rivers are a major source of ^{7}Be in coastal marine sediments, 26–50 cm of ^{7}Be activity, as seen at Raccoon Island and Sandy Point, indicates rapid and long-distance transport from a likely fluvial-source within approximately the past six months relative to the time of sample analysis. On average there is about 0.5–1 m/yr. sediment deposition calculated from ^{7}Be radionuclide data. This is confirmed by our time-series bathymetric data using difference of depths methods, as well as the acoustically opaque infilling seismic facies on sonar subbottom profiles collected in the study areas. The infilling of the Sandy Point and Raccoon Island pits is in a relatively early stage (within three years post-dredge), but our results from Peveto Channel show that the pit does fill up to 100%. All three dredge pits turn out to be efficient sediment traps. Our study reveals an infilling rate that is an order of magnitude higher than the cm/yr accumulation near the Atchafalaya and Mississippi River mouths, and much higher than the mm/yr seen on the mid-shelf offshore Louisiana.

Nairn et al. (2005) predicted sediment infilling rates at both Sandy Point and Peveto Channel dredge pits, but not at Raccoon Island pit. At Sandy Point dredge pit, Nairn et al. (2005) estimated that the infilling rate will be ~70% in 2.7 years after dredging, but the observed infilling from our bathymetric data was ~15% (Figure 60). Nairn et al. (2005) also predicted that it will take about 10 years to fill up Sandy Point dredge pit, but the actual time may be closer ~15 years, as shown in Figure 63. Note that Sandy Point is the deepest pit ever dredged on the OCS at ~ 10 m below undisturbed seafloor. At the Peveto Channel dredge pit, Nairn et al. (2005)'s estimated infilling rates are slightly greater than the observed values from our bathymetric data (Figure 62).

The parameters that are most challenging to quantify in the Nairn et al. (2005) model are probably settling velocity and sediment concentration, both of which vary substantially in space and time. Long-term time-series observations of these parameters are required in order to better quantify the pit filling process. In addition, as of now there is no explicit sediment consolidation process in the Nairn et al. (2005) model. To improve the predictions, consolidation needs to be added to better capture the morphological evolution. As explained in Section 4.4, consolidation is an ongoing process and plays a key role on morphological evolution even after the pit is 100% filled.

The type of infilling sediment was mainly mud in the Sandy Point and Raccoon Island dredge pits. Although no cores were collected at Peveto Channel, the low backscatter of sidescan data indicates a fine-grained texture in Peveto Channel. Considering the high mud percent, the infilling sediment is probably not suitable for the reuse for future barrier island restoration, as restoration sediment should contain at least ~80% beach-compatible sand. Gas-charged sediment, as indicated by an acoustically opaque seismic facies, was observed on the subbottom profiles in all three pits, indicating the decay of organic matter buried with mineral mud inside the pits.

4.3 Pit Margin Evolution

BOEM requires that all pipelines inshore of the 200 ft depth contour be buried by at least 3 ft (0.9 m) below the seabed surface to avoid impacts with navigation and commercial fishing activity as well as to prevent scour and spanning or movement of pipeline sections. Nairn et al. (2005) reported that the distance from the edge of the pit to a location beyond which there is less than 0.9, 0.5, or 0.1 m of vertical erosion varies widely depending on pit width or length, dredge depth, pre-existing water depth, and equilibrium concentration.

Two scenarios were tested in Nairn et al. (2005)'s calculations for muddy settings. The first scenario included an elongated pit with a length of 2000 m, a pit depth of 10 m and a pit width 125 m, in a water depth of 10 m. The second scenario featured a more typical case with a pit length of 650 m, a pit width of 650 m, a pit depth of 6 m, in a water depth of 8 m. The sizes of the Sandy Point, Raccoon Island, and Peveto Channel dredge pits studied in this project are approximately 1200 m × 350 m, 800 m × 200 m, 600 m × 400 m, respectively, and all three pits are in muddy settings. These three pits are not the same as the sizes used in two model scenarios, and all of them are less than 2000 m long. The cut depths of these three pits varied between 6 m and 10 m.

Nairn et al. (2005) calculated the buffer distance requirements to avoid more than 0.9, 0.5, or 0.1 m of vertical erosion for both scenarios. They reported that the required buffers range from 100 m to 1,500 m for the long pit (first scenario) and 50 m to 1,200 m for the average pit (second scenario). They also assumed that for the average pit with typical pre-existing water depth (5 to 10 m) and dredge depths (5 to 10 m) the required buffer distance was generally less than about 200 m.

Comparisons of bathymetric data collected at the Sandy Point, Raccoon Island, and Peveto Channel dredge pits in different periods show that the pit margins have been relatively stable in all three pits. In general, the pit margin movements were not more than 50 m in the Sandy Point, Raccoon Island, and Peveto Channel dredge pits. For example, Figure 73 shows the margins of the Peveto Channel dredge pit in 2003, 2004, and 2006, which were defined as the areas steeper than 16°, 7°, and 3°, respectively, in our calculations. The overlay color map of Figure 73 shows that the outward migrations of pit walls were not more than 10s of meters horizontally three years after the dredging. Sidescan map on Figure 50 also reveals minimal pit margin movement even 13 years after the dredging. Differing from sandy dredge pits, it seems that the cohesive "mud caps" prevent widespread pit wall collapse and help preserve the localized pit morphology in the Sandy Point, Raccoon Island, and Peveto Channel dredge pits.

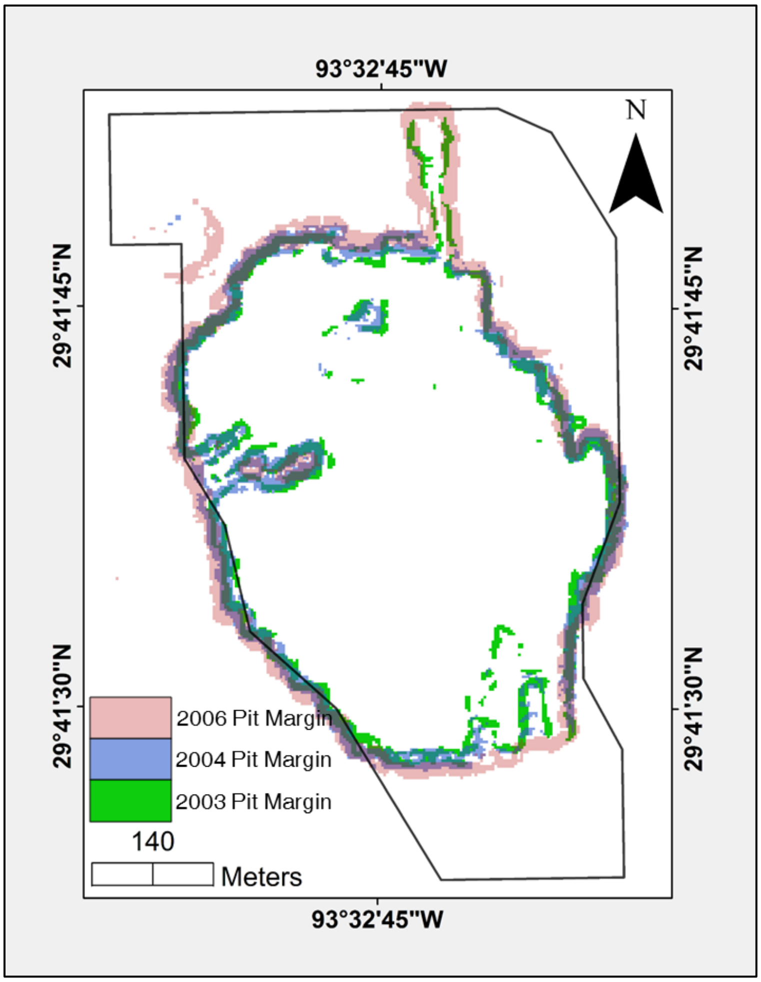

Figure 73. Map showing pit margins of Peveto Channel from 2003–2006.

The colored outline encompasses the entirety of the wall slope, and thus captures the pit from the outside edge to the inside of the pit. Minute amounts of lateral migration can be seen each year, showing that the pit walls move outward very little. From Robichaux et al. 2020.

The average slope of the pit margins at the Peveto Channel dredge pit decreased from 2003 to 2006. Similar results are found in the Sandy Point dredge pit. Figure 38 shows the temporal and spatial changes of slopes in the Sandy Point dredge pit walls. The eastern wall of the Sandy Point dredge pit was steeper than western wall after the dredging, and maintained this geometry three years after construction. This is in contrast with evolution of the western wall which has lost some of its steepness (become flatter) since construction.

The estimated erosion of pit margin using Nairn model varies between 0.1 and 1.0 m vertically (Figure 57). The Edgetech 4600 bathymetric system used in this project has a vertical resolution of about 0.25 m in 10 m deep water, and the difference of depths yields an error of 0.5 m, which is comparable to the modeled 0.1–1.0 m pit margin vertical erosion. In other words, pit margin erosion less than 0.25 m may not be easily identified in our bathymetric data. Despite this challenge, our gradient map analysis and sidescan data help identify the pit wall edges easily on Figure 50.

It should be noted that some rapid pit margin evolution may have happened during the dredging, or before the first survey after the dredging. This period is difficult to observe because the dredging takes several months to finish, and the first post-dredging survey typically does not occur until ~1 month or longer after sand excavation. In this phase, locally derived sediment may dominate pit infill as steep pit walls slump and fail to achieve equilibrium.

4.4 Post 100% Infilling

When the dredge pits are filled up with sediment, a flat and smooth surface is expected. However, complex morphology is found in some portions of seafloor in the Peveto Channel dredge pit (Figure 49). Both smooth and rough surfaces are found inside the Peveto Channel dredge pit. A comparison of 2003, 2016, and 2003+2016 overlay maps show that the surface morphology in 2016 has been greatly impacted by 2003 bathymetry (Figure 67). For instance, blue and orange rectangles in Figure 74 highlight the thirteen-year footprint effect of 2003 bathymetry in the Peveto Channel dredge pit. The cause of rough surfaces might be related to the degassing and consolidation of fresh, fine-grained infilling sediment at Peveto Channel, which is a long term and ongoing process. It is possible that freshly deposited sediment in the deeper part of pit had undergone a much thicker consolidation processes, which had not been totally compensated by infilling. In contrast, the consolidation magnitude of thin deposit on shallower part of pit was smaller. This vertical differential consolidation could lead to the current layout of smooth and rough surfaces. Other related processes can be wave-impacted mass wasting, which could lead to downslope horizontal submarine mudslides. Denommee (2015) reported active mass wasting processes in western Louisiana shelf due to active wave impact on fluid muds at very low seabed gradients. Similar footprint effect can also be seen in the Sandy Point dredge pit. As illustrated in Figure 38, an E-W trending “stair” in the middle of pit in 2012 and 2015 bathymetric data corresponds with the designing plates of the Sandy Point dredge pit.

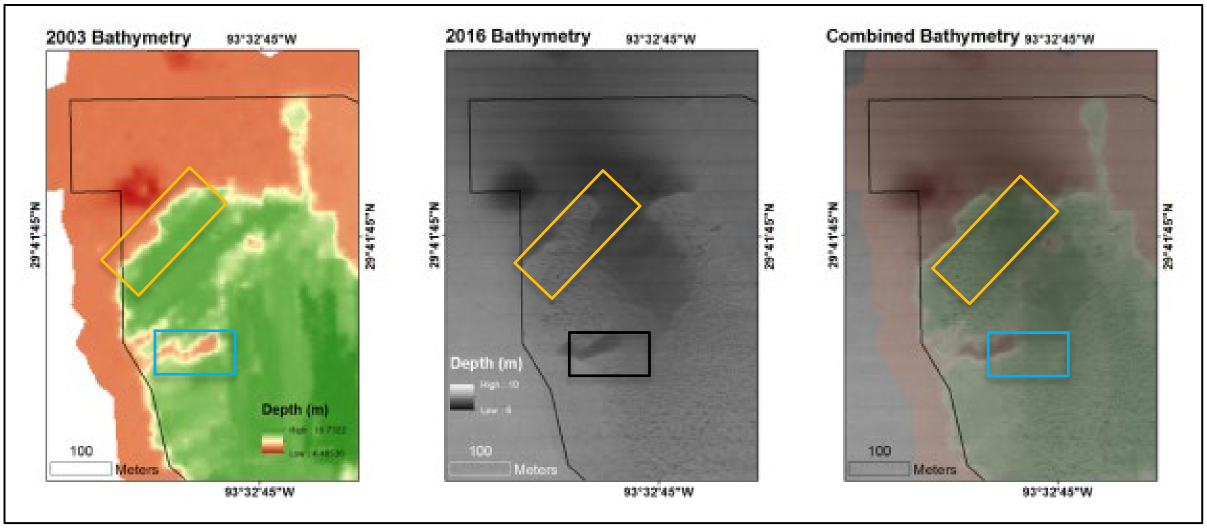

Figure 74. Left, 2003 Peveto Channel dredge pit bathymetry; middle, 2016 bathymetry; right; overlaying 2003 with 2016 using 50% transparency.

Blue and orange rectangles highlight the thirteen-year footprint impact of 2003 on 2016 data. From Robichaux et al. 2020.

Considering the active processes in Sandy Point and Peveto Channel, the protocols to manage the 100% infilling dredge pits need to be carefully considered by the managers and decision makers. A pipeline constructed before 2016 in the middle of the Peveto Channel dredge pit was detectable using our magnetometer (Figure 52). The location of this pipeline was not far from morphologically active and rough surface. Whether the ongoing subsidence may potentially expose the pipeline needs further investigation. Because the geotechnical properties of newly filled pit material is different than the surrounding undisturbed seafloor, properties such as water content, organic matter content, pore pressure, shear strength should be evaluated before the construction of any new infrastructure. Because consolidation is a long, ongoing process, continued monitoring the 100% infilling dredge pits is needed because new collapse and uneven surfaces can be formed even after the development of flat surface.

4.5 Existing Mitigations

Based on the bathymetric and sidescan data collected from all three pits, the horizontal pit wall migrations and erosions are limited to about 50 meters from the original pit walls. To avoid 0.1–0.9 m erosion, Nairn et al. (2005) suggested some setback buffer distances of up to 1,200 m to 1,500 m, and these values seem to be conservative for mud-capped dredge pits. Three pits share some similarities, but differ greatly in hydrodynamics, sediment dynamics and filling in processes. The morphological evolution is a long term processes that should be accessed and tested using some longer-term data. Currently there are only two surveys performed after the dredging at Sandy Point and two at Raccoon Island. The calibrations of sediment infilling model apparently require more data to be collected.

4.6 Pit Monitoring Protocols

To better monitor the dredge pits, long-term and repeat surveys are needed. Repeat bathymetric surveys using multi-beam or swath interferometric systems are highly recommended. All the bathymetric data should be referenced to a common horizontal and vertical datum so that multiple datasets can be compared. In addition, about 1,200 to 1,500 m outside of the dredge pits should be surveyed based on the values from Nairn et al. (2005). This distance seems to work well in the Sandy Point, Raccoon Island, and Peveto Channel dredge pits. Single-beam survey is not recommended because of the complex morphology of the dredge pit walls and floor as it fills. Our bathymetric and sidescan data show that there are highly localized features and erosional hot spots surrounding the dredge pits. If only sparse single-beam data are collected in the study area, it would be hard to detect these areas. The calculation of volume using single beam data is also highly dependent on the interpolation methods. A suite of geophysical data acquisition like bathymetry, sidescan, and subbottom can provide rich 3-D datasets that can be used for comprehensive data analyses. Sidescan and subbottom profiling surveys are highly recommended because they are complementary with bathymetric data. When bathymetry, sidescan, and subbottom work is performed at the same time, the cost of ship time can be saved.

Quick updates of bathymetric and pipeline databases are needed, and these data should be shared among academia, industry, stakeholders, and federal and state agencies. The permitting process to construct new pipelines over 100% infilling pits need to be established. Consolidation is a long ongoing process and should be taken into consideration in the infrastructure permitting process, even several years after 100% infilling.

Works Cited

Barnhardt WA (ed.). 2009. Coastal change along the shore of northeastern South Carolina—the South Carolina coastal erosion study. USGS Geological Survey Circular 1339. 77 p. Reston (VA): US Geological Survey.

Bea RG, et al. 1983. Wave-induced slides in south pass block 70, Mississippi Delta. J Geotech Eng. (109.4): 619–644.

Bendat JS, Piersol AJ. 2000. Random data–analysis and measurement procedures, 3rd edition. 594 p. New York (NY): John Wiley and Sons.

Broussard L, Boustany R. 2005. [CD-ROM.] Restoration of a Louisiana barrier island: Raccoon Island case study. In: Proceedings of the 14th Biennial Coastal Zone Conference, July 17–21, 2005, New Orleans, Louisiana. Charleston (SC): NOAA Coastal Services Center.

Chaichitehrani N, Li C, Xu KH, Allahdadi MN, Hestir EL, et al. 2019. A numerical study of sediment dynamics over Sandy Point dredge pit, west flank of the Mississippi River, during a cold front event. Cont Shelf Res. 183: 38–50.

Coastal Planning and Engineering, Inc. 2013. Pelican Island restoration (BA-38-I), CWPPRA project: project completion report. 27 p. Boca Raton (FL): Coastal Planning and Engineering, Inc.

Cochrane JD, Kelly FJ. 1986. Low frequency circulation on the Texas-Louisiana continental shelf. J Geophys Res. 91:10, 645–10,659.

Coleman JM, Prior DB, Garrison LE. 1980. Subaqueous sediment instabilities in the offshore Mississippi River Delta. Open File Report 80-01. New Orleans (LA): US Department of Interior, Bureau of Land Management, New Orleans Outer Continental Shelf Office. 60 p.

Deltares. 2014. User manual Delft3D-FLOW, Simulation of multi-dimensional hydrodynamic flows and transport phenomena, including sediments. 710 p. Delft (NL): Deltares.

Denommee K. 2015. Developing recognition criteria for current-wave-enhanced sediment gravity flows [dissertation]. Baton Rouge (LA): Louisiana State University.

Goring DG, Nikora V. 2002. Despiking acoustic doppler velocimeter data. J Hydraul Eng. 128: 117–126.

Henkel DJ. 1970. The role of waves in causing submarine landslides. Géotechnique. 20:75-80.

IHIS™ Energy Technical Global. 2016. Kingdom® 2016.1 installation guide. 104 p. Houston (TX): HIS..

Kim JH, Yoneya M, Yokoyama H. 2002. Tristable nematic liquid-crystal device using micropatterned surface alignment. Nature. 420(6912): 159-62.

Karimpour A. 2015. OCEANLYZ Ver. 1.4, Ocean Wave Analyzing Toolbox, user manual. [accessed 9 Aug 2018]; http://www.arashkarimpour.com/oceanlyz.html.

Kobashi D. 2009. Bottom boundary layer physics and sediment transport along a transgressive sand body, Ship Shoal, south-central Louisiana: implications for fluvial sediments and winter storms [dissertation]. Baton Rouge (LA): Louisiana State University.

Lee HJ, Edwards BD. 1986. Regional method to assess offshore slope stability. J Geotech Eng. 112.5: 489–509.

Li C, Valle-Levinson A, Atkinson L, Royer TC. 2000. Inference of tidal elevation in shallow water using a vessel-towed ADCP. J Geophys Res C: Oceans. 105(C11): 26225–26236.

Li C. 2002. Axial convergence fronts in a barotropic tidal inlet–Sand Shoal Inlet, VA. Cont Self Res. 22: 2633–2653.

Liu H, Xu KH, Wilson C. 2020. Sediment infilling and geomorphological change of a mud-capped Raccoon Island dredge pit near Ship Shoal of Louisiana shelf. Estuarine Coast Shelf Sci 245:106979.

Lu Q, Nairn RB. 2010. Prediction on morphological response of dredged sand-borrow pits. Coastal Eng. 32: 1–9.

Muhammad Z., Bentley SJ, Febo LA, Droxler AW, Dickens GR, et al. (2008). Excess 210Pb inventories and fluxes along the continental slope and basins of the Gulf of Papua. J Geophys Res F: Earth Surface. 113: F1.

Nairn RB, Langendyk SK, Michel J (Baird & Assoc., Madison, Wisconsin, and Research Planning Inc., Columbia, SC). 2004. Preliminary infrastructure stability study, offshore Louisiana. 179 p. New Orleans (LA): US Department of Interior, Minerals Management Service. Contract No.: 35-0001-31051. Report No.: MMS 2005-043

Nairn RB, Lu Q, Langendyk SK, Michel J (Baird & Assoc., Madison, Wisconsin, and Research Planning Inc., New Orleans, Louisiana). 2005. A study to address the issue of seafloor stability and the impact on oil and gas infrastructure in the Gulf of Mexico. 228 p. New Orleans (LA): US Department of Interior, Minerals Management Service. Contract No.: 1435-01-04-CT-335085. Report No.: MMS 2005-043.

Nairn RB, Lu Q, Langendyk SK, Hayes MO, Montagna PA. et al. (Baird & Assoc., Madison, Wisconsin). 2007. Examination of the physical and biological implications of using buried channel deposits and other non-topographic offshore features as beach nourishment material. 471 p. New Orleans (LA): US Department of Interior, Minerals Management Service. Contract No.: 1435-01-05-CT-39150. Report No.: MMS 2007-048.

Nittrouer JA, Allison MA, Campanella R. 2008. Bedform transport rates for the lowermost Mississippi River. J Geophys Res F: Earth Surface. 113: F03004. doi: 10.1029/2007JF000795.

Nowlin WD Jr, Jochens AE, Reid RO, DiMarco SF (Texas A&M University, College Station, Texas). 1998a. Texas-Louisiana shelf circulation and transport processes study: synthesisrReport, volume 1 technical report. 502 p. New Orleans (LA): US Dept. of the Interior, Minerals Management Service. Contract No.: 14-35-0001-30509. Report No.: MMS 98-0035

Obelcz J, Xu KH, Bentley SJ, O'Connor M, Miner M. 2018. Mud-capped dredge pits: an experiment of opportunity for characterizing cohesive sediment transport and slope stability in the northern Gulf of Mexico. Estuarine Coast Shelf Sci. 208: 161–169.

Penland S, McBride RA, Williams SJ, Kindinger JL, Boyd R. 1989. Holocene sand shoals offshore of the Mississippi River delta plain. Gulf Coast Assoc Geol Soc Trans. 39: 471–480.

Roberts HH, Huh OK, Hsu SA, Rouse LJ Jr, Rickman D. 1987. Impact of coldfront passages on geomorphic evolution and sediment dynamics of the complex Louisiana coast. In: Kraus NC, editor. Coastal sediments '87: Proceedings of a Specialty Conference on Advances in Understanding of Coastal Sediment Processes, New Orleans, Louisiana, May 12–14, 1987. 2 vols. New York (NY): American Society of Civil Engineers.

Robichaux P, Xu KH, Bentley SJ, Miner M, Xue Z. 2020. Morphological evolution of a mud-capped dredge pit on the Louisiana shelf: Nonlinear infilling and continuing consolidation. Geomorph. 354: 107030.

Soulsby RL, Dyer KR. 1981. The form of the near-bed velocity profile in a tidally accelerating flow. J Geophys Res C: Oceans. 86.C9: 8067–8074.

Stone G, Xu J. 1996. Wave climate modeling and evaluation relative to sand mining on Ship Shoal, offshore Louisiana, for coastal and barrier island restoration. 182 p. New Orleans (LA): US Department of Interior, Minerals Management Service. Report No.: MMS 96-059.

Stone G (Louisiana State University, Baton Rouge, Louisiana). 2000. Wave climate and bottom boundary layer dynamics with implications for offshore sand mining and barrier island replenishment in south-central Louisiana. 94 p. New Orleans (LA): US Department of Interior, Minerals Management Service. Contract No.: 14-35-0001-30660-19911b. Report No.: MMS 2000-053.

Stone GW, Condrey RE, Fleeger JW, Khalil SM (Louisiana State University, Baton Rouge, Louisiana). 2009. Environmental investigation of the long-term use of Ship Shoal sand resources for large-scale beach and coastal restoration in Louisiana. 314 p. New Orleans (LA): US Department of Interior, Minerals Management Service. Contract No.: 1435-01-04-CA-35162. Report No.: MMS 2009-024.

Styles R, Glenn MS. 2000. Modeling stratified wave and current bottom boundary layers on the continental shelf. J Geophys Res. 105(C10): 24119–24139.

Suter JR, Berryhill HL Jr, Penland S. 1987. Late Quaternary sea-level fluctuations and depositional sequences, southwest Louisiana continental shelf. In: Nummedal D, Pilkey OH, Howard JD, editors. Sea-level fluctuation and coastal evolution. SEPM Special Publication 41. Tulsa (OK): Society of Economic Paleontologists and Mineralogists. p. 199–219.

Tang G, Zhao M, Li T, Liu Y, Zhang T. 2003. Simulation on slope uncertainty derived from DEMs at different resolution levels: a case study in the Loess Plateau. J Geogr Sci. 13(4): 387-394

TetraTech EM, Inc. 2004. Final tier 1 evaluation of Sandy Point overburden: Plaquemines Parish, Louisiana. Barataria/Plaquemines Barrier Shoreline System Complex Project, CWPPRA Project Fed No. BA-38. 21 p. Miami (FL): National Oceanic and Atmospheric Administration, National Marine Fisheries Service.

Wahl TL. 2002. Discussion of ‘‘despiking acoustic doppler velocimeter data” by Derek g. Goring and Vladimir I. Nikora. J Hydraul Eng. 129: 484–487.

Wang L, Justić D. 2009. A modeling study of the physical processes affecting the development of seasonal hypoxia over the inner Louisiana-Texas shelf: circulation and stratification. Cont Shelf Res. 29(11–12):1464–1476.

Wang J, Xu KH, Obelcz J, Li C. 2018. Forces driving the morphological evolution of a mud-capped dredge pit, Northern Gulf of Mexico. Water. 10: 1001.

Wright SG, Dunham RS. 1972. Bottom stability under wave induced loading. In: Proceedings of Offshore Technology Conference, May 1-3, 1972, Houston, Texas. Houston (TX): Offshore Technology Conference. p. 852–862.

Wright L, Sherwood C, Sternberg R. 1997. Field measurements of fairweather bottom boundary layer processes and sediment suspension on the Louisiana inner continental shelf. Mar Geol. 140(3): 329–345.

Willmot, CJ. 1982. Some comments on the evaluation of model performance. Bull Am Meteorol Soc. (63):1309–1313.

Xu KH, Harris CK, Hetland RD, Kaihatu JM. 2011. Dispersal of Mississippi and Atchafalaya sediment on the Texas-Louisiana shelf: model estimates for the Year 1993.Cont Shelf Res. (31):1558–1575. doi:10.1016/j.csr.2011.05.008

Xu KH, Bentley SJ, Robichaux P, Sha X, Yang H. 2016. Implications of texture and erodibility for sediment retention in receiving basins of coastal Louisiana diversions. Water. 8: 26. doi:10.3390/w8010026.

Xu K, Wang J, Li C, Bentley S, Miner M. 2021. Geomorphic and hydrodynamic impacts on sediment transport on the inner Louisiana Shelf. Geomorphol. 108022.

The Department of the Interior Mission

As the Nation's principal conservation agency, the Department of the Interior has responsibility for most of our nationally owned public lands and natural resources. This includes fostering sound use of our land and water resources; protecting our fish, wildlife, and biological diversity; preserving the environmental and cultural values of our national parks and historical places; and providing for the enjoyment of life through outdoor recreation. The Department assesses our energy and mineral resources and works to ensure that their development is in the best interests of all our people by encouraging stewardship and citizen participation in their care. The Department also has a major responsibility for American Indian reservation communities and for people who live in island territories under US administration.

The Bureau of Ocean Energy Management Mission

The Bureau of Ocean Energy Management (BOEM) promotes energy independence, environmental protection and economic development through responsible, science-based management of offshore conventional and renewable energy resources.

The BOEM Environmental Studies Program Mission

The mission of the Environmental Studies Program (ESP) is to provide the information needed to predict, assess, and manage impacts from offshore energy and marine mineral exploration, development, and production activities on human, marine, and coastal environments.